LUND UNIVERSITY

Numerical investigation on the formation mechanism of residual stress in metal cutting

Liu, Yang

2021

Document Version:
Publisher's PDF, also known as Version of record

Link to publication

Citation for published version (APA):
Liu, Y. (2021). *Numerical investigation on the formation mechanism of residual stress in metal cutting*. Lund University.

Total number of authors:
1

General rights
Unless other specific re-use rights are stated the following general rights apply:
Copyright and moral rights for the publications made accessible in the public portal are retained by the authors and/or other copyright owners and it is a condition of accessing publications that users recognise and abide by the legal requirements associated with these rights.
• Users may download and print one copy of any publication from the public portal for the purpose of private study or research.
• You may not further distribute the material or use it for any profit-making activity or commercial gain
• You may freely distribute the URL identifying the publication in the public portal

Read more about Creative commons licenses: https://creativecommons.org/licenses/

Take down policy
If you believe that this document breaches copyright please contact us providing details, and we will remove access to the work immediately and investigate your claim.

LUND UNIVERSITY

PO Box 117
221 00 Lund
+46 46-222 00 00

Download date: 27. Apr. 2024

Numerical investigation on the formation mechanism of residual stress in metal cutting

YANG LIU
DIVISION OF PRODUCTION AND MATERIALS ENGINEERING | LUND UNIVERSITY

Printed by Media-Tryck, Lund 2021 NORDIC SWAN ECOLABEL 3041 0903

Faculty of Engineering
Department of Mechanical Engineering Sciences
Division of Production and Materials Engineering

ISBN 978-91-8039-077-4
ISRN: LUTMDN/(TMMV-1072)/1-101/(2021)

Numerical investigation on the formation mechanism of residual stress in metal cutting

Yang Liu

LUND
UNIVERSITY

DOCTORAL DISSERTATION

by due permission of the Faculty LTH, Lund University, Sweden.
To be defended in lecture hall KC:A, KC-building, LTH

on 2021-12-17 at 09:00 AM

Faculty opponent
Prof. Tomas Beno, University West

Organization LUND UNIVERSITY	**Document name:** DOCTORAL DISSERTATION
	Date of issue: December 2021
Author(s) Yang Liu	Sponsoring organization: CSC

Title and subtitle:
Numerical investigation on formation mechanism of residual stress in metal cutting

Abstract

Residual stress can be introduced unintentionally into the workpiece with various magnitudes and distributions through all manufacturing processes. These stresses have a significant effect upon the performance of the final component. Understanding the residual stress imparted by machining is an essential aspect of understanding the machining process and overall part quality. Although many investigations have been conducted over the past few decades in measurement, modelling and mechanisms of residual stresses induced by the different manufacturing processes, the insights of residual stresses induced during the machining are still far from being completely understood. Several crucial issues still have to be investigated. In particular, the residual stress generation under different circumstances (segmented chip, the variation of tool geometries, multiple cuts, and curved surface turning) still has to be fully assessed. In this dissertation, finite element method (FEM) was employed to simulate and analysis the residual stress induced by the metal cutting process aiming to contribute to further understanding of the machining-induced residual stress.

The dissertation covers four aspects of research, which are included in the published papers. Paper I focused on the analysis and prediction of the cyclic residual stress distribution in machined workpiece when a segmented chip is formed. With a fine enough mesh, formation of the single-chip segment is investigated in-depth to explain such residual stress distribution. It is shown that the feed force increase firstly and then decrease during one segment genesis. It is the increased feed force that cause an increase in the local normal/tangential stress acting on the machined surface, leading to a less tensile residual stress in the lower stress zone.

Paper II, III and VI address the effect of tool geometry on residual stresses induced in an orthogonal cutting process. The thermal and mechanical contribution to the formation of residual stress was distinguished in the study. The local normal/tangential stress is used to determine the degree of the tensile plastic deformation induced by the tool, providing a reasonable explanation for the variation of subsurface compressive residual stress with the changing of tool geometry.

Paper IV reveals the influences of multiple cuts and correspondent cutting parameters and tool geometry on residual stresses evolution. For the first time, material loading cycles are developed in multiple cutting operations based on the quantified stress/strain that is obtained numerically. The results indicate that the existence of previous cut tends to generate more compressive residual stress in the finished workpiece, and this effect is more evident when the previous cut is implemented at the cutting conditions producing a larger compressive stress/tensile strain in the subsurface.

Paper V simulates the residual stress evolution when turning a fillet surface. The variation of the size and shape of uncut chip cross-section in outer/end surfaces turning was analyzed. It is shown that the residual stress becomes more compressive when the tool position changes from outer face to end face, although the difference is not significant.

All four aspects of research present new and novel contributions to the field of metal cutting simulations and numerical analysis. The key physical quantities (i.e., stresses, plastic strains, shear angle, material degradations, forces, and temperatures) generated in the cutting processes are thoroughly evaluated and analyzed to significantly increase the interpretation and understanding of residual stresses formation under different aspects.

Key words: Residual stress, FEM, Inconel 718, Metal cutting, Thermal-mechanical load, Plastic deformation

Classification system and/or index terms (if any)

Supplementary bibliographical information	**Language:** English
ISSN and key title	**ISBN** 978-91-8039-077-4 (print) **ISBN** 978-91-8039-078-1 (pdf)
Recipient's notes	**Number of pages** 101 / Price
	Security classification

I, the undersigned, being the copyright owner of the abstract of the above-mentioned dissertation, hereby grant to all reference sources permission to publish and disseminate the abstract of the above-mentioned dissertation.

Signature Yang Liu Date 2021-11-08

Numerical investigation on the formation mechanism of residual stress in metal cutting

Yang Liu

LUND
UNIVERSITY

Copyright © Yang Liu and Division of Production and Materials Engineering

Faculty of Engineering, Department of Mechanical Engineering Sciences
Division of Production and Materials Engineering
Lund university, Box 118, SE 221 00 Lund, Sweden

ISBN: 978-91-8039-077-4 (print)
ISBN: 978-91-8039-078-1 (pdf)
ISRN: LUTMDN/(TMMV-1072)/1-101/(2021)

Printed in Sweden by Media-Tryck, Lund University
Lund 2021

Media-Tryck is a Nordic Swan Ecolabel certified provider of printed material. Read more about our environmental work at www.mediatryck.lu.se
MADE IN SWEDEN

Abstract

Residual stress can be introduced unintentionally into the workpiece with various magnitudes and distributions through all manufacturing processes. These stresses have a significant effect upon the performance of the final component. Understanding the residual stress imparted by machining is an essential aspect of understanding the machining process and overall part quality. Although many investigations have been conducted over the past few decades in measurement, modelling and mechanisms of residual stresses induced by the different manufacturing processes, the insights of residual stresses induced during the machining are still far from being completely understood. Several crucial issues still have to be investigated. In particular, the residual stress generation under different circumstances (segmented chip, the variation of tool geometries, multiple cuts, and curved surface turning) still has to be fully assessed. In this dissertation, finite element method (FEM) was employed to simulate and analysis the residual stress induced by the metal cutting process aiming to contribute to further understanding of the machining-induced residual stress.

The dissertation covers four aspects of research, which are included in the published papers. Paper I focused on the analysis and prediction of the cyclic residual stress distribution in machined workpiece when a segmented chip is formed. With a fine enough mesh, formation of the single-chip segment is investigated in-depth to explain such residual stress distribution. It is shown that the feed force increase firstly and then decrease during one segment genesis. It is the increased feed force that cause an increase in the local normal/tangential stress acting on the machined surface, leading to a less tensile residual stress in the lower stress zone.

Paper II, III and VI address the effect of tool geometry on residual stresses induced in an orthogonal cutting process. The thermal and mechanical contribution to the formation of residual stress was distinguished in the studies. The local normal/tangential stress is used to determine the degree of the tensile plastic deformation induced by the tool, providing a reasonable explanation for the variation of subsurface compressive residual stress with the changing of tool geometry.

Paper IV reveals the influences of multiple cuts and correspondent cutting parameters and tool geometry on residual stresses evolution. For the first time, material loading cycles are developed in multiple cutting operations based on the quantified stress/strain that is obtained numerically. The results indicate that the existence of previous cut tends to generate more compressive residual stress in the finished workpiece, and this effect is more evident when the previous cut is implemented at the cutting conditions producing a larger compressive stress/tensile strain in the subsurface.

Paper V simulates the residual stress evolution when turning a fillet surface. The variation of the size and shape of uncut chip cross-section in outer/end surfaces turning was analyzed. It is shown that the residual stress becomes more compressive when the tool position changes from outer face to end face, although the difference is not significant.

All four aspects of research present new and novel contributions to the field of metal cutting simulations and numerical analysis. The key physical quantities (i.e., stresses, plastic strains, shear angle, material degradations, forces, and temperatures) generated in the cutting processes are thoroughly evaluated and analyzed to significantly increase the interpretation and understanding of residual stresses formation under different aspects.

Keywords:

Residual stress, FEM, Inconel 718, Metal cutting, Thermal-mechanical load, Plastic deformation

Popular science summary

Machining processes are the techniques using various kinds of tool to remove excess material to shape the workpiece into the desired geometries, dimensions, and surface conditions. It is common that some stresses will be preserved within the finished parts after the machining processes, which is called residual stress. The machining-induced residual stresses have attracted wide attention for the last decades because they were closely related to the quality and performance of the machined components. Residual stresses can be induced with various magnitudes and distributions by any machining operation. The final residual stress depends on the material of the components, and the employed cutting conditions: cutting speed, cutting feed, depth of cut, tool geometries, tool wear, lubrication, etc., and pre-existing stresses in the parts. Therefore, the investigation of the effect of different cutting parameters on residual stress and the underlying mechanism of residual stress formation is very important to optimize the machining process and improve the work performance of the machined products.

There are three commonly used methods for residual stresses investigation: experimental measurement, analytical modeling, and finite element simulation. Generally, cutting processes operate at severe deformation conditions, involving very high strain, strain rate, stress, and temperature. These extreme conditions increases the difficulty in the measurement of the cutting temperatures, stress, plastic strains, shear angle, etc., which are critical parameters to understand the mechanism of residual stresses. The analytical method has been developed is a good alternative to achieve a better understanding about the phenomena occurring during the cutting processes. The drawback of the analytical models is the lack of accuracy of the results due to the significant simplification of the process. Moreover, some essential aspects, such as the multiple cuts and the pre-stress conditions due to prior manufacturing processes, are difficult to investigate with analytical models. With the continuous development of finite element techniques, the model of machining processes has attracted plenty of attention by many researchers over the last decades. This method not only realize the visualization of the cutting process, but also incorporate the complexity of the actual cutting process.

In this dissertation, orthogonal cutting and fillet surface turning models are established to predict the residual stress induced by metal cutting process under different cutting parameters. With the validated models, this dissertation is further aimed to visualize the cutting process and formation of residual stresses. Therefore, some process variables (i.e., stresses, strains, forces, and temperatures) which are not measurable or difficult to measure experimentally can be obtained to explore the underlying mechanisms of residual stress formation. With a deeper understanding of the influence from each process parameter in detail, an optimization of the machining conditions is possible in the practical machining process.

Acknowledgement

This work was carried out between October 2017 and December 2021 at the Division of Production and Materials Engineering, Lund University. The candidate was financially supported by the China Scholarship Council (CSC). The computational resources were provided by the Swedish National Infrastructure for Computing (SNIC) at LUNARC, Lund University.

This work would have been impossible without the support of many people. I would like to thank my main supervisor, Prof. Jinming Zhou, for his continuing guidance, support and advice throughout my work. I thank him for providing me the opportunity to perform my doctoral study at the Department of Mechanical Engineering Sciences at Lund University. He inspired me to think over scientific questions as a researcher and I got benefit from his serious attitude towards work. I would also like to thank Dr. Mathias Agmell for his support in the early phase of my research work. Special thanks goes to Dr. Rachid M'Saoubi for the valuable discussion with him and crucial support in the arrangement of my experiment work at Seco tools. My gratitude also goes to Prof. Aylin Ahadi for her valuable advice, productive discussions and encouragement. It is my honor to be supervised by them.

I would like to thank all the staff members in the Department of Mechanical Engineering Sciences. In particular, I would like to thank Dr. Andrii Hrechuk for his assistance in measuring chips and machined surface, and Dr. Jian Weng for the great help with experiment and all the interesting discussions. I would like to thank Johan Persson for helping me solve all the problems I ran into with the computer when doing the simulations. I also want to thank the collaborator Dr. Dongdong Xu, who put a lot of effort into the RS measurement and gave me valuable feedback to improve the quality of papers. Further, I would like to thank Mr. Per Alm from Seco tools for his technical support in the preparation of the cutting experiment, also Seco tools for providing experiment equipment, materials and tools in this study.

I would like to thank all my Chinese friends: Shijie Xu, Yuanyuan Cao, Senbin Yu, Miao Zhang, Miao Yang, Huaduo Gu, Shenghui Zhong, Yan Zhang, Yaopeng Li, Xiufei Li, Yuanxin Qi, Tian Wang, and others. All the beautiful moments I spent with you enriched my life during the past four years.

I would like to express my deepest gratitude to my family members. Thank my kind parents and my sisters for their support and encouragement. Special thanks to my mother and father, they encouraged me to move forward and face difficulties and challenges bravely. To my mother and my mother-in-law, thanks for all the sacrifice you made to take care of my daughter. Thanks also go to my father-in-law for his support. I am deeply grateful to my daughter, Xinrui Xu, who is an angel to help me get through the toughest period in my life. She accompanies me, loves me, admires me, gives me smiles and hope. All her love, kindness, and need for me make me stronger and more determined. Last, I would like to thank the best person in the

world, Leilei Xu, my husband, and great father to our child. He is the most charming man I have ever met: kind, clever, witty, and diligent. Thanks for all the help you provide me both in work and life. Your considerate companionship has lighted and warmed this long and challenging journey.

List of publications

Publications included in this dissertation:

I: **Yang Liu**, Mathias Agmell, Dongdong Xu, Aylin Ahadi, Jan-Eric Stahl, Jinming Zhou
Numerical contribution to segmented chip effect on residual stress distribution in orthogonal cutting of Inconel718.
The International Journal of Advanced Manufacturing Technology, 2020, 109(3), 993-1005.

II: **Yang Liu**, Dongdong Xu, Mathias Agmell, Rachid M' Saoubi, Aylin Ahadi, Jan Eric Stahl, Jinming Zhou
Numerical and experimental investigation of tool geometry effect on residual stresses in orthogonal machining of Inconel 718.
Simulation Modelling Practice and Theory, 2021, 106: 102187.

III: **Yang Liu**, Andrii Hrechuk, Mathias Agmell, Aylin Ahadi, Jan-Eric Stahl, Jinming Zhou
FE analysis on the association between tool edge radius and thermal-mechanical load in machining Inconel 718.
Procedia CIRP, 2021, 102: 91-96.

IV: **Yang Liu**, Dongdong Xu, Mathias Agmell, Aylin Ahadi, Jan-Eric Stahl, Jinming Zhou
Investigation on residual stress evolution in nickel-based alloy affected by multiple cutting operations.
Journal of Manufacturing Processes, 2021, 68: 818-833.

V: **Yang Liu**, Jian Weng, Rachid M' Saoubi, Aylin Ahadi, Jinming Zhou
Analysis of residual stress in fillet surface when turning stainless steel.
Submitted to Journal of Materials and Manufacturing Processes

VI: Dongdong Xu, **Yang Liu**, Jinming Zhou, Rachid M'Saoubi
Experimental and numerical investigation of Inconel 718 machining with worn tools.
Submitted to Journal of Manufacturing Processing, under review.

Publications not included in this dissertation:

VII: Jian Weng, **Yang Liu**, Kejia Zhuang, Dongdong Xu, Rachid M'Saoubi, Andrii Hrechuk, Jinming Zhou
An analytical method for continuously predicting mechanics and residual stress in fillet surface turning.
Journal of Manufacturing Processes, 2021, 68: 1860-1879.

VIII: Dongdong Xu, Liang Ding, **Yang Liu**, Jinming Zhou, Zhirong Liao
Investigation of the influence of tool rake angles on machining of Inconel 718.
Journal of Manufacturing and Materials Processing, 2021, 5(3): 100.

Author's contributions in each papers

I: Yang performed conceptualization, simulation, data analysis and original draft writing work.

II: Yang performed conceptualization, simulation, analysis and original draft writing work.

III: Yang performed conceptualization, simulation, analysis and original draft writing work.

IV: Yang performed conceptualization, simulation, analysis and original draft writing work.

V: Yang performed simulation, data analysis and original draft writing work.

VI: Yang contributed to simulation work and wrote the sections on numerical modelling and analysis.

List of symbols and abbreviation

A	Initial yield stress
B	Hardening modulus
C	Strain rate dependency coefficient
D	Stiffness degradation
$D_{i(i=1\sim5)}$	Constants in the Johnson-Cook damage model
d_1	Depth of cut in outer face turning
d_2	Depth of cut in end face turning
E	Young's modulus of workpiece material
F_c	Cutting force in cutting speed direction
F_f	Cutting force in feed direction
F_r	Cutting force in radial direction
F_t	Cutting force in tangential direction
f	Feed rate
G_f	Hillerborg's fracture energy
h_1	Uncut chip thickness
h_c	Mechanical induced compressive area depth
h_t	Mechanical induced stretched area depth
$h(P)$	Heat conduction coefficient
K_c	Fracture toughness
K_r	Major cutting edge angle
L	Characteristic length associated with an integration point
m	Thermal softening coefficient
n	Strain-hardening exponent
PEEQ	Equivalent plastic strain
$\dot{Q}_p$	Heat generation due to plastic work
$\dot{Q}_f$	Heat generation due to friction
η_p	The fraction of the plastic deformation energy converted to heat
η_f	The fraction of the frictional energy converted to heat
q	Heat flux per unit of area
R	Curved surface radius
r_β	Tool edge radius
r	Tool nose radius
S	Stagnation point
T_{melt}	Melt temperature of workpiece material
T_{room}	Room temperature
V_c	Cutting speed
V_s	Sliding velocity
VB_s	Flank wear
$\bar{u}$	Equivalent plastic displacement
$\overline{u_f}$	Equivalent plastic displacement at failure
$\bar{\varepsilon}$	Equivalent plastic strain
$\dot{\bar{\varepsilon}}$	Equivalent plastic strain rate
$\dot{\bar{\varepsilon}}_0$	Reference strain rate
$\Delta\bar{\varepsilon}$	Increment of equivalent plastic strain
$\bar{\varepsilon}_0$	Plastic strain at damage initiation
$\bar{\varepsilon}_f$	Equivalent plastic strain at failure
$\bar{\sigma}$	Equivalent flow stress
$\tilde{\sigma}$	Flow stress during damage evolution

σ	Flow stress followed by damage evolution
σ_n	Normal stress along tool-workpiece interface
σ_{SF}	Normal contact stress on the flank/workpiece interface
p	Hydrostatic stress
ω	Scalar damage parameter
v	Poisson's ratio of workpiece material
γ	Rake angle
γ_n	Normal rake angle
ε_r	Tool included angle
μ	Friction coefficient
τ_f	Frictional stress along tool-workpiece interface
τ_y	Yield shear stress of the workpiece material
τ_{SF}	Tangential contact stress on the flank/workpiece interface
λ_s	Tool cutting edge inclination angle

Table of Contents

1 Introduction

This chapter provides an introduction to the research performed, including the background, hypothesis, research questions, objective, methodology, dissertation scope and limitations, and the dissertation outline.

1.1 Background

The rapid development of the manufacturing industry has increased the demands in quality and performance of components, especially for those applied in safety-critical areas, such as components used in aerospace and energy areas, in which the surface integrity achieved by final machining process plays the vital role. As one of the most important surface integrity, the residual stress has a significant effect on the final products in terms of static strength, fatigue strength, creep life and resistance to stress corrosion cracking [1]. It is recognized that tensile residual stresses are detrimental to the service life of components since they cause stress corrosion cracking and fatigue damage, while compressive residual stresses can increase the lifetime of the component because they can inhibit crack nucleation [2]. The residual stress in machined components usually reaches the depth of 300 μm from the surface and is determined by complex interactions among a large number of different parameters such as material properties, the employed cutting conditions (cutting speed, cutting feed, depth of cut, tool geometries, tool wear, lubrication, etc.) and pre-existing stresses in the workpiece. Nevertheless, there is some lack of agreement in the literatures with regards to the specific trend of residual stress with each cutting parameters and tool geometry, and the underlying mechanism of residual stress formation are not fully understood yet. Insights into this topic are essential for industrial manufacture, which can suggest possible directions to optimize the cutting conditions to obtain the desired residual stress state and thus to enhance the lifetime and functional performance of the machined components.

The understanding of basic mechanisms of residual stress generation in the metal cutting process is difficult due to the complex mechanics of deformation taking place during the process. In a typical machining process, the workpiece material in the vicinity of the cutting edge is subjected to extreme conditions with strain rates in the order of 10^5 s^{-1} while the temperature in the shear zones can exceed 1200 °C [3]. Due to these extreme conditions, it is difficult to measure the interesting aspects

during the process with experiment method, such as cutting temperatures at newly machined surface, stress, plastic strains, and shear angle, etc., which are critical parameters to understand the mechanism of residual stresses induced during machining of the component. Furthermore, current experimental techniques of the residual stress profiles measurement are not only sensitive to measurement uncertainties [4], but the most accurate techniques also tend to be expensive and time-consuming. To address the issues, analytical modelling and finite element simulation were proposed aiming to provide more information during the cutting process. The analytical method is a good method to investigate residual stress in the metal cutting process since it achieves a rapid residual stress prediction and allows a deeper understanding of the influence of each parameter in detail, thus enabling the optimization of the entire process as well. Nevertheless, due to the inherent complexity of the cutting process itself, a significant simplification of the process is required when establishing an analytical model, thus reducing the accuracy of the results. Moreover, some essential aspects, such as the sequential cuts and the pre-stress conditions due to prior manufacturing processes, are difficult to investigate with analytical models [5]. These aspects can, however, be taken into account by the finite element models. Therefore, although this type of method is more time-consuming than the analytical model, it can not only incorporate the complexity of the actual cutting process, but also capture the process phenomena such as forces, cutting temperature, chip morphology, tool stress distributions, and machined surface integrity characteristics (residual stresses, plastic deformation, white layer thickness [6]) as comprehensively as possible. Furthermore, the development of the sub-models in FE simulation makes it possible to capture complex phenomena, such as phase transformations [7], dynamic recrystallization [8], etc., that influence the surface integrity. There has been significant progress in finite element modelling of residual stress generated in machining processes over the past few decades [9].

Despite all these efforts, the mechanism of residual stress generation is still far from being completely understood, and several crucial issues still have to be investigated. Mabrouki et al. [10] proposed a numerical methodology concerning to study the orthogonal cutting of an aeronautic aluminum alloy (A2024-T351). The simulation result shows that the chip serration may cause wavy stress distribution on the machined surface and rippled geometry of machined surface. Unfortunately, the relationship between the segmented chip and residual stress distribution was still unclear. There is a need for exploring the effect of chip morphology on the residual stress distributions. Also, it is known that the final residual stress distributions are significantly influenced by the utilized cutting tool geometry (i.e. rake angle, edge radius). Although many researchers have studied the impact of tool geometries on residual stresses generated in machining, different trends and explanations have been reported in the study [11]. For example, it was reported [12] that surface tensile stress decreased and the magnitude and depth of subsurface compressive residual stress increased when using a more negative rake angle in turning hardened steel. However, the surface tensile residual was found increase with the same variation of

tool rake angle in the investigation of Outeiro et al. [13] and M'Saoubi et al. [14]. Therefore, a detailed knowledge of the mechanisms involved in the generation of residual stresses for different tool geometries is highly desirable. It is common that in the practical machining a final component is produced by multiple cuts other than a single cut. Naturally, the strain/stress and temperature that are produced by the previous cuts will be brought to the final operation, which eventually affects the final residual stress distribution. However, a few studies were made on the effects of multiple cuts on residual stress and residual stress evolution during multiple cuts is still not well understood. Furthermore, most of the studies focus on the machining process with straight tool path, such as longitudinal and end face turning process, and the prediction of the fillet surface turning was seldom reported, and thus the evolution of the thermal-mechanical load and residual stress during the fillet surface turning need to be further studied.

These above aspects all represent a vital shortcoming of current cutting models. The overall objective of this dissertation is therefore separated into the four mentioned parts, aiming to provide useful insights for comprehensive understanding the residual stress formation so that the machining parameters can be optimally selected to enhance fatigue life of machined components by inducing favorable residual stresses.

1.2 Hypothesis

The following hypothesis were established for this research project:

- It is possible to explore the effect of segmented chip on the residual stress evolution using the FE simulation.
- It is possible to distinguish the thermal and mechanical effect on the formation of residual stress during cutting process through FE method and provide a unified explanation for the formation mechanism of residual stress when using various tool geometries.
- Accumulated cutting effect on residual stresses can be simulated through FE simulation.
- Through simplification, it is possible to predict the residual stresses in the fillet surface by using FE method.

1.3 Research questions

Based on the hypothesis, the research questions of this dissertation were formulated accordingly as follows:

RQ1: Can FE simulation be a practical and efficient means to reveal the formation mechanism of residual stress induced by metal cutting process under various cutting conditions?

RQ2: Is it possible to simulate and visualize the evolution of residual stress in multiple cuts and curved surface turning by FE model?

1.4 Objective

The overall objective of this dissertation is to establish FE models to predict the residual stress induced by metal cutting process under some important and easily overlooked circumstances (segmented chip, tool geometries, multiple cuts, fillet surface turning). With the validated models, the dissertation further aims to visualize the cutting process and formation of residual stresses. Therefore, some process variables (such as stresses, strains, shear angle, material degradations, cutting forces, and temperatures), which are non-measurable or difficult to measure through experiment, can be evaluated in order to explore the underlying mechanisms of residual stress formation. With a deeper understanding of the influence of each cutting parameters and tool geometry in detail, an optimization of the machining conditions is possible in the practical machining process. Specifically, more detail objectives are presented as followings:

- Study the effect of the segmented chip on the residual stress evolution through the analysis of thermal and mechanical loadings acting on the machined surface.
- Analyze the effect of tool geometries on residual stress formation and explore a unified explanation for the generation mechanism of residual stress through dividing the mechanical or thermal influence separately.
- Investigate the effect of the cutting parameters and tool geometries utilized in the previous cuts on the residual stresses evolution in the subsequent cuts.
- Investigate the evolution of the residual stress distribution during fillet surface turning.

1.5 Methodology

The research methods depend on the purpose of study. In this dissertation, the research methods address the research questions with strong emphases on numerical simulation and analysis. Models for orthogonal cutting and fillet surface turning were established using the finite element method based on Coupled Eulerian-Lagrangian (CEL) technique. The corresponding cutting tests were conducted to validate the proposed numerical models in terms of temperature distribution, cutting

forces, chip morphology, and residual stress distribution. The validated models were therefore employed to simulate the cutting processes under the aforementioned circumstances. Fig. 1.1 schematically illustrates the implemented research approach in this dissertation.

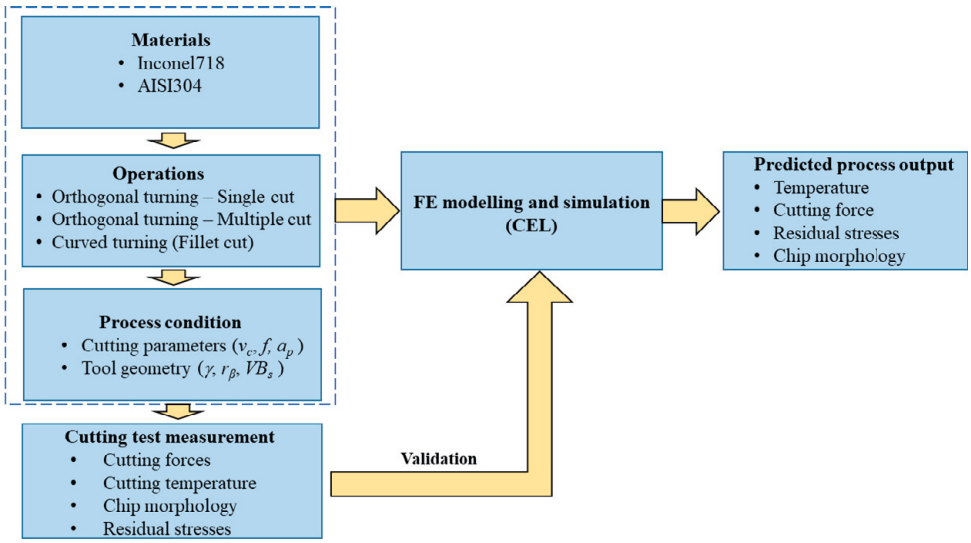

Figure 1.1.
Schematic of the implemented research approach.

1.6 Scope of the work and limitations

There are many different areas and variables in the machining investigation, including workpiece material, tool wear and geometries, and cutting parameters. Only selected machining cases were studied and validated in this dissertation. The following limitations were employed during this study:

- This research is limited to the machining of workpiece material of Inconel 718 and AISI 304 stainless steel with the tool material of cemented carbide.
- The finite element method was employed to simulate the cutting process, in which the Johnson-Cook material model is employed to describe the plastic behaviour of the material. As an isotropic hardening plasticity model, the Johnson-Cook model doesn't introduce the Bauschinger effect occurring in cyclic deformation of the workpiece material.
- The workpiece materials in simulation investigation are considered as pure homogenous materials absence of grain structure or phase content.
- The simulation work has been limited to being accomplished in Abaqus/Explicit using Coupled Eulerian-Lagrangian (CEL) technique.

1.7 Outline of the dissertation

This dissertation is organized as follows:

Chapter 1: Introduction
This chapter introduces the research topic and presents the research questions and the limitations of this research.

Chapter 2: Review of study on residual stresses and simulation in metal cutting
This chapter presents fundamental aspects of residual stresses and review of study on residual stresses induced in the metal cutting process. Experimental techniques for the residual stress measurement and the most commonly used numerical methods for simulation of the metal cutting process are also summarized in this chapter. In addition, the literature review mainly focused on the residual stress stresses investigation in orthogonal cutting and fillet surface turning.

Chapter 3: Numerical modelling
This chapter introduces all the details of the CEL model used for this work, including the geometry, mesh, and boundary conditions, material modelling, friction modelling and thermal modelling.

Chapter 4: Experimental setup
This chapter focuses on the presentation of the experimental work used in the validation of the predicted results. Details of the workpiece, tools as well as experimental procedures are presented.

Chapter 5: Results and discussion
This chapter presents the results of the current work. A detailed discussion about the influences of the segmented chip (Paper I), various tool geometries (Paper II, III and VI), multiple cuts (Paper IV), and the fillet surface turning (Paper V) on the residual stress evolution are presented.

Chapter 6: Conclusions and future work
This chapter ends up with the main conclusions drawn from this study and future outlook.

2 Review of study on residual stresses and simulation in metal cutting

This chapter presents fundamental aspects of residual stresses and review of study on residual stresses induced in metal cutting process. Experimental techniques for the residual stress measurement and the most commonly used numerical methods for simulation of the metal cutting process are also summarized in this chapter. In addition, the literature review mainly focused on the residual stress stresses investigation in orthogonal cutting and fillet surface turning.

2.1 Fundamentals of metal cutting process

Cutting parameters and tool geometry. Metal cutting is the process of shaping the workpiece into the desired geometries, dimensions, and surface conditions by removing a layer of unwanted material in the form of a chip. Common cutting processes include turning, milling, drilling, boring, shaping, broaching, reaming and others. This dissertation will focus on the turning process especially the orthogonal cutting process since most of the cutting phenomenon that occurred in the cutting process could be simplified to orthogonal cutting.

Three cutting parameters, i.e. cutting speed (v_c), feed rate (f), and depth of cut (a_p), need to be determined in a turning operation (Fig. 2.1a). Cutting speed is defined as the relative velocity between the workpiece and cutting tool. Feed rate is defined as the axial distance of the tool in one revolution of the workpiece. The cutting depth is the thickness of material that is required to remove by machining. Fig. 2.1b shows the cutting tool geometry parameters used in orthogonal cutting, including rake angle, edge radius, flank wear, and clearance angle.

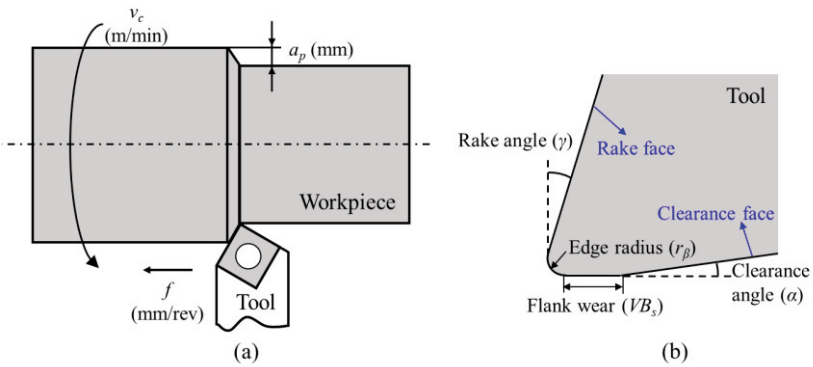

Figure 2.1.
Cutting parameters and tool geometry: (a) Cutting parameters for a turning operation; (b) cutting tool geometry parameters in two dimensions.

Cutting forces. The magnitude of cutting forces is mainly determined by the chip area, i.e. the depth of cut and the feed rate. The properties of the workpiece material also have a significant influence on the cutting forces. Some other factors, such as cutting speed and tool geometries also influence the cutting forces. The resultant force in a longitudinal turning process can be divided into three force components, as shown in Fig. 2.2. The cutting force acting on the rake face of the tool and in the cutting speed direction is called the main cutting force F_c. This is often the largest force component. The force component acting in the axial direction is referred to as feed force F_f. this is usually the second-largest force component. The force component acting in the radial direction is called the passive force F_p.

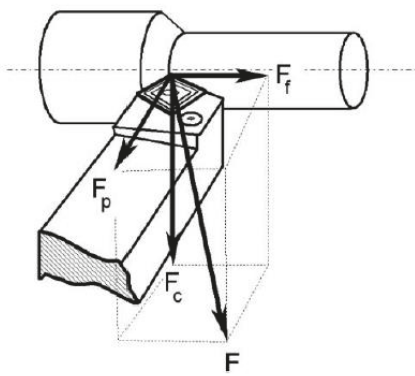

Figure 2.2.
Cutting force components that contribute to the resultant cutting force (*F*) during a conventional turning operation [15].

Deformation zones and heat generation. In a cutting process, the major part of the energy provided is converted to heat through plastic deformation of the workpiece material and friction work in the workpiece-tool interface. The material deformation region in machining can be divided into three deformation zones as shown in Fig. 2.3. In the primary deformation zone (ε_I), the material is sheared from the workpiece and is taken away in the form of chips. The primary deformation zone extends from the tip of the cutting tool to the intersection between the surface of the undeformed workpiece and the deformed chip. In this region, the heat is generated due to the plastic deformation and the rapidly increased temperature causes softening of the material and allows the greater deformation. This region consumes about 70% of the total energy applied.

The secondary deformation zone (ε_{II}) happens near the interface between the tool rake face and chip accompanied by further squeezing and friction of the material. The heat generated by the secondary deformation zone is due to the plastic deformation of the chip and the friction between the tool rake face and the chip. The tertiary deformation zone (ε_{III}) is formed in the newly machined surface under the stretching stress of the clearance face of the tool. The heat generated in this region is due to plastic deformation of the new surface and frictional work between the clearance face and the newly machined surface.

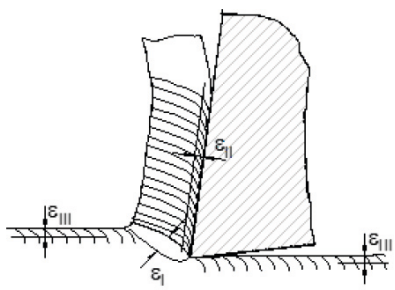

Figure 2.3.
Illustration of the deformation zones: ε_I, ε_{II}, ε_{III} [15].

Stagnation zone. As mentioned previously, during the cutting process the workpiece material in front of the tool tip is either pushed upward by the rake face to form a chip or ploughed under the cutting edge and finally become the machined surface. The point where the material flow separates to form the chip and machined surface is the stagnation point, marked as S in Fig. 2.4a. For this reason, the friction force applied on the tool edge opposes each other on opposite sides of point S. Therefore, the location of the stagnation point S can be determined by the distribution of tangential force acting on the cutting tool, and the friction force shows a value of null around this point. The chip leaves the tool rake face at point A. The newly machined surface leaves the tool at point B. The line DS is the actual

material separation line during the cutting process. The thickness of material that is ploughed into the newly machined surface is called ploughed depth. It has been recognized that material stagnation induced by the cutting edge has a significant influence on the cutting process and the resultant surface integrity. The material ploughed underneath the tool experiences will be stretched by the clearance/flank face of the tool, experiencing severe plastic deformation and elevated temperature and forming the top layer of the machined surface. The deformation state and temperatures of this layer have a critical influence on the final surface integrity. FEM is a visible and effective method to illustrate the stagnation zone in detail. As shown in Fig. 2.4b, the ploughed depth is larger with a larger edge radius.

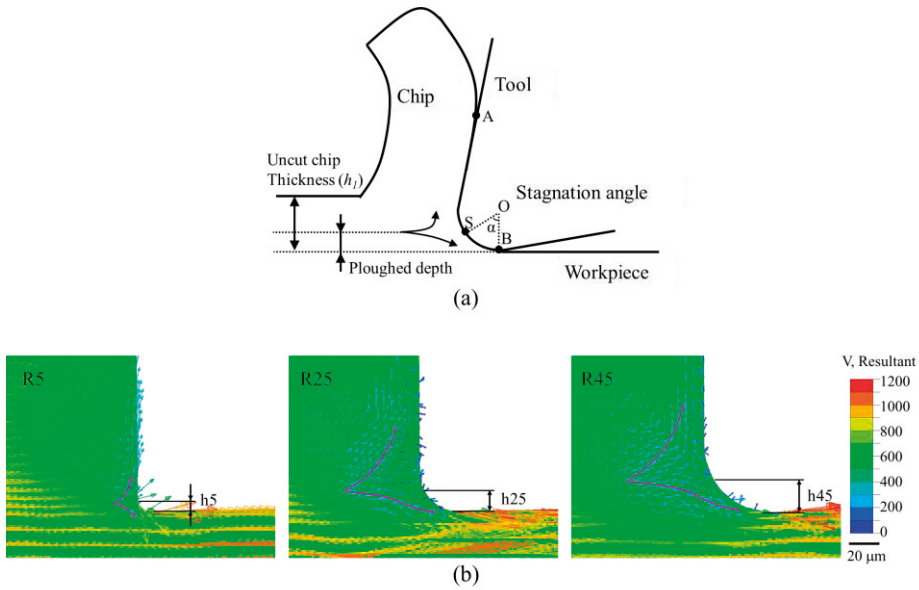

Figure 2.4.
Illustration of stagnation zone: (a) stagnation point, and (b) effect of edge radius on ploughed depth.

2.2 Surface integrity

Surface integrity is the conditions of the surface and subsurface produced by the manufacturing processes. Surface integrity can have a significant impact on the performance (fatigue strength, fracture strength, corrosion rate, tribological behaviour, dimensional accuracy, etc.) of a component during use, particularly for demanding applications in the aerospace, automotive and bearing industries. Surface quality is closely related to the cutting parameters, tool geometries, tool wear, cooling and lubrication conditions during machining. The typical surface

integrity characteristics include surface topography (surface defects and surface roughness), microstructural alterations (plastic deformation, grain refinement and texture, and white layer), and mechanical properties (microhardness and residual stress) [16], as shown in Fig. 2.5. Among these, residual stress is one of the most concerns since it has a significant effect on the final products in terms of static strength, fatigue strength, creep life and resistance to stress corrosion cracking [1]. It is recognized that tensile residual stresses are detrimental to the service life of components since they cause stress corrosion cracking and fatigue damage, while compressive residual stresses can increase the lifetime of the component because they can inhibit crack nucleation [2].

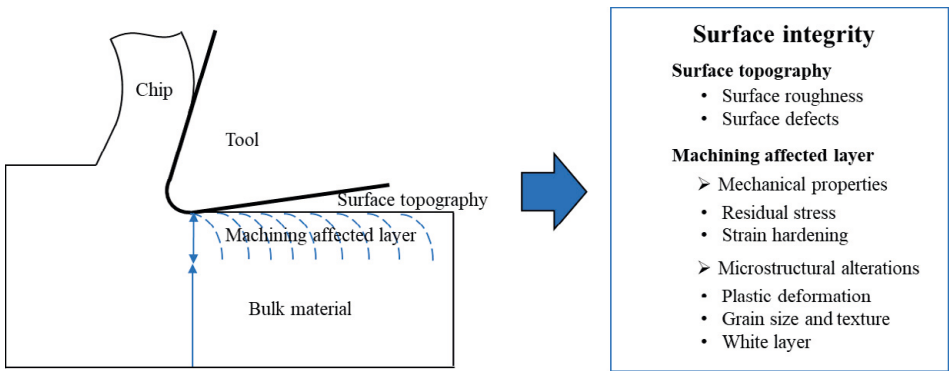

Figure 2.5.
Schematic of machined surface integrity characteristics.

2.3 The definition and classification of residual stress

Residual stresses are inherent stress keeping in equilibrium state within components in the absence of external forces or moments, thermal gradients and phase transition [17]. Residual stress can be classified as macro or micro stresses according to the length scale over which they are nearly constant in magnitude and direction. There are three different types of residual stresses which are defined as follows:

- Type I: The macro residual stresses that equilibrate over the bulk of the material. Such stresses can be estimated using continuum models which ignore the polycrystalline or multiphase nature of the material, often predicted using the finite element method. This is the type of residual stress which is investigated in this dissertation.
- Type II: The micro residual stresses that are equilibrated between grains. The variations of this type of residual stress may result from different phases in the material.

- Type III: The sub-micro residual stresses that exist over atomic dimensions and balance within a grain, arising from the line defects (dislocations) and point defects (vacancy and interstitial) of the solid body.

2.4 Residual stresses induced in metal cutting

Residual stresses can be presented in the unprocessed raw material, unintentionally introduced into the workpiece with various magnitudes and distributions through all manufacturing processes such as machining, joining, forming, casting, heat-treating and coating or can be generated during service life under complicated conditions (mechanical, thermal and chemical) [17]. In essence, the origins of residual stresses generated within a part can be classified as three mechanisms: non-uniform mechanical deformation, non-uniform temperature gradients and volume change induced by phase transformations. There exists more than one mechanism simultaneously and the final residual stresses field are the superposition of the residual stress induced by each mechanism. In the cutting process, transformations occur in the superficial material if the temperature is higher than phase transition temperature, thus residual stress is induced by the volume change of metallographic structure. Without considering phase transformations, this study will focus on the residual stresses generated by the first two factors. It was proven [18,19] that the residual stresses generated in the feed direction depends largely on that in the cutting direction and a similar trend of residual stresses was achieved in both directions. Thus, only the residual stresses in the cutting direction will be discussed in detail throughout the present work.

Mechanical-induced residual stress. During the cutting process, the workpiece material around and ahead of the tooltip is seriously compressed by the primary shear plane and tool edge, which generates compressive plastic deformation. After the cutting forces disappear, the elastically deformed region below will always try to restrain the above compressed region. Thus, tensile residual stress is generated in this plastically deformed region, while slight compressive residual stress comes into being in the below elastically deformed area to reach a balanced state. With the tool advancing, a portion of these materials will be ploughed into the newly machined surface and stretched by the part of the tool behind stagnation point S (Fig. 2.4a), generating tensile deformation. After the tool moves away, compressive residual stress will appear in the tensile deformed region under the action of the beneath elastic region, while slight tensile residual stress is generated in the elastically deformed region as a result. Therefore, if the absolute value of the tensile plastic deformation is larger than that of the compressive deformation previously produced in front of the tool tip, the machined workpiece will present compressive residual stress and vice versa.

Thermal-induced residual stress. Thermal-induced residual stress also contributes to the final residual stress distribution. In the metal cutting process, the heat is mainly generated from the plastic deformation in the mentioned three deformation zones and the friction work between tool and workpiece. Some of the heat energy is transferred into the machined surface and thus the temperature of the surface/near-surface layer will significantly increase and material in this region will expand rapidly. The expanded region is hindered by the bulk material below and thus, compressive thermal stress is generated in this area during the cutting process. It was reported [20] that the thermal stress along the cutting direction is found predominantly compressive. It is known that for the majority of materials, the yield strength decreases with increasing temperature. If the thermal stress exceeds the yield strength of the materials in the surface/near-surface layer, the compressive strain is generated in this region and after cooling down, the inner material imposes restrictions on the shrinkage of surface material. Thus, the thermal gradients will result in tensile residual stress in the surface/near-surface layer and slight compressive residual stress in the beneath elastically deformed layer.

Consequently, residual stress distribution in surface/near-surface layer is the superposition of the mechanical-induced residual stress and thermal-induced tensile residual stress. Regarding the residual stress distributed in the subsurface layer, it is purely influenced by the mechanical load since the thermal influence cannot penetrate so deep.

2.5 Effect of residual stress

Residual stress in the machined workpiece is an important evaluation criterion of surface integrity. It has a detrimental or favourable influence on the functional behaviour and the service life of a component concerning dimensional stability, static strength, fatigue strength and corrosion cracking [21]. When the workpiece is in service, the residual stress, which acts as a pre-stress state of the components, can add to, or subtract from the external loadings. The stress field acting on the material is the summation of the service stress and residual stress. The tensile residual stress will cause a local overload of the component while compressive residual stress can relieve some of the load locally. Therefore, tensile residual stresses are generally perceived as a potential risk to components since they can contribute to, and are often the main cause of fatigue failure and stress corrosion cracking, and leads to premature failure of the workpiece as a result. Schwach et al. [22] found that tensile residual stresses work closely with the white layer and they significantly reduced the rolling contact fatigue life of hard turned surfaces. The initiation of stress corrosion cracking has been found to be promoted by a larger residual stress induced by machining [23]. On the contrary, a number of studies have shown that

compressive residual stress, which can be introduced to the surface or interior of a component deliberately through such processes as shot-peening [24], autofrettage [25], or ball burnishing [26], are usually beneficial since they prevent origination and propagation of fatigue cracks, and increase wear and corrosion resistance [27]. Consequently, an in-depth study of the residual stress prediction, formation and prevention in different processing conditions and service environments is essential to avoid the occurrence of unexpected failure.

2.6 Measurement of residual stress

There are several experimental methods available for residual stresses measurement. They are categorized generally as mechanical methods (destructive or semi destructive) and non-destructive methods. The mechanical method is also called the stress-relaxing method. In this method, the change of the strain or displacement caused by removing stressed materials is measured, thus the values of the residual stresses present in the part before the metal was removed can be determined by analyzing the successive state of equilibrium [4]. Hole drilling method, deep hole drilling method, sectioning method, and contour method are the commonly used destructive and semi destructive techniques to measure residual stresses in components. The non-destructive residual stress measurement techniques are aimed to calculate the residual stress by determining the variation of the physical constants within crystalline materials in the stress field without destroying the component. These methods include diffraction-based methods (X-ray or neutron diffraction), synchrotron, magnetic and ultrasonic methods. Fig. 2.6 compares the penetration and resolution of each kind of measurement method.

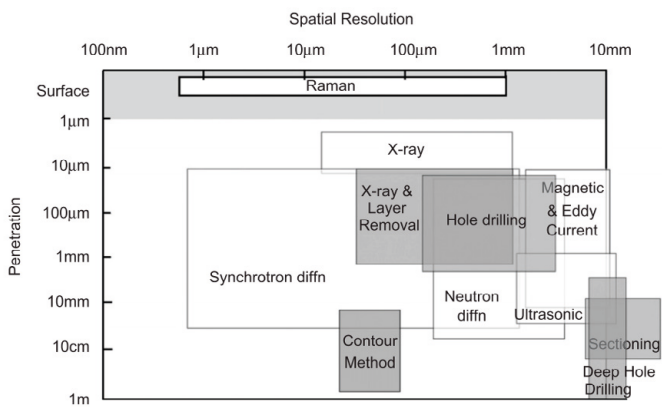

Figure 2.6.
The capabilities of the different techniques used to measure residual stress (the destructive techniques are shaded) [28].

X-ray diffraction method. X-ray diffraction method is one of the most commonly used non-destructive residual stress measurement techniques. The basic principle of this method relies on the measurement of inter-planar atomic spacing and elastic strains in surfaces when subjected to an applied or internal stress from which the residual stress can be determined [29]. Since the wavelength of an X-ray is similar to the distance between atoms in a crystal, a special interference effect called diffraction can be used to measure the distance between the atoms. When the atomic planes are exposed to an X-ray beam, X-rays are scattered by the regularly spaced atoms. The diffraction occurs where the scattered waves constructively interfere, as shown in Fig. 2.7a. Thus, the relationship between the lattice plane distance d and the diffraction angle 2θ can be described by Bragg's law, cf. Eq. 2.1:

$$n\lambda = 2d\sin\theta \qquad (2.1)$$

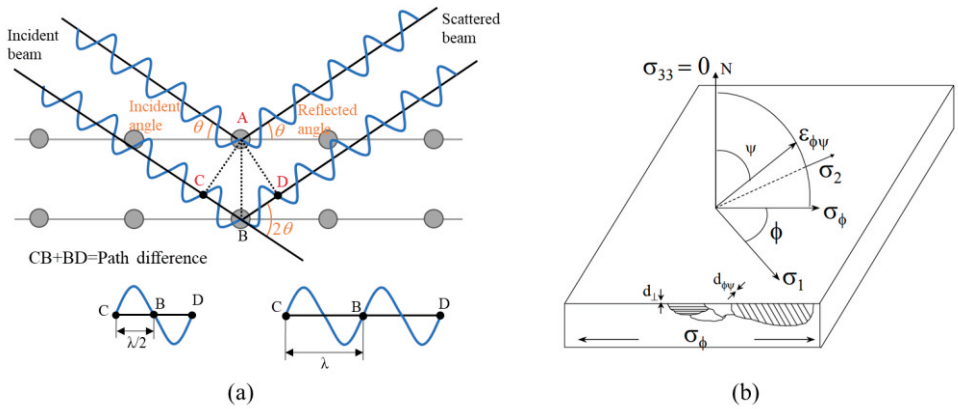

Figure 2.7.
(a) Diffraction of X-rays by a crystal lattice; (b) schematic showing diffraction planes parallel to the surface and at an angle $\phi\psi$. (σ_1 and σ_2 both lie in the plane of the specimen surface) [30].

When a metal is under stress, elongations and contractions are produced within the crystal lattice, which alters the inter-planar spacing of the lattice planes (d). Any change in the lattice spacing results in a corresponding shift in the diffraction angle (2θ). By precise measurement of this angle, the change in the inter-planar spacing can be evaluated and thus the strain within the material is deduced; from this quantity, the total stress on the metal can then be obtained according to simple elastic theory. The most commonly used method for stress calculation is the $\sin^2\psi$ method. In this method, a number of XRD measurements are made at different angle $\phi\psi$ (Fig. 2.7b) to obtain a number of inter-planar spacing d or 2θ, which is used to plot a straight line against $\sin^2\psi$. The stress σ_ϕ can then be calculated from such a plot by calculating the gradient of the line and with basic knowledge of the elastic properties of the material, as shown in Eq. 2.2:

$$\sigma_{\phi} = (\frac{E}{1+v})m \quad (2.2)$$

where m is the gradient of the d vs $\sin^2\psi$ line, E and v are the Young's modulus and poisson's ratio of the material.

X-ray method is regarded as the most accurate and efficient way to determine residual stress among the non-destructive methods, especially when the residual stress changes tremendously within a narrow range. One of the most severe limitations of X-ray method is that X-ray wavelengths have very small penetration depths of around 10-30 μm [31], thus only the residual stress in the superficial can be detected through this method. Therefore, it is usually combined with some form of layer-removal technique to establish a stress profile. In addition, limited space is available on most beam lines or X-ray diffractometers, which means the samples often need to be cut down in order to be measured.

Neutron diffraction. Similar to the X-ray method, the neutron diffractions method also relies on elastic deformations within a polycrystalline material that causes changes in the spacing of the lattice planes from their stress-free condition. Neutron diffraction has advantages over X-ray diffraction in performing the residual stress determination in terms of the measurement within the interior of components due to its nearly 1000 times deeper penetration into materials. The high spatial resolution of this method makes it capable of obtaining complete three-dimensional strain fields of the test components. The major disadvantage of this method is that the intense neutron beams are necessary in the experiment to obtain high resolution, which is available only at a medium or high-flux reactor or an accelerator-based neutron source [32]. This limits its use as the neutron sources of sufficient intensity is expensive and not as portable as the instruments for X-ray measurement.

The hole-drilling method. The hole-drilling method is one of the most widely used techniques to determine residual stress (Fig. 2.8). A small hole is drilled in the specimen in the area of interest and the electrical resistance strain gauges are glued around the hole to measure the resulting strains. The corresponding residual stress can then be calculated from these strains using formulae. This method has the advantages of relatively simple and cheap, standardized test procedures, and convenient practical implementation, and it applies to a wide range of materials and components. The damage caused to the specimen is localized to the small, drilled hole, and is often tolerable or repairable [33]. One of the limitations of hole drilling is that it is difficult to obtain accurately residual stress in a depth greater than half the hole diameter [34]. Therefore, it is mainly used for in-plane residual stress measurement. In addition, the technique suffers from limited strain sensitivity and resolution, and its accuracy is influenced by the dimensions of the hole (diameter, concentricity, profile, depth etc.), surface roughness, flatness, and specimen preparation [31].

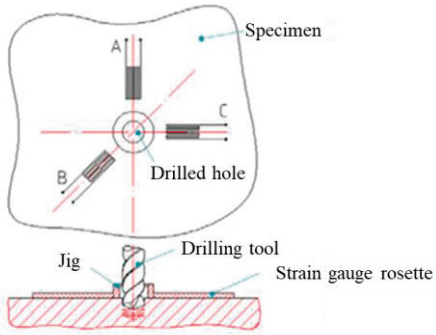

Figure 2.8.
Principle of the hole-drilling method [35].

Ultrasonics method. The ultrasonic method is one of the most promising methods for non-destructive techniques of residual stresses measurement. This technique is based on the effect of acoustic-elasticity – the dependency of the acoustic wave velocity on the magnitude and direction of applied stresses [36]. It can detect residual stress through the thickness of the samples and is not limited by the types of materials. The main difficulty with such a method is that the relative deviations of ultrasonic velocities produced by the presence of stress are extremely small and sensitive to the material's texture (grain alignment), which often restricts its spatial resolution [31].

2.7 Numerical simulation of cutting process

Finite element modelling of machining processes has witnessed significant progress over the last few decades with the help of the ever-improving performance and power of computers. Currently, most of the published research works were mainly carried out for the simplest configuration of machining known as orthogonal cutting, with a focus on a wide range of different sub-topics such as predicting cutting forces, temperatures, chip morphology, tool wear, residual stresses, white layer formation, and sequential cuts modelling [5]. Fig. 2.9 summarises the major inputs (the mechanical and thermal properties of the workpiece and tool, cutting conditions, boundary and interaction conditions, etc.) and outputs (cutting force, temperatures, chip morphology, residual stresses, etc.) parameters for FEM simulation in metal cutting. Among the inputs, the flow stress of the workpiece and tool-chip friction laws are two of the most essential parameters for efficiently acquiring cutting forces, chip morphology, temperature field and residual stress distribution.

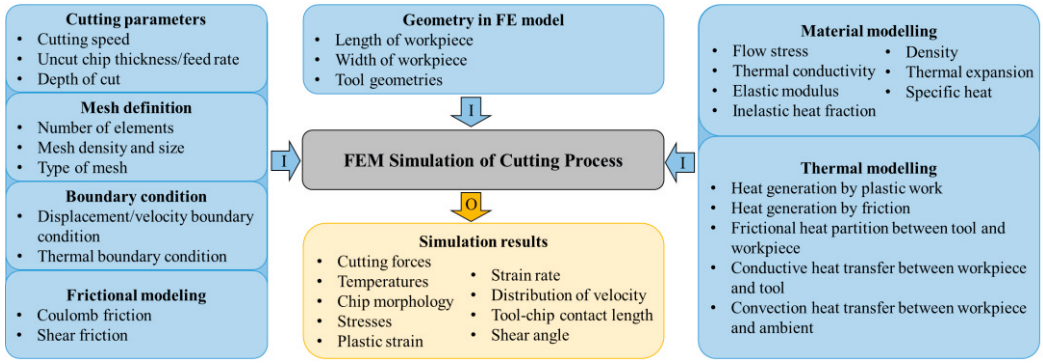

Figure 2.9
Input (I) and output (O) parameters for cutting process simulation.

There are four commonly used FE formulations to predict residual stress generated during the metal cutting process: Lagrangian, updated Lagrangian (Re-meshing), Arbitrary Lagrangian-Eulerian (ALE) and Coupled Eulerian and Lagrangian (CEL).

Lagrangian method is probably the earliest and most commonly used technique in metal cutting simulations. In this method, the motion of the material is easy to visualize as the mesh is the representation of the material. Although this method is straightforward and able to simulate the segmented chip morphology, many disadvantages exist. The biggest drawback is that excessive element distortion will occur especially at the chip-tool interface due to the large deformation of the material in this area, leading to termination of the simulation. To handle this problem, some researchers adopt a damaged layer coupled with a separation criterion to successfully separate chips from the substrate. These criteria can be divided into two categories: geometrical and physical (stress, strain, and strain energy) [37]. However, it was reported [38] that the magnitude of the separation criteria significantly affects the stress field in the machined surface and the strain distributions both in the chip and in the machined surface. Thus, a trial and error method should be adopted to determine the magnitude of these separation criteria based on the observation of mesh deformation and stress state on the machined surface, which adds a large degree of uncertainty to the model. In addition, the highly distorted element reaching the damage criterion is deleted during the simulation, resulting in the absence of the material having the higher values of temperature, stress and strain and the results accuracy could be influenced. Grissa et al. [39] developed three kinds of finite element models to investigate surface integrity. The results showed that both the residual stress and temperature level at the machined surface are lower when using Lagrangian formulation for the suppressing of elements in this model. Furthermore, it is hard to get the stagnation zone using Lagrangian method due to the deletion of the severely distorted elements in front of the tool tip.

In updated Lagrangian formulation (re-meshing) method, when the mesh is highly distorted during the simulation a new mesh based on the deformed geometry of the workpiece will be created. A mapping process is employed to transfer the solution data from the old distorted mesh to the new mesh, and interpolations usually take place during this process as the nodes of the old mesh and those of the new mesh don't usually coincide. The new mesh can have different types and numbers of elements but it must share the same geometry boundary with the old mesh. Re-meshing has disadvantages in that it decreases the accuracy of the results because of the accumulated errors after the repetitive interpolation process [40]. With this method, Agmell et al. [41] successfully predicted and validated the subsurface deformation of machined Inconel718 and temperature distribution in the segmented chip.

The Arbitrary Lagrangian-Eulerian (ALE) technique can be considered as a special case of re-meshing technique. This method permits the independent movement of the mesh and the deformed material compared to traditional re-meshing. However, it cannot be able to alter the topology (elements and connectivity) of the mesh, which restricts the ability of this method to deal with the largely distorted mesh. There are two types of boundary conditions applied in ALE: Eulerian-Lagrangian mixed boundaries (ALE-EL) and pure Lagrangian boundary (ALE-LG). When Lagrangian-Eulerian mixed boundaries are used (Fig. 2.10), a segmented chip could be obtained [42]. Nevertheless, to reduce time calculation it is suitable to approximate a convenient initial shape of the chip by testing different shapes and dimensions before final calculation [43]. It was shown [42] that in the ALE-LG model the latter generated chip segments show clear waviness while the former segments gradually faded away with the approaching of the cutting tool, as presented in Fig. 2.11. In this type of model, the total element numbers and their connectivity remains consistent during the entire adaptive process. Thus, the high density of the nodes and shrinking elements occurred in the chip root and the latter formed segments inevitably inflate the elements in the previously generated valleys of the free chip surface and decrease the curvatures of this valley. The restoration of chip segments generated by this method was also reported in the study [44], which was proven to be far from the experimental results.

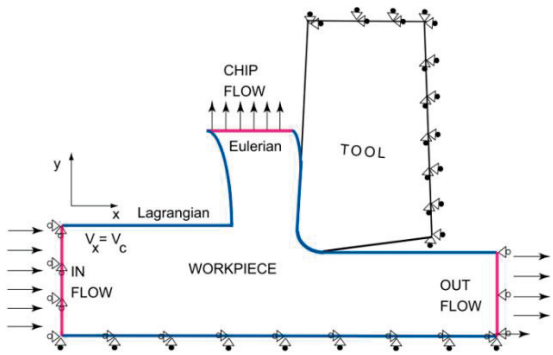

Figure 2.10
Boundary conditions of the ALE-EL model [45].

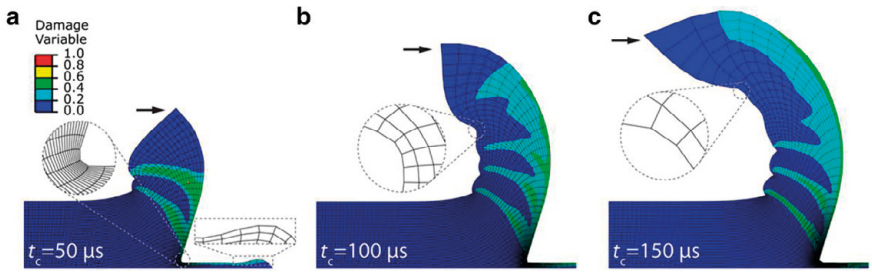

Figure 2.11
Chip morphology evolution from the ALE-LG model [42].

Coupled Eulerian and Lagrangian (CEL) formulation is another method for metal cutting simulation. The CEL model consists of both Eulerian and Lagrangian formulations, where the workpiece is modelled with an Eulerian formulation and the tool by a Lagrangian formulation. For the Eulerian part, the mesh is fixed in space and the material flows through it, which can completely avoid the problem with severe element distortion. The mesh grids of Lagrangian and Eulerian parts can be overlapped. When comparing with the ALE method, it was reported [46] that the chip morphology and cutting forces were better predicted by CEL model in orthogonal cutting of the titanium alloy Ti6Al4V, and the absence of mesh deformation in CEL simulation lead to a decrease in computing time. The CEL method has been successfully used in metal cutting simulations by [47–49] with promising results as well.

Among these methods, Lagrangian formulation has superiority in terms of computational efficiency. ALE formulation models take a longer computational time due to the application of adaptive meshing algorithm. For CEL model it needs a fine mesh used in the large 3D Eulerian domain to ensure the accuracy of the results, which will increase time consumption. All the advantages and disadvantages

of various formulations for simulating the cutting process are summarised in Table 2.1. The CEL method is selected in this dissertation to guarantee both the accuracy of the results and segmented chip generation, although costs a longer time than Lagrangian formulations.

Table 2.1.
Advantages and disadvantages of various formulations for simulating the cutting process.

Formulations	Advantages	Disadvantages
Lagrangian	• Straightforward; • The mesh is the representation of the material; • Be able to predict segmented chip.	• Element will be severely distorted; • Separation criteria are needed; • Parameters of the separation criteria need to be tuned; • Cannot capture stagnation zone; • Accuracy may be decreased due to the deletion of the severely distorted elements.
Updated Lagrangian (Re-meshing)	• Doesn't need separation criteria; • The simulation is able to continue through the mapping process where the solutions are transferred from highly distorted mesh to the new mesh; • New mesh can have different types and numbers of element with the old mesh; • Be able to predict segmented chip.	• Interpolations will be employed during the mapping process; • Accuracy of the solution will deteriorate as the errors may accumulate after repetitive interpolation.
ALE	• Doesn't need separation criteria; • Allow the independent movement of the mesh and the deformed material.	• Cannot alter the topology (elements and connectivity) of the mesh; • Frequent adaptive meshing is needed, which increased time consumption; • Restoration of chip segments will occur using ALE-LG method; • The initial shape of the chip should be predefined using the ALE-EL method.
CEL	• Completely avoid the problem with severe element distortion; • Be able to predict segmented chip.	• Finer mesh is needed to get reasonable chip morphology; • Fail to capture the cracks in the chip.

2.8 Analysis of residual stress

In the last decades, many numerical models have been developed to explore the influence of cutting conditions, tool geometries, chip morphology, pre-stressed condition, and workpiece-tool materials, etc. on the residual stress distributions [5,37]. Despite all these efforts, the mechanism of residual stress generation is still far from being completely understood, and several crucial issues still have to be investigated. This section reviews the progress and limitations in the area of residual stress investigation in orthogonal cutting and fillet surface turning.

2.8.1 Flow stress and segmented chip

It was reported that [50] the right type of chip modelling is extremely critical in correctly predicting the magnitude and distribution of the residual stress. This is because there is a substantial difference in temperature and cutting forces with continuous and segmented chips. However, how the segmented chip morphology affects temperature and cutting forces have not been explained. A rippled surface and a cyclic evolution of residual stress in the machined aeronautic aluminium alloy with a generated segmented chip were found [10], but the relationship between the segmented chip and machined surface integrity was still unclear. One of the objectives of this dissertation is to explore the effects of the segmented chip morphology on the residual stress distribution through FE method. An appropriate description of the stress-strain curve of the workpiece material is essential for successfully simulating the segmented chip.

In practical machining, the segmented chip is a common type of chip morphology for many materials [15]. Some authors consider that segmented chip formation is due to a thermoplastic instability in the shear band, while others explain this phenomenon by considering the initiation and propagation of cracks inside the primary shear zone of the workpiece material [51,52]. In either theory, the strain-softening phenomenon – stress is decreased with an increasing strain beyond a critical strain value – is an indispensable factor in the material constitutive law for a segmented chip prediction [44]. The strain-softening phenomenon was identified by carrying out uniaxial compression tests at temperatures close to those found in machining (21-1050 °C) and high strain rates ($10°$-10^2 s^{-1}) on Inconel 718 [53]. It was found that the strain hardening reached a certain strain followed by a strain-softening range where stress decreases with further increasing strain. This type of flow stress-strain curve has also been obtained for AISI 304 steels [54]. The representative flow curves of Inconel 718 and AISI 304 stainless steel are shown in Fig. 2.12.

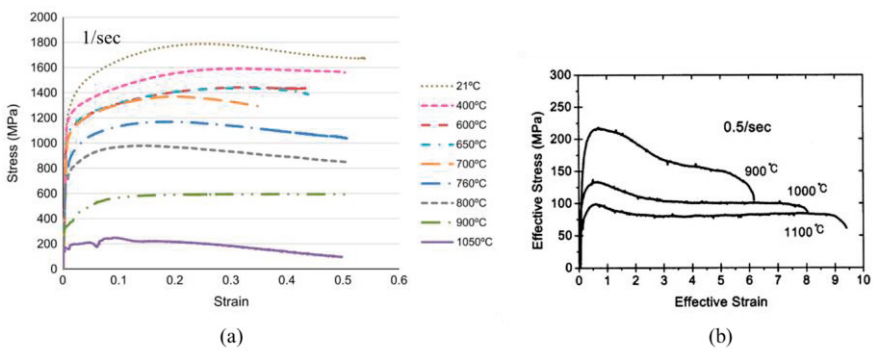

Figure 2.12
Influence of temperature on the flow behavior of different materials: (a) Inconel 718 [53]; (b) AISI 304 stainless steel [54].

Thus, when predicting residual stress induced by machining the mentioned materials, a material model used to characterise their flow stress curves should consider the strain-softening phenomenon. Johnson-Cook constitutive law is the most popular used material model in metal cutting simulation because it can effectively reflect the strain hardening, strain rate hardening and temperature softening phenomenon of material under the conditions of large deformation, high strain rate and high temperature. However, the classic constitutive Johnson-Cook laws exhibit a flow stress increase with increasing strain whatever the temperature and strain rate conditions, which is invalid in predicting the segmented chip formation due to the absence of strain-softening behaviour. According to this, many researchers proposed modified constitutive models introducing the strain-softening effect.

A successful modification (TANH model) based on J-C model was proposed by Calamaz et al. [52], in which the flow stress begins to decrease until a specified strain after which nearly constant stress is obtained. The TANH model also achieves the function that the degree of strain-softening increased with the increase of temperature. This model was further improved in the study [51] by considering the observation that the strain-softening should appear from about 0.3 times the melting temperature. Subsequently, Sima et al. [55] introduced an exponent S to TANH model to cause a dependency of strain-softening phenomenon on the strain. The literature shows that most of the developed models can provide a good prediction of chip morphology, temperatures and cutting forces in the cutting simulation.

Some other researchers introduced a damage model (damage initiation and evolution) to characterize strain-softening behaviour (Fig. 2.13). Atlati et al. [56] used a fracture energy based ductile damage model to simulate segmented chip generation and analyse the segmentation intensity ratio for A2024–T351 alloy cutting. Zhang et al. [57] adopted the fracture energy based ductile damage model to correctly predict the limiting shear stress at the tool–chip contact surface and investigate the effect of cutting speed and tool-rake angle on chip morphology in Ti-6Al-4V cutting simulation. Similarly, the J-C plastic model was combined with material damage and its fracture energy to study the dry cutting of an aeronautic aluminium alloy (A2024-T351) [10]. The distributions of equivalent von Mises plastic stresses, temperature and equivalent plastic strain during one chip segment formation were predicted in this study.

Previous works indicate that both the modified constitutive models and the damage modelling strategies can give a good description of the strain-softening phenomenon. The latter method is used in this dissertation.

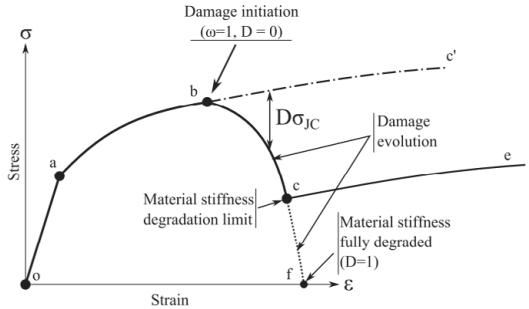

Figure 2.13
Stress-strain response of a metal specimen with damage behaviour [58].

2.8.2 Effect of cutting parameters and tool geometry

The effect of cutting parameters and tool parameters on residual stresses attracts lots of research, and different results can be found in the literature. Christian et al. [59] found that increasing cutting speed (from 10 to 1200 m/min) leads to higher tensile stresses at the surface and higher compressive stresses below the surface when turning Inconel 718 at the feed rate of 0.5 mm/rev. The same trend of surface residual stress induced by a higher cutting speed was also revealed [14] when turning AISI 316L steels. On the other hand, Pawade et al. [60] found that the surface residual stress increased as the cutting speed changed from 125 to 300 m/min, and decreased with the cutting speed further increasing to 475m/min in the machining of Inconel 718. It was attributed that at a lower cutting speed the rate of heat dissipation by the chip is lower than that at the higher cutting speed due to the lower volume removal rate. At the same time, the chips stay in the machining zone for a relatively longer duration. Consequently, more heat dissipates into the machined surface. When increasing cutting speed, a greater fraction of heat is carried away with the chip due to a higher volume removal rate, leading to decreased heat entering the workpiece. Moreover, findings from Sharman et al. [61] suggested that surface residual stress became more compressive with increasing cutting speed from 40 to 80 m/min when turning Inconel 718. It is explained that increased chip flow rate with increasing cutting speed reduces the time for the generated heat in the shear zone to dissipate to the workpiece surface, which weakens the effect of thermal load and thus, the mechanical load results in more compressive residual. Regarding the effect of feed rate, it is found that higher and deeper compressive residual stresses in the subsurface were induced with increasing feed rate when turning AISI 316L steels [14] and hard turning of bearing steel [62,63]. The increased compressive field with increasing feed rate was explained by the mechanical effects. As feed rate increased, cutting and feed forces become larger, which leads to an enhancement of the tensile deformation of the workpiece and the

compressive residual stress increased as a result. On the other hand, Sharman et al. [61] found that the increase in feed rate resulted in a decreased magnitude of compressive residual stress in the subsurface layer when turning Inconel 718. Furthermore, it was found [61] that the tensile stress at the machined surface increased with an increasing feed rate, while another study reported that the surface residual stress barely varied as the feed rate increased [14].

The influence of cutting tool geometry (i.e. rake angle, edge radius) on residual stresses were investigated by many research works. It was reported [12] that surface tensile stress decreased and the magnitude and depth of subsurface compressive residual stress increased when using a more negative rake angle in turning hardened steel. The trend to be more compressive of the residual stress was explained by the increased cutting force and feed force with a more negative rake angle. However, the surface tensile residual was found to increase with the same variation of tool rake angle in the investigation of Outeiro et al. [13] and M'Saoubi et al. [14]. As to the influence of edge radius, it was found that a larger tool edge radius induces larger tensile stress at the machined surface and also compressive stress in the sublayer [19,64]. In addition, the effect of tool wear on residual stresses is also studied by many researchers. It was reported [65–67] that the magnitude/depth of both the tensile stress in the surface and compressive stress in the subsurface increased with increasing tool wear. The residual tensile stresses at the machined surface were caused by the thermal impacts due to the increase of the friction, and the increased compressive stress at the subsurface was explained by the larger mechanical impact induced by tool wear. However, it was reported that [50] a worn tool produced less compressive residual stress in the sublayer in orthogonal cutting of Ti-6AI-4V.

As seen, despite all these efforts, contradictory residual stress distribution findings can be found in the literature. Since most of these studies were carried out through experimental methods, it is difficult to measure or divide the mechanically or thermally induced plastic deformation separately through experimental investigation of the machined workpiece. The mechanism of residual stress generation is therefore hard to explore. In this dissertation, the numerical method is employed to make up this fact. Using the numerical method, the local normal/tangential stress acting on the material behind the tooltip can be taken as an indicator for evaluating the extent of mechanical induced tensile plastic deformation in surface/near-surface and subsurface layer. The temperature field as a function of depth beneath the machined surface can indicate the level of thermal-induced compressive strain in the surface/near-surface layer. In this case, the machining induced plastic strain (either from mechanical effect or thermal aspect) is continuously captured to analyse the evolution process thus facilitating understanding of the mechanism of the residual stress generation.

2.8.3 Residual stresses induced in multiple cuts

In practical machining processes, multiple-cuts operations are often needed to achieve the designed dimensional accuracy, surface roughness, or to meet the operational specifications of the machine (i.e. the maximum cutting power allowed) [68]. During multiple cuts, the accumulated strain/stress and temperature produced by the previous cuts will be brought to the subsequent cuts. Cutting of the affected layer leads to the variation of cutting forces, chip morphology, temperature and strains in subsequent cuts, and eventually affects the final residual stress distribution. In order to investigate the residual stress evolution during multiple cuts, a number of researchers have developed so-called sequential cut modules.

It was found in the study [69] that when applying the same cutting parameters for each cut, the surface tensile residual stress was lower after the second cut than that after the first cut in orthogonal cutting of 304 stainless steel. The same trend of residual stress was also reported in the numerical study of micro-cutting process prediction [70], as well as in the experimental work of orthogonal cutting AZ31B Mg Alloy [71] and hard turning AISI52100 Steel [72]. However, the underlying mechanism behind this phenomenon was not fully explored in these studies. To investigate the effect of uncut chip thickness on the residual stress evolution during multiple cuts, Mohamed et al. [73] established two multiple-cut FE models with two different uncut chip thicknesses and found that the lower tensile residual stress induced by the second cut is more obvious with a larger uncut chip thickness. In addition, a lower magnitude of compressive plastic strain (PE11) ahead of the tooltip was simulated during the second cut compared to the one during the first cut, which explained why lower surface tensile residual stresses were generated in the second cut. On the other hand, a different finding was reported in the experimental study [13], where a gradually increased surface residual stress was obtained from the first cut to the third cut in orthogonal cutting AISI 316L steel. In addition, different uncut chip thickness was also applied in a single multiple-cut model by some researchers. For example, Guo et al. [74] utilized four different uncut chip thicknesses in the second cut and found that compressive residual stress distribution could be induced by the second cut with an uncut chip thickness below the critical value. Regarding the influence of repetition of finishing operations on the residual stress evolution, Sasahara et al. [75] revealed the finish machining following the rough machining caused the compressive residual stress on the surface while more repetition of the finish machining changed the surface residual stress to be tensile.

Many studies were carried out to investigate the influence of pre-existing stress distributions on residual stresses evolution. Yuan et al. [76] uniformly applied initial stresses with different values and distribution depths to the workpiece followed by the cutting simulation process. It was found that the existence of initial tensile stress strengthens the tensile residual stress distribution in the finished workpiece, while initial compressive stress has opposite effects. Ruitao et al. [77] developed a novel pre-stressed loading device for ring parts to perform the pre-stressed cutting

experiment and demonstrated that residual stress of the machined surface decreases sharply with the pre- stress increasing. Nevertheless, in these studies, the workpiece material is employed either with a homogeneous initial stress field or free of plastic deformation, which is far from the case in practical machining.

It is shown in the literature review that most of the studies linked to multiple cuts mainly focused on either implementing successive cutting using identical cutting conditions or only considering the influence of subsequent machining on the final stress state. The influence of the previously caused accumulated strain/stress that is in accordance with the practical machining on the residual stresses in multiple cuts was not fully explored.

2.8.4 Residual stresses induced in turning curved surface

From the previous studies, a large number of researches about machining induced residual stresses distributions were mostly focused on straight line tool paths. In industrial applications, curved surface parts are widely used for their aesthetics functionality like in home appliances, plastic products, etc. or enhancing the operating capability of parts in automotive and aerospace fields [78], demonstrating an urgent need for deep research into the residual stress distribution induced by the machining of curved surface parts.

Several studies on the optimization of machining parameters in curved surface machining have been conducted. Jian et al. [79] suggested that both the cutting force and the cutting vibration increased when the tool-path curvature radius increased in high-speed milling of TC4 curved surface. It has been shown [80] that the cutting force became smaller and the change of cutting force was smoother with an increasing spindle speed in high-speed milling of Inconel 718 curved surface. Kuldeep et al. [81] stated that the feed rate is the most influencing parameter for surface roughness in diamond turning of the curved surface. Xiaohui et al. [82] found that the curved surface residual stress and deformation can be effectively reduced when using a larger tool radius and smaller depth of cut in milling of curved thin-walled parts. In addition, the cutting force prediction model for milling of the complex curved surface was also proposed [83,84] to enrich the processing and manufacturing theory. However, the residual stress research for the turning of the curved surface is seldom involved. Based on the experimental observations [85], the residual stress profiles strongly differ between the longitudinal turning and end face turning while turning a fillet surface, indicating the necessity to better understand the thermal-mechanical load and residual stress evolution along the fillet surface turning. Therefore, one of the motivations of this dissertation is to take the curved tool path into account and investigate the residual stress variation in the component induced by fillet surface turning.

3 Numerical modelling

The CEL method was employed in the present study to guarantee both the accuracy of the results and segmented chip generation. This chapter introduces all the details of the CEL model used for this work, including the geometry, mesh, and boundary conditions, material modelling, friction modelling and thermal modelling.

3.1 Geometry, mesh, and boundary conditions

Orthogonal cutting and fillet surface turning simulations were carried out in Abaqus/Explicit 6.14-2 in this dissertation. The workpiece material for the orthogonal cutting is Inconel 718, and the fillet surface turning is AISI 304 stainless steel. The carbide insert is used for both cases.

3.1.1 Orthogonal cutting model

In orthogonal cutting modelling, the Euler-part is initially filled with workpiece according to the blue area, while the rest of the Euler- space is regarded as void. An 8-node thermally coupled linear Eulerian brick element (EC3D8RT) is adopted for the Euler space and an 8-node thermally coupled brick element (C3D8T) is employed for the tool. The influence of element size of the Eulerian part in CEL model on the simulated results (chip morphology, temperatures and forces) is investigated in the study [86]. It was recommended to use square elements to avoid any influence of the results due to the orientation of the elements. In addition, it was found that convergence is reached for 5 μm square elements and larger elements with a length of 10 μm, could be used to achieve fast results computing with lower accuracy. Therefore, the mesh size in the region where generating machined surface and chips is set to 5 μm square elements to get a precise chip morphology and describe a reliable residual stress profile. Since the CEL method is only implemented in 3D in Abaqus/Explicit v6.14-2 [87], the developed CEL model is a tridimensional model rather than a planar one. It was also demonstrated in the study [86] that the element's width doesn't influence the chip morphology, temperature fields and cutting forces. Thus, one element with a width of 0.03 mm was used in the width of the model. To further make the model as close as possible to a 2D plane

strain one, the velocity in the z-direction for the two x-y planes of the Euler-part is set to zero. The workpiece is fixed in space and the tool that is set as a rigid body advances into the workpiece with the cutting speed until the chip is completely cut off. The velocity constraints applied on the Euler-part are shown in Fig. 4.1.

In single cut modelling, three steps have been conducted. Firstly, simulate the cutting process; secondly, remove the tool; and thirdly, cool down machined workpiece to room temperature for residual stresses calculation. In multiple cuts modelling, the boundary conditions applied on the Euler-part keeps consistent in each cutting sequence and a short cooling down step (0.02 seconds) is performed after each cut for residual stress calculation.

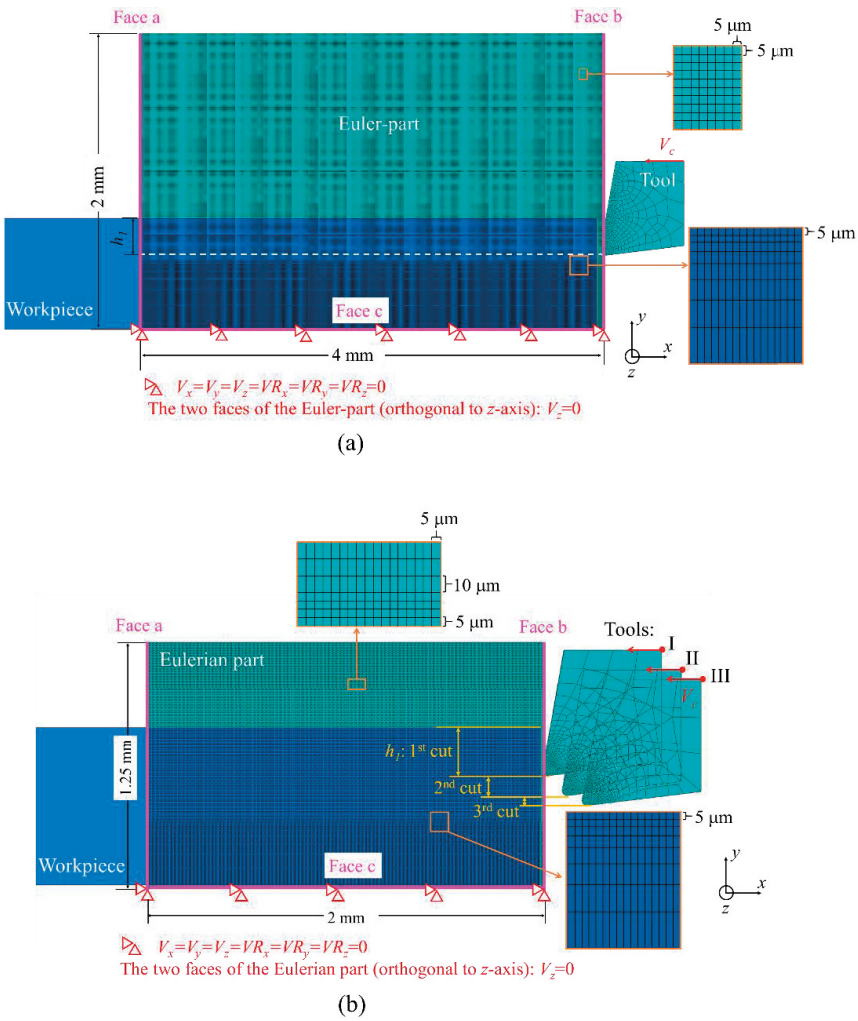

Figure 4.1
Initial geometry and boundary conditions of the orthogonal CEL model: (a) single cut; (b) multiple cuts.

3.1.2 Modelling fillet surface turning

It is extremely time consuming to accomplish the whole fillet surface turning process from outer face to end face with the numerical method. To make it possible to reveal the evolution of residual stress during this process, four simulations were carried out corresponding to the four cutting faces shown in Fig. 3.2. The position of the tool in Deg30 (point C) and Deg60 (point D) faces can be calculated according to the known angles and dimensions. Based on this, the positions of the tool in the previous cut (point C' and D') were therefore obtained with the help of feed rate. The previous machined surface profile was created in each cutting face using the "Merge/Cut Instances" technique in Abaqus.

The initial configuration of the CEL model for outer face turning is illustrated in Fig. 3.3. The tool is fixed in space and set as a rigid body with a reference point. The Euler part is initially filled with workpiece material in the crossed region of the workpiece and Euler-part. The left face of the Euler-part is velocity constrained with an inflow of material $V_z = -V_c$ and unrestricted in all other degrees of freedom. The bottom face of the Euler-part is velocity constrained with $V_x = V_y = 0$ and unrestricted in all other degrees of freedom. An 8-node thermally coupled linear Eulerian brick element (EC3D8RT) is used for the Euler space and a 4-node thermally coupled tetrahedron element (C3D4T) is employed for the tool. Considering the large number of elements (more than $2.5e10^6$) employed in the Euler-part, the cooling down step is avoided in the fillet surface simulation due to the limited computing resources. Accordingly, the extraction position of the residual stresses should be away from the cutting edge as far as possible where the temperature is lower to limit the temperature gradient influence.

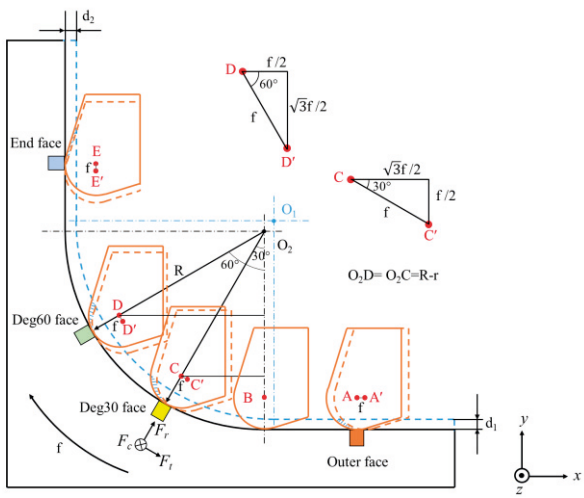

Figure 3.2
The four cutting faces selection in simulation and the evolution of uncut chip cross-section geometry from outer face to end face.

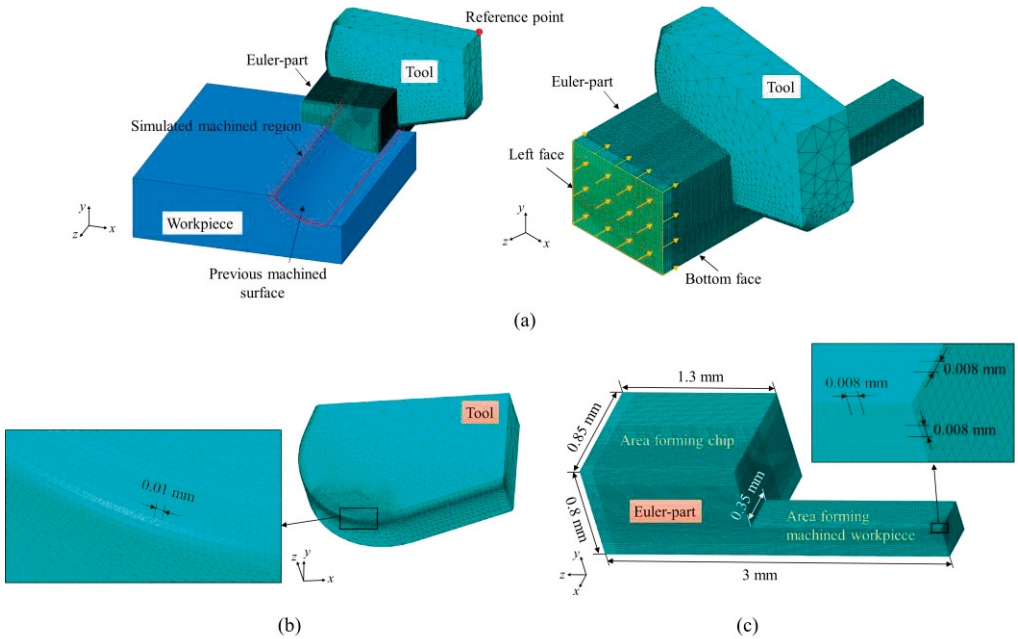

Figure 3.3
The initial configuration of the CEL model for outer face turning: (a) boundary conditions acting on the Euler-part; (b) meshing for the tool; (c) geometry and mesh size of the Euler-part.

3.2 Material modelling

In this dissertation, the Johnson-Cook plasticity model is selected to describe the plasticity behaviour of the workpiece material. The J-C damage model (damage initiation) and Hillerborg's fracture energy model (damage evolution) were adopted to describe the strain-softening phenomenon, which is previously illustrated in Fig. 2.13. The Johnson-Cook constitutive law is expressed in the Eq. (3.1).

$$\bar{\sigma} = [A + B(\bar{\varepsilon})^n]\left[1 + Cln\left(\frac{\dot{\bar{\varepsilon}}}{\dot{\bar{\varepsilon}}_0}\right)\right]\left[1 - \frac{T - T_{room}}{T_{melt} - T_{room}}\right]^m \qquad (3.1)$$

where $\bar{\sigma}$ is the equivalent flow stress; $\bar{\varepsilon}$ is the equivalent plastic strain; $\dot{\bar{\varepsilon}}$ is the equivalent plastic strain rate; $\dot{\bar{\varepsilon}}_0$ is the reference strain rate; A is the initial yield stress; B is the hardening modulus; C is the strain rate dependency coefficient; n is the strain-hardening exponent; m is the thermal softening coefficient; T_{melt} is the melting point of material; and T_{room} is the room temperature. The Johnson– Cook parameters used for the workpiece are specified in Table 3.1. The Inconel 718 used in this study was solution heat treated (1052°C) followed by ageing treatment

(877°C), which is quite similar to the heat treatment condition of the Inconel 718 specimens in the study [53]. Thus, the same parameters of A, B, n, C and m are adopted. There are many sets of J-C parameters of AISI 304 available in the literature. Several set of data were tested and it was found that the parameters provided in the study [88] are the most suitable one because they can predict more accurate cutting forces and residual stress distribution when compared with the experimental results. The thermo-mechanical properties of both the tool and the workpiece in the simulation are presented in Table 3.2.

Table 3.1.
Constants of the Johnson-Cook constitutive model for Inconel 718 [53] and AISI 304 [88].

Material	*A* (MPa)	*B* (MPa)	*n*	*C*	*m*	T_{melt}	T_{room}
Inconel718	1377	1243.5	0.6767	0.0045	1.29	1344	20
AISI 304	277	556	0.794	0.0096	0.944	1400	20

Table 3.2.
Properties of workpiece and cutting tool material [41,89,90].

Properties	Inconel718	AISI 304	Carbide Tool
Density (kg/m^3)	8221	7930	14860
Thermal conductivity (W/m°C)	12(20 °C) 24(900 °C)	16.2	82
Thermal expansion (°C^{-1})	1.2e-5(20 °C) 1.7e-5(900 °C)	16e-6	5.2
Young's modulus *E* (GPa)	212	193	600
Poisson's ratio *v*	0.294	0.28	0.2
Specific Heat (J/Kg°C)	440(20 °C) 680(900 °C)	500	249.8

The criterion used to identify the damage initiation (point b in Fig. 2.13), is the Johnson-Cook damage model [91]. The equivalent plastic strain at damage initiation $\bar{\varepsilon}_0$ is defined by Eq. (3.2),

$$\bar{\varepsilon}_0 = \left[D_1 + D_2 \exp\left(D_3 \frac{P}{\bar{\sigma}}\right)\right]\left[1 + D_4 \ln\left(\frac{\dot{\bar{\varepsilon}}}{\dot{\bar{\varepsilon}}_0}\right)\right]\left[1 + D_5\left(\frac{T - T_{room}}{T_{melt} - T_{room}}\right)\right] \quad (3.2)$$

where $D_{i(i=1\sim5)}$ are five constant failure parameters and p is hydrostatic stress.

For a given element, failure begins when scalar damage parameter ω, cf. Eq.(3.3), exceeds 1,

$$\omega = \sum_{i=1}^{n} \left(\frac{\Delta\bar{\varepsilon}}{\bar{\varepsilon}_0}\right)_i \quad (3.3)$$

where $\Delta\bar{\varepsilon}$ is the increment of equivalent plastic strain at unit integration point during an increment (i).

In the damage evolution stage, Hillerborg's fracture energy G_f [92] is introduced to describe the energy dissipated during the damage evolution process,

$$G_f = \int_{\bar{\varepsilon}_0}^{\bar{\varepsilon}_f} L\bar{\sigma}\, d\bar{\varepsilon} = \int_0^{\bar{u}_f} \bar{\sigma}\, d\bar{u} \quad (3.4)$$

where, L is the characteristic length associated with an integration point; $\bar{\sigma}$ is the flow stress in this stage; $\bar{\varepsilon_f}$ is the equivalent plastic strain when the material is fully degraded corresponding to point f in Fig. 2.13. $\bar{\varepsilon_0}$ is the equivalent plastic strain at damage initiation corresponding to point b in Fig. 2.13. $\overline{u_f}$ is the equivalent plastic displacement. The fracture energy G_f of Inconel718 is offered as an input parameter by G_f=$K_c^2(1-v^2)/E$ where K_c is the fracture toughness determined by [93].

The stiffness degradation D during the material softening process is in the range of 0 ~ 1.

$$D = 1 - \exp(-\int_0^{\bar{u}} \frac{\bar{\sigma}}{G_f} d\bar{u}) \tag{3.5}$$

During the softening phenomenon (curve bc in Fig. 2.13), the flow stress in the material is given by the following equation:

$$\bar{\sigma} = (1 - D)\tilde{\sigma} \tag{3.6}$$

where $\tilde{\sigma}$ is the stress in the material if it had not been damaged. The material softening stops when the stiffness degradation D reaches the specified value, visualized by point c and start to follow the curve c-e in Fig. 2.13. The parameters of $\bar{\varepsilon_0}$ and D are manually adjusted until the forces and chip morphology are good agreement with experimental data, and the procedure to determine these two parameters are shown in Fig. 3.4. In this study, the selected $\bar{\varepsilon_0}$ and D for different workpiece materials are presented in Table 3.3.

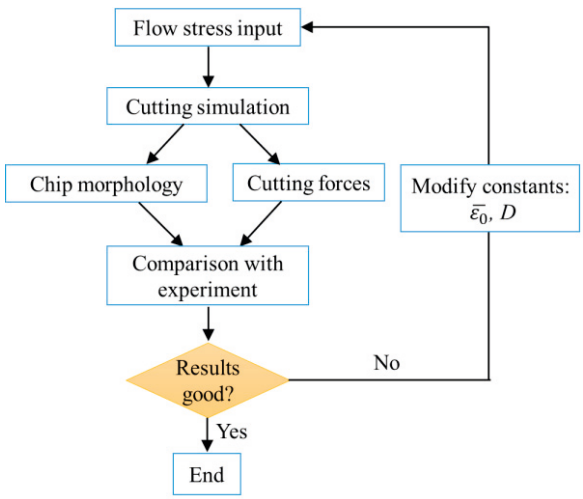

Figure 3.4.
Flow chart for determining the equivalent plastic strain at damage initiation ($\bar{\varepsilon_0}$) and the critical damage value (D).

Table 3.3.
The values of $\bar{\varepsilon}_0$ and D for different workpiece materials.

Parameters	$\bar{\varepsilon}_0$	D
Inconel718	0.9	0.6
AISI 304	2.6	0.5

3.3 Friction modelling

One of the most commonly used friction models in machining is proposed by Zorev [94], which is shown in Fig. 3.5. In Zorev's model, the interface area between the chip and cutting tool is divided into two regions: the sticking and the sliding regions. Sticking zone is located close to the cutting edge where very high normal stresses cause high plastic deformation. In general, the frictional stress cannot exceed the shear yield strength of the material. Therefore, shear friction model is developed to discribe frictional behaviour, in which friction stress is proportional to the shear strength of the workpiece. The firction stress is determined by the relationship $\tau_f=k\tau_y$, where τ_f is the friction stress; τ_y is the shear strength of the workpiece material and is defined as $\tau_y=\sigma_y/\sqrt{3}$, where σ_y is the yield stress of the material; k is the shear friction factor. A maximum constraint on the friction stress is equal to the shear strength of the workpiece material, that is, the constant k is set as 1. This is the case adopted in this dissertation. Sliding region is located next to the sticking region up till the point where the chip leaves the tool, where the normal stresses is relatively low. Coulomb's friction model was generally used in this sliding region. In this model, the friction stress is determined by the relationship $\tau_f=\mu\sigma_n$, where μ is the friction coefficient and σ_n is the normal stress along the tool-chip interface. Accordingly, Zorev's model is defined by Eq. (3.7). The reason for using this model is that the mechanism behind the frictional problem is not fully understood therefore this model has been used for simplicity reasons.

$$\tau_f = min(\mu\sigma_n, \tau_y) \tag{3.7}$$

The friction coefficient μ in simulation is defined as Eq. (3.8) [95],

$$\mu = \frac{F_c tan\gamma + F_f}{F_c - F_f tan\gamma} \tag{3.8}$$

where F_c and F_f are the mean cutting force and mean feed force which can be measured in the experiment, respectively; and γ is the tool rake angle.

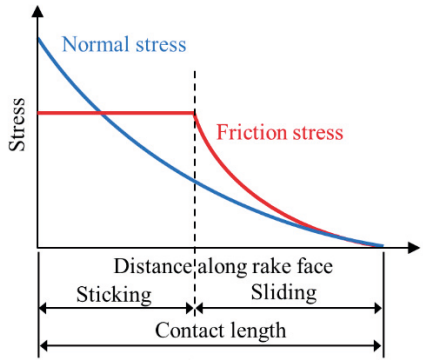

Figure 3.5.
Curves representing normal and shear stress along rake face from Zorev's model [94].

3.4 Thermal modelling

The heat is generated from two sources in metal cutting process: plastic deformation and friction. The rate of heat generation due to plastic work ($\dot{Q}_p$) is given by [96]:

$$\dot{Q}_p = \eta_p \bar{\sigma} \dot{\bar{\varepsilon}} \tag{3.9}$$

where $\bar{\sigma}$ is the flow stress, $\dot{\bar{\varepsilon}}$ the plastic strain rate and η_p is the fraction of the plastic deformation energy converted to heat, which is set to 0.9 according to [41].

The rate of heat generation by friction ($\dot{Q}_f$) at the tool-workpiece interfaces is described according to the following relationship:

$$\dot{Q}_f = \eta_f \tau_f V_s \tag{3.10}$$

where τ_f is the friction stress given by Eq. (3.7), V_s is the sliding velocity, and η_f is the fraction of the frictional energy that is converted to heat. By assuming all the frictional work converted into heat, $\eta_f = 1$ is considered in this dissertation [41]. In addition, the frictional work is divided equally between tool and workpiece [97].

The heat conduction between the tool and workpiece is performed through the tool-workpiece contact face from the workpiece with higher temperature to the tool with lower temperature during the cutting process. This conduction heat transfer is calculated as:

$$q = h(P)(T_a - T_b) \tag{3.11}$$

where q is the heat flux which is a flow of energy per unit of area per unit of time crossing the interface from point a on the workpiece to point b on the tool; T_a and T_b are the temperature of the points on the respective surfaces; $h(P)$ is the heat conduction coefficient which is defined as a function of the pressure and adopted from the study [41]. In the cutting process, the simulation time is too short to allow the convection heat transfer to occur, and therefore, this heat transfer is often ignored. In the cooling down step for the orthogonal cutting, convection heat transfer occurs between the surfaces (faces a, b and c in Fig. 3.1) and the ambient. The convection coefficient is set to be 10 $W/m^2°C$ according to the study [98]. In addition, heat radiation was neglected throughout the simulation as it is negligible when compared to the thermal conduction and convection.

4 Experimental setup

To provide the validation of the proposed cutting models, the experiment work for obtaining the cutting forces, temperature and residual stress profiles were performed under the same cutting condition applied in FE modelling. In this chapter, the cutting tests for orthogonal cutting and fillet surface turning are described in detail. The measurement of temperatures, cutting forces, chip morphology, and residual stress are also presented.

4.1 Workpiece and tool materials

The workpiece material used in the orthogonal cutting experiments is a solution treated and aged nickel-based superalloy Inconel 718 with the hardness of 45 HRc; while the one used in the fillet surface turning is AISI 304 stainless steel. Both Inconel 718 and AISI 304 stainless steel belong to difficult-to-cut materials. Inconel 718 is one of the Nickel-based superalloys which are widely used in the aviation and aerospace industries since it exhibits outstanding mechanical properties and corrosion resistance at elevated temperatures [11]. However, Inconel 718 is one of the difficult-to-machine materials due to its poor thermal conductivity, work hardening behaviour, and tendency to adhere to cutting tools [99]. AISI 304 stainless steels are also difficult-to-machine materials due to their high strength, high ductility and low thermal conductivity. They are used to fabricate chemical and food processing equipment, as well as machinery parts requiring high corrosion resistance [100]. The poor machinability of the two types of materials leads not only to high tool wear but also to poor surface integrity due to the severe thermo-mechanical loads induced during the machining process [101]. It becomes more essential to investigate the surface integrity of the machined workpiece with difficult-to-cut materials to improve the service life and quality of the finished components especially those working in extremely harsh environment. The cutting tools used for orthogonal cutting tests are customised uncoated carbide insert and for the fillet surface turning is the CVD coated carbide tool.

4.2 Orthogonal cutting tests

Orthogonal cutting tests were implemented in dry condition as shown in Fig. 4.1a, where a solution treated and aged nickel-based superalloy (Inconel718; Hardness of 45 HRc) with a dimension of 32 mm×3.25 mm×30 mm was employed as the workpiece, and a customised uncoated carbide insert WC-6%Co with the width of 3.9 mm was used. Table 4.1 summarises the tool geometry and cutting parameters used in the cutting tests. The clearance angle α of the tool is 7° in all the cases. Prior to the experiment, the edge radius of the tools were measured under Alicona Infinite Focus Optical 3D microscope to ensure their accuracy, as shown in Fig. 4.2. An infra-red thermal camera with a frame rate of 650 Hz was used to monitor the cutting temperature during the machining process. The chips produced during the experiment were collected for analysing with the help of Alicona Infinite Focus Optical 3D microscope. Residual stress distribution in both machined workpiece surface and subsurface was measured by X-ray diffraction technique using $sin^2\psi$ method with the help of electropolishing technique. An aperture with a diameter of 1 mm was employed, and a manganese (Mn) tube was applied for residual stress measurement. The measurement was carried out in a range of -30° to 30° angles and 5 times repetition were done. More details of the residual stress measurement are presented in Table 4.2. In order to measure the cutting force and feed force, the additional experiment was carried out as shown in Fig. 4.1b, in which the forces were measured with a Kistler force dynamometer under the mentioned cutting conditions.

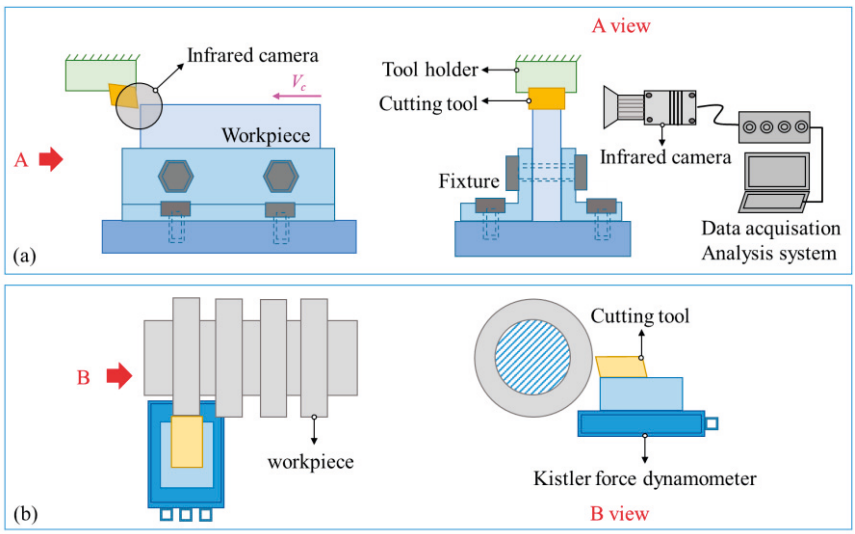

Figure 4.1.
The schematic of experimental set-up for orthogonal cutting illustrating the (a) temperature measurement and (b) cutting forces measurement.

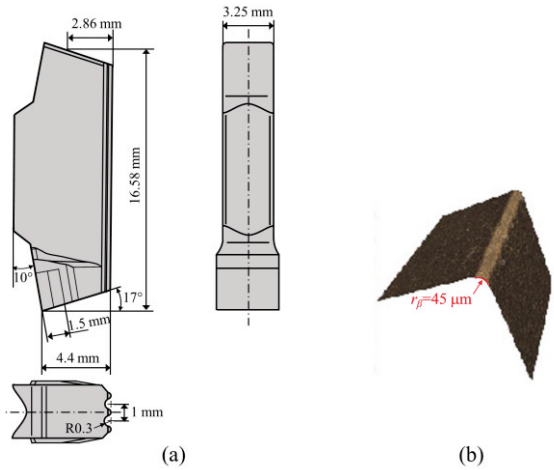

Figure 4.2.
Cutting tool used in the cutting tests with γ=0°, r_β=45 μm: (a) geometry parameters; (b) measured edge geometry.

Table 4.1.
Cutting parameters and tool geometry used in the experiment.

Test	Cutting speed (V_c/m·min^{-1})	Uncut chip thickness (h_1/mm)	Rake angle (γ/°)	Tool egde (r_β/μm)	Flank wear (VB_s/μm)
1	80	0.25	10	25	0
2	40	0.05	10	25	0
3	80	0.05	10	25	0
4	80	0.05	-10	25	0
5	60	0.15	0	5	0
6	60	0.15	0	25	0
7	60	0.15	0	45	0
8	60	0.15	0	25	200
9	80	0.25	-10	25	0
10	80	0.25 (1st cut); 0.05 (2nd cut);	10	25	0

Table 4.2.
XRD conditions for residual stress measurement.

Type	Constants
Tube	Mn Kα
Diffraction plane, Brag angle	{311}, 2θ=151.88°
Peak location	Gaussian
Number of β inclinations	6 (-30°≤ψ≤30°)
1/2S_2 (Elastic constants)	6.33E-6 MPa^{-1}
-S_1 (Elastic constants)	1.42E-6 MPa^{-1}

4.3 Fillet surface turning

Machining tests were conducted on an SMT 500 CNC lathe, as shown in Fig. 4.3a. AISI 304 stainless steel was used as workpiece material. Machining was done with CVD coated carbide tools (ISO DNMA150608) and the tool holder is DDHNL2525M15. The workpiece has been pre-machined as a fillet surface, and then a new tool is employed to start the experiments. The edge radius of the tool was pre-measured by Edge Master Module of Alicona to ensure its accuracy (Fig. 4.3b). The tool geometry and cutting parameters used in the experiments are summarized in Table 4.3. The cutting forces were measured with the Kistler 9129AA dynamometer. The residual stress distribution along the machined workpiece depth at both the outer face and the end face were inspected by X-ray diffraction technique that has been previously described. Since it is difficult to detect the residual stress underneath the fillet surface, only the surface residual stress at the position of Φ=30° and 60° on the arc face were detected. As to the residual stress measurement, five times repetition were implemented to minimize the measurement errors.

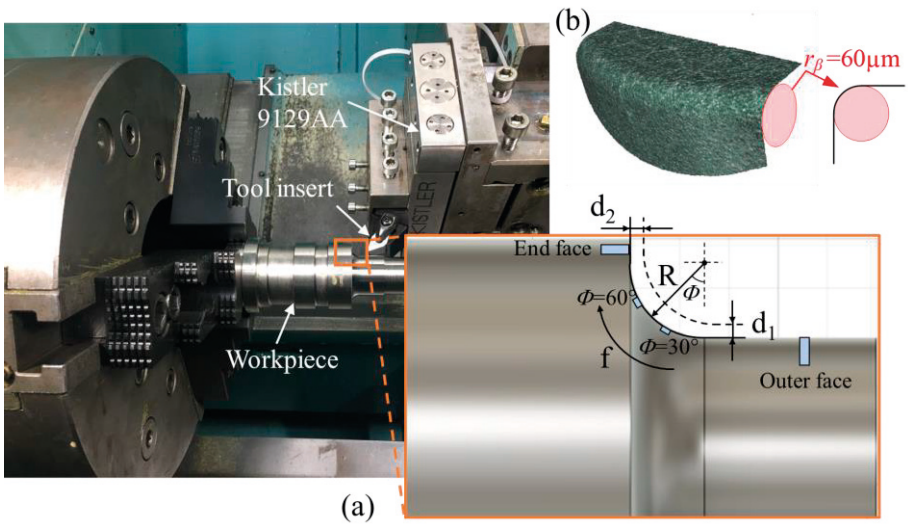

Figure 4.3.
Experimental setup: (a) cutting experiments and force measurements; (b) edge geometry.

Table 4.3.
Tool geometry and cutting conditions.

Tool geometry	Major cutting edge angle, K_r (°)	72.5
	Tool cutting edge inclination angle, λ_s (°)	-6
	Normal rake angle, γ_n (°)	-6
	Insert included angle, ε_r (°)	55
	Tool nose radius, r (mm)	0.8
	Tool edge radius, r_β (μm)	60
Cutting conditions	Fillet surface radius, R (mm)	5
	Depth of cut in outer face turning, d_1 (mm)	0.3
	Depth of cut in end face turning, d_2 (mm)	0.3
	Cutting speed, V_c (m/min)	180
	Feed, f (mm/r)	0.15

5 Results and discussion

This chapter presents results from simulation and related discussion. The model validation in terms of temperature, forces, chip morphology and residual stresses are conducted, and the discrepancy between the experimental and simulated results are discussed. In addition, the residual stress generated from different circumstances (segmented chip, tool geometries, multiple cuts, fillet surface turning) are analyzed in detail.

5.1 Model validation

5.1.1 Validation of orthogonal cutting modelling

The temperature fields obtained from the experiment and simulation are compared in Fig. 5.1. The comparison of temperature fields from the experiment was conducted at the cutting times of around 0.01s and the ones from the simulation were carried out at the cutting times of about 5e-4 s. It should be noted that there are different sources of error that both arise from the experiment (emissivity issues, out of plane measurements, etc.) and simulation (friction modelling, heat transfer at the interface, very short cutting times due to the computational cost, etc.). Even so, the measured and predicted temperature fields presents good agreement in terms of the changing trend as a function of rake angle and uncut chip thickness. Table 5.1 shows the comparison between the experimental cutting forces and the predicted ones. It is shown that the FE model has a better correlation for cutting force than feed force. Apart from the deviation of the material flow stress and simplified friction model used in the FE model, the underestimated feed force is also likely attributed to the rapid deformed shape that occurred to the tool edge in the actual cutting test. With the coupling numerical simulation and experimental investigation of orthogonal cutting of AISI 304 with WC-10%Co tool, Laakso et al. [102] found that the cutting edge deformation in the first seconds of tool life has a significant effect on the magnitude of feed force. In addition, Fig. 5.1 presents the chip morphology from both simulation and experiment, showing that the predicted chip morphology is in good agreement with the experiment ones regarding the type and dimensions of the chip morphology.

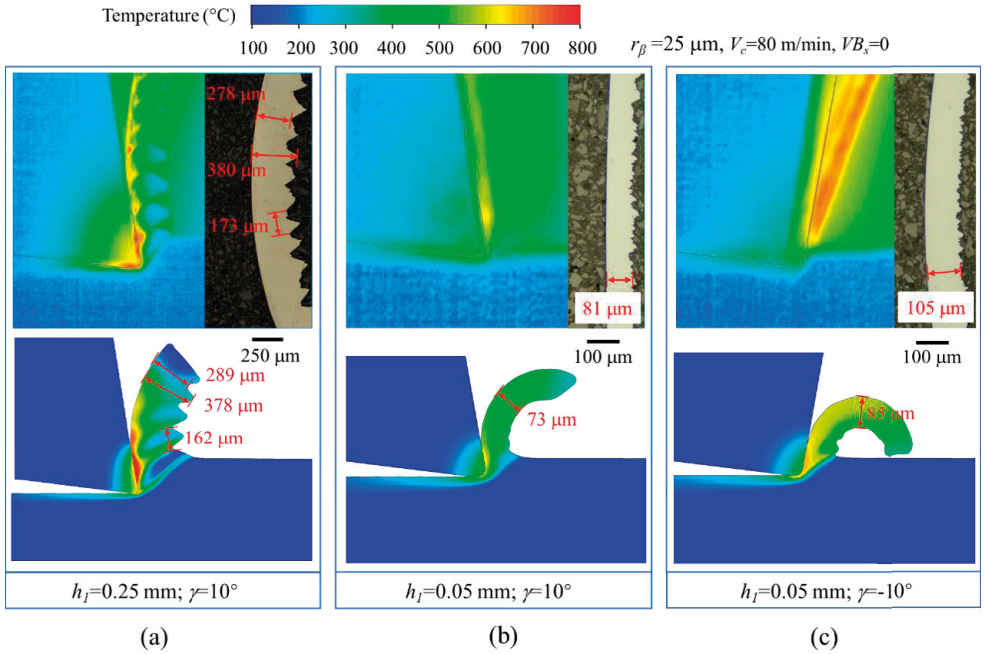

Figure 5.1
Comparison of the measured (the upper figures) and simulated (the bottom figures) temperature fields and chip morphology under different cutting conditions.

Table 5.1.
Comparison of cutting forces between experiment and simulation.

Cutting conditions	Experiment		Simulation (average value)	
(r_β=25 μm, V_c=80 m/min, VB_s=0)	F_c (N/mm)	F_f (N/mm)	F_c (N/mm)	F_f (N/mm)
γ=10°, h_1=0.05 mm	190±10	175±5	160	115
γ=10°, h_1=0.25 mm	575±20	250±10	570	170
γ=-10°, h_1=0.05 mm	260±15	201±5	193	160

When finishing the cases, many paths from different locations on the simulated surface to the bottom are selected, and the average residual stress curves are calculated to improve the reliability (Fig 5.2a). It is shown in Fig. 5.2b that the prediction of residual stresses on the machined surface and in the subsurface follows the experimental profile very well. For the maximum tensile and compressive stress prediction, the prediction error is below 26.1% and 17.5% respectively. In general, an exact match between numerical and experimental results could not be expected because of the different sources of errors in each one of them. The main sources of errors in simulation could be summarized as: homogeneous material assumption, simplicity of the material model and friction laws, neglect of the complex microstructural changes (twinning, grain refinement, etc.) in the superficial of the workpiece under the action of the elevated temperature and serious deformation, as

well as the invariable of the tool edge geometry throughout the cutting process. On the other side, the main sources of errors encountered in experiment could come from the measurement error of residual stress [4]. In addition, prior to the experiment, more than one cut is required to clear and flatten the workpiece surface, which brings a certain magnitude and depth of residual stress and plastic strains within the workpiece [103]. The final residual stress distribution achieved in experiment will be more or less affected by these accumulated residual stresses and plastic strains.

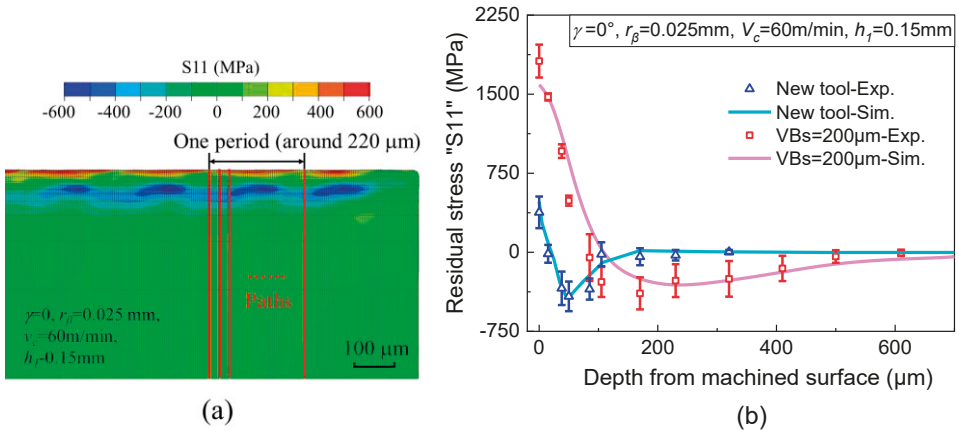

Figure 5.2
Simulated residual stress distribution: (a) the selected paths; (b) comparison of the measured and predicted residual stress profiles.

5.1.2 Validation of fillet surface turning modelling

The simulated forces components, chip morphology and residual stresses are compared with the experimental results in this section. It is shown in Fig. 5.3 that the FE model has a better correlation for F_c compared to F_t and F_r. The discrepancy of F_c are within 4.1–19.4% while the other two force components are predicted 32.3–62.5% lower than the experimental results when analyzing the mean value of the force components. However, even if the mismatch between the experimental and simulated forces is caused by many sources which are already mentioned above, the present fillet surface turning model can predict the same trend of the force components.

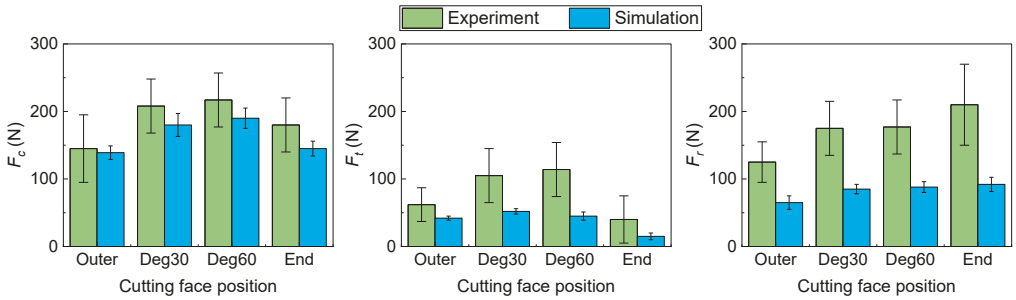

Figure 5.3
Comparison of the predicted force and measured forces.

The average chip thickness (T) and width (W) are investigated to quantitatively compare chip morphology obtained from experiments and simulation. It is shown in Fig. 5.4 that an obvious segmented chip morphology is produced both in simulation and experiment. In addition, the same trend of chip geometry changing is achieved both in experiment and in simulation. Based on the results, the difference in average chip thickness and width between simulation and experimental values are in the range of 3.9-10.8% and 3.9-18.8% respectively, showing the accuracy and reliability of proposed FE models.

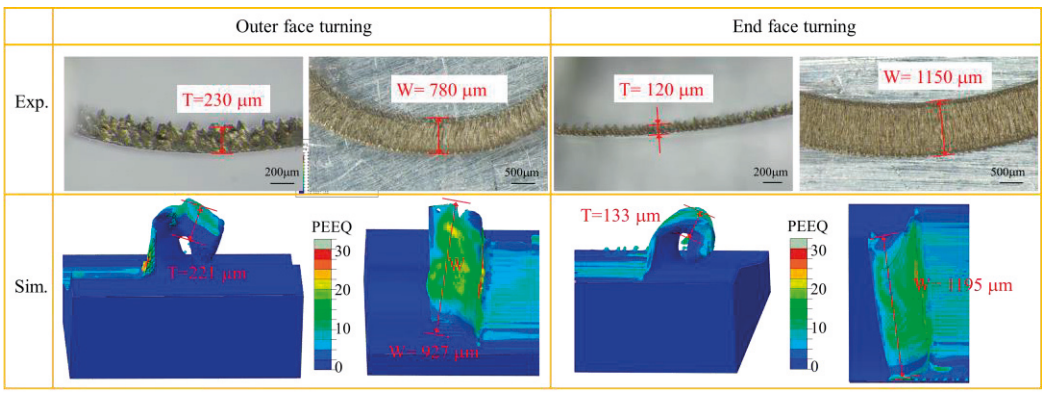

Figure 5.4
Comparison of the predicted and measured chip morphology.

Fig. 5.5 compares the experimental and simulated surface residual stress at the four specific cutting faces. The simulated results match reasonably well with the measured results, showing a similar decreased trend with the maximum difference of around 20.0% when compare the average value. It is possible to deduce that the

proposed model was able to predict distribution of residual stresses with reasonably accuracy.

The sources of errors encountered in residual stresses prediction during fillet surface turning could be summarized as: not a very refined mesh, absence of cooling down step due to the limited computing resources, and some already mentioned reasons (the discrepancy of material flow stress, simplicity of friction model, assumption of a pure homogeneous material, and a consistent tool geometry utilised in the F.E. model, etc.). On the other side, the sources of errors from experiment is related to the residual stress measurement error [4] and the pre-existed residual stresses fields produced by the pre-machined operation prior to the experiment.

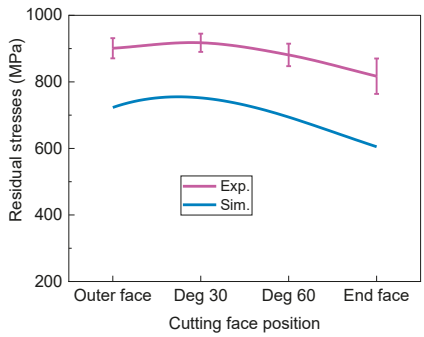

Figure 5.5
Comparison of the measured and simulated surface residual stresses.

5.2 Effect of chip morphology

It was recognized [37] that the homogeneous distribution of residual stress at a machined surface was observed when giving rise to a continuous chip. However, the residual stress distributions under the segmented chip and the corresponding mechanism are rarely reported. Our simulation results show that there are two types of cyclic evolution of residual stresses when producing segmented chips, as shown in Fig. 5.6. It is shown that the residual stress distribution in higher stress zones (paths1 and 3) shows a similar trend of hook-shaped profiles in the two cases, while the residual stress profiles in the lower stress zone are significantly different. In case 1 (path 2), compressive residual stress of -507 MPa is generated on the surface, followed by a maximum tensile of 823 MPa at a depth of 7 μm and again the peak compressive of -613 MPa penetrating to 50 μm below the surface. However, in case 2 (path 4), a hook-shaped residual stress profile is obtained with a lower magnitude of peak tensile and compressive values compared to that along path 3. A similar type of cyclic residual stress fields to that in case 2 was also reported in the study [10]. Despite the discrepancy of the two types of residual stress evolution, they share

the common characteristic that there exist higher and lower stress zones in the machined workpiece in both cases. In addition, the residual stress on the surface in the lower stress zone has the potential to become compressive. To explore the reason for the generation of the lower residual stress zones, attention is focused on the steps portraying the generation of one chip segment during the cutting period from 380 μs to 560 μs in case 1.

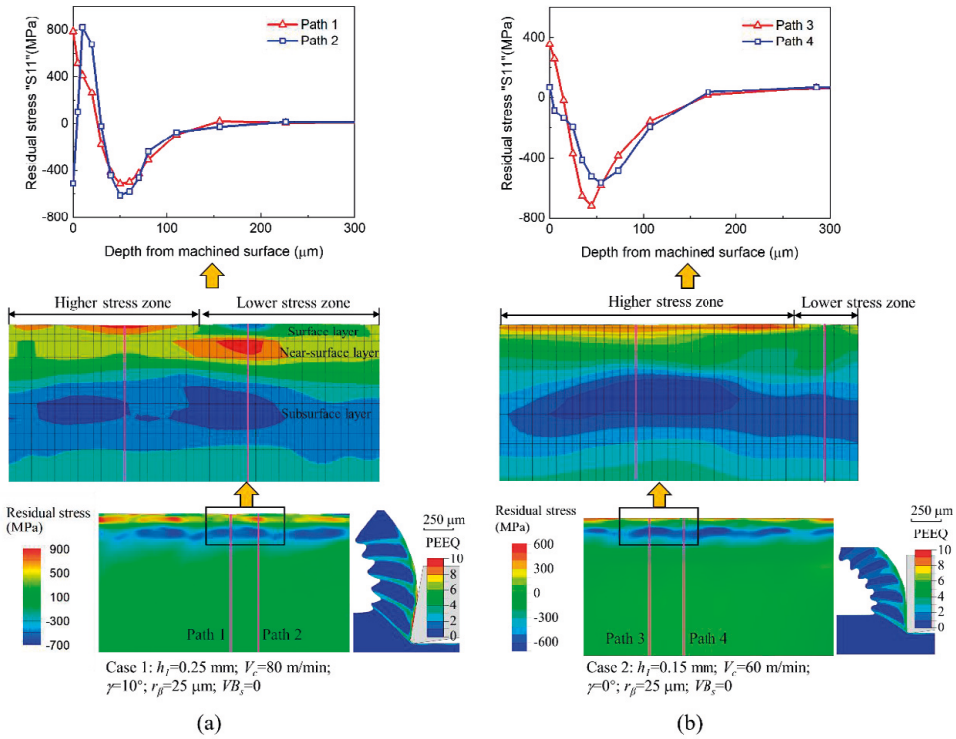

Figure 5.6
The two types of cyclic residual stress distributions and the corresponding chips under different cutting conditions.

Fig. 5.7a gives the evolution of material degradation during one chip segment generation, presenting that the formation of one segment includes two stages. The first stage takes place during 380 μs to 460 μs, in which the shear band starts at the tool tip and propagates toward the chip free surface with the advancement of the tool. The second stage characterizing the upward movement of the generated shear band along the tool rake face occurs from 460 μs to 560 μs of the cutting time. The generated residual stress distribution during this time period before the workpiece cooling down is shown in Fig. 5.7b. It is demonstrated that the lower stress zone is produced at the intermediate time during one chip segment generation. To reveal the mechanism of this reduced surface residual stress, the variation of the

mechanical and thermal loadings acting on the machined surface during the same period are analysed.

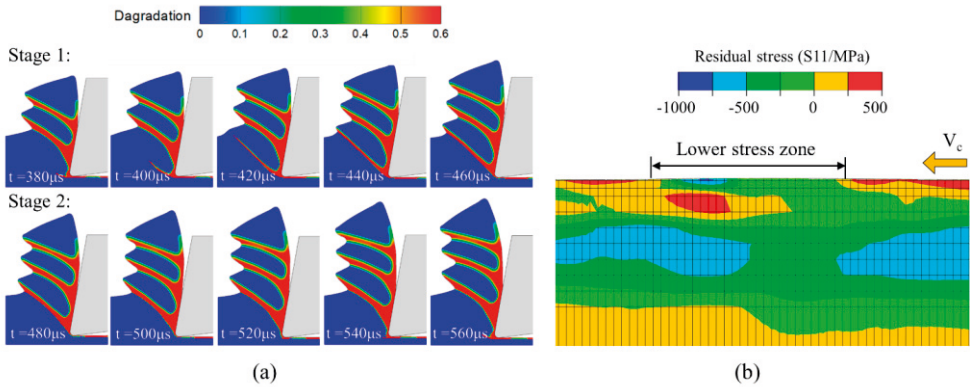

Figure 5.7
(a) Distribution of material degradation during one chip segment genesis, and (b) the generated residual stress distribution during this period before the workpiece cooling down.

The evolution of the maximum temperature on the machined surface is extracted during this period (Fig. 5.8a). This value increases during stage 1 and decreases during stage 2. The reason for this phenomenon is that the equivalent plastic deformation near the tool tip increase during stage 1 with the formation of the shear band. This leads to an increase in temperature around this area. On the contrary, with the move away of the generated shear band during stage 2, the temperature decreases as a result. It is also noted that the value of maximum surface temperature varies within 56 °C, which is limited to generate the cyclic residual stress field. Furthermore, the periodical residual stress field shown in Fig. 5.7b is formed directly after the tool pass by. At this moment, the temperature in this region is still high enough (higher than 300°C) and the thermal-induced residual stress is not fully introduced. Therefore, it can be deduced that the periodical residual stress distribution is primarily related to the variation of the mechanical load acting on the machined surface.

The evolution of the cutting and feed forces during the cutting process are shown in Fig. 5.8b, It can be seen that an evident cyclic evolution of the forces is found which is caused by the generation of segmented chips, while the same trend of cutting forces with the segmented chip is also observed in [104]. This cyclic evolution of forces is related to the material degradation distribution that is shown in Fig. 5.7a. At stage 1, a decrease in cutting force is noted due to a loss in material stiffness propagating through the shear band, while the feed force increases as a counter effect. At stage 2, the cutting force recovers resulting from the transferring damaged material, and, on the contrary, a reduction of feed force is found. This

cycle repeats throughout the cutting process, and it means that a greater degree of serration should give a larger amplitude of the cutting force and feed force.

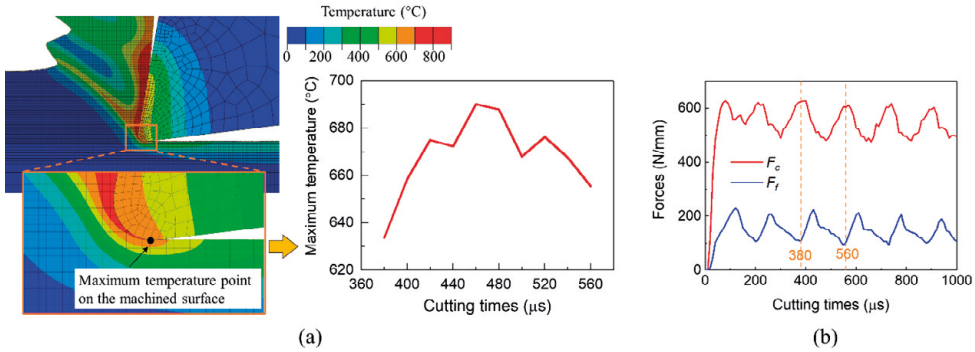

Figure 5.8
Thermal and mechanical load: (a) the evolution of maximum temperature on the machined surface; (b) the variation of cutting and feed forces.

To further reveal the effect of mechanical load on residual stress distribution, local normal/tangential stress is introduced. As it is known, during the cutting process a certain amount of work material is either pushed upward by the rake face and separates from a bulk material to form chip or ploughed under the cutting edge and finally become the machined surface. The point where the material flow separates to form the chip and machined surface is stagnation point S, as presented in Fig. 5.9a. As mentioned previously, severe compressive deformation takes place around and ahead of the cutting edge, becoming the source of mechanical induced tensile residual stress. On the other hand, the material ploughed down the tool experiences severe tensile plastic deformation exerted by the tool flank face when the cutting edge passes by it, and thus the compressive residual stress is induced in the machined workpiece. Therefore, the generation of a lower stress zone during one segment chip formation is likely attributed to the variation of tool stretching effect, which is indicated by the local normal/tangential contact stress on the flank/workpiece interface in the present study. These two kinds of stress are the calculation of the normal (CNORMF) and tangential (SHEARF) components of the local contact force divided by the flank/workpiece contact area (Fig. 5.9a). The local normal/tangential stress variation acting on the SF part of the tool during the specific time period is shown in Fig. 5.9b. An increase in both stresses is noticed during stage 1, which is due to the increased feed force in this period as mentioned above, and vice versa for stage 2. It can be deduced that when the local stresses are relatively lower, the stretching effect applied on the newly machined surface is weakened thus more tensile residual stress is produced at the surface layer. With the increase in these stresses, the material below the tool edge is stretched more severely thus less tensile residual stress is generated in the surface layer. When producing a

lower degree of chip serration, a slightly increased feed force (local normal/tangential stress) is expected during stage 1. Thus, the decrease in surface residual stress in the lower stress zone is not significant, as the case 2 in Fig. 5.6b. However, in the cutting process giving rise to a larger degree of chip serration a significant increase in feed force (local normal/tangential stress) is induced during stage 1, leading to a significant decrease in the surface residual stress in the lower stress zone, as the case 1 in Fig. 5.6a. Since the compressive residual stress is induced in the subsurface layer, the corresponding tensile residual stress is generated in the near-surface layer to maintain an equilibrium state.

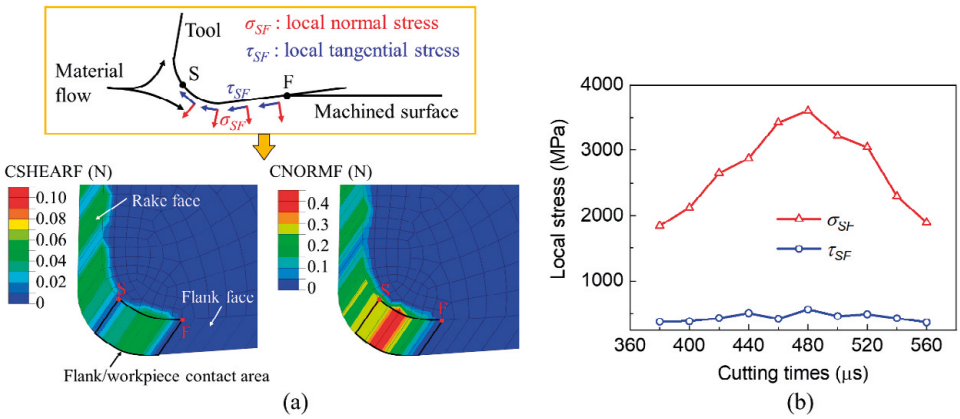

Figure 5.9
(a) Method for obtaining the local normal/tangential stress acting on the tool flank face, and (b) the variation of local normal/tangential stress during one chip segment generation.

It can be concluded that a cyclic residual stresses distribution are generated on the machined workpiece when a segmented chip is formed. This is mainly attributed to the periodical change of mechanical load on the machined surface during chip segments generation rather than the thermal load. Specifically, the feed force increase firstly and then decreases during one segment genesis. It is the increased feed force that causes an increase in the local normal/tangential stress acting on the machined surface, leading to a less tensile residual stress in the lower stress zone. This effect is more obvious when producing a larger degree of chip serration, in which compressive residual stress will be generated at the surface layer of the lower stress zone. To maintain an equilibrium state, tensile residual stress is formed in near-surface layer in this region.

5.3 Effect of tool geometries

The contradictory residual stress distribution findings have been briefly reviewed in section 2.8.2. In this section, the formation mechanism of residual stress will be explored in detail for different tool geometries by identifying the role of mechanical and thermal loads in the cutting process. To achieve this, six simulation cases are employed, as shown in Table 5.2. The values of the friction coefficient for each case that are calculated according to the experimentally obtained forces (Eq. (3.8)) are also presented.

Table 5.2.
Cutting parameters and tool geometry used in the numerical simulation.

Test	Cutting speed (V_c/m·min^{-1})	Uncut chip thickness (h_1/mm)	Rake angle (γ/°)	Tool egde (r_β/μm)	Flank wear (VB_s/μm)	Friction coefficient (μ)
1	80	0.05	10	25	0	1.32
2	80	0.05	-10	25	0	0.52
3	60	0.15	0	5	0	0.69
4	60	0.15	0	25	0	0.75
5	60	0.15	0	45	0	0.89
6	60	0.15	0	25	200	0.98

5.3.1 Temperature distribution on workpiece in cutting area

Fig. 5.10a shows that the workpiece temperature around the tool tip slightly increases when using a rake angle of -10º compared to the one with the rake angle of 10º. This can be explained by the fact that more severe deformation in the shear zone is induced by the rake angle of -10º with a smaller shear angle (Fig. 5.11). In addition, when using the rake angle of -10º, a severer extrusion and friction between tool rake face and chip is also expected. As a consequence of the combined plastic deformation and frictional work, the temperature around the cutting tool with the rake angle of -10º is higher than that with a rake angle of 10º.

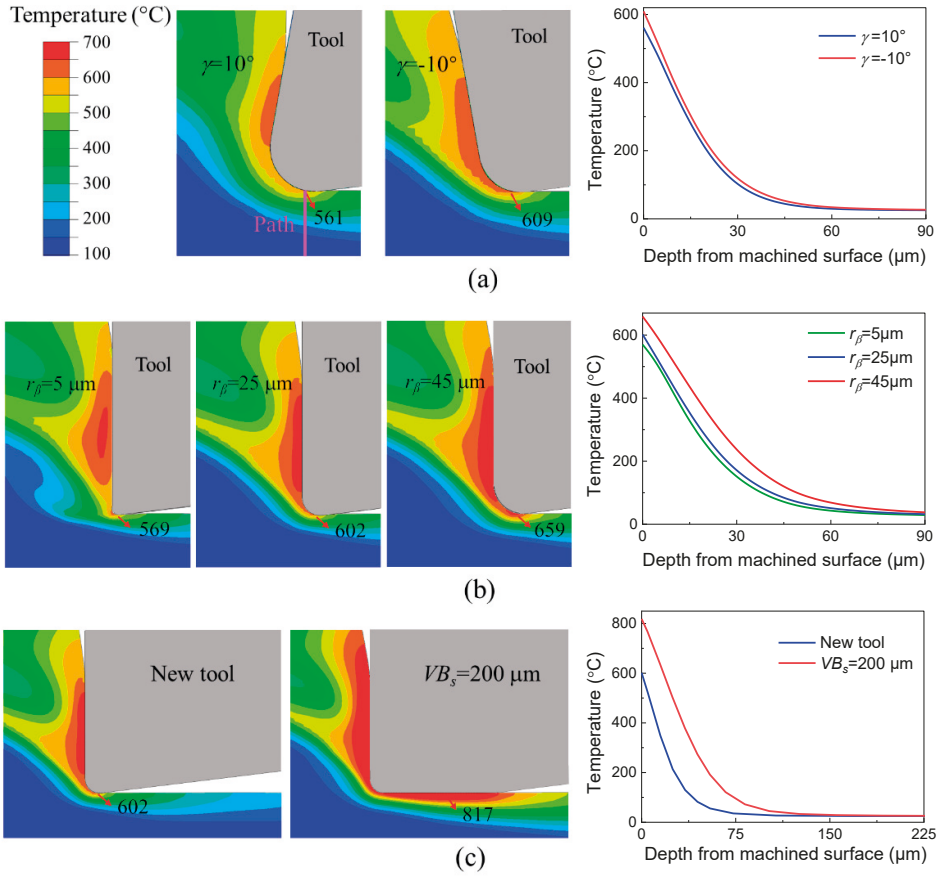

Figure 5.10
Workpiece temperature distribution around tool edge and along workpiece depth with different tool geometries. Effect of (a) tool rake angle; (b) edge radius; and (c) flank wear.

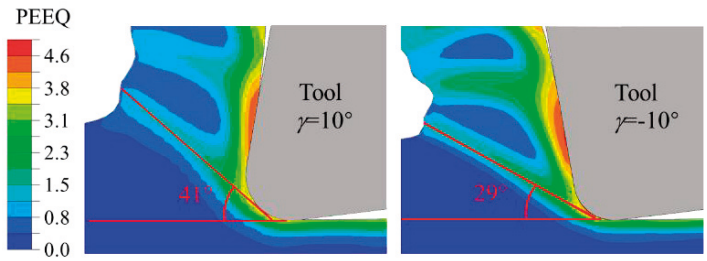

Figure 5.11
Equivalent plastic strain and shear angle under different rake angle tools.

It is shown in Fig. 5.10b that the surface temperature increases with the increasing tool edge radius. As described previously, the compressed material ahead of the tool tip will be split into two parts: one forms the chip and the other one forms the newly machined surface. Fig. 5.12 illustrates the material flow around the tool with different edge radius. It is shown that the length of part SA is much longer for the edge radius of 45 μm than that with 5 μm. This means that when using a larger edge radius, the material flowing upwards along the rake face experiences more deformation of extrusion by a larger area of part SA which somehow shows an influence on the temperature like employing a negative effective rake angle tool. Meanwhile, the height of the ploughed material (d) increases with an increasing edge radius, producing a larger plastic deformation in the machined surface side. The plastic deformation increase on both side with the edge radius increasing from 5 μm to 45 μm, generating more heat around the tool edge. Also, a larger contact area between tool edge and workpiece is found with a larger tool edge radius, in which more heat is generated from frictional work. As a joint result of more serious plastic deformation and increased frictional work when using a larger tool edge radius, the workpiece temperature will significantly increase.

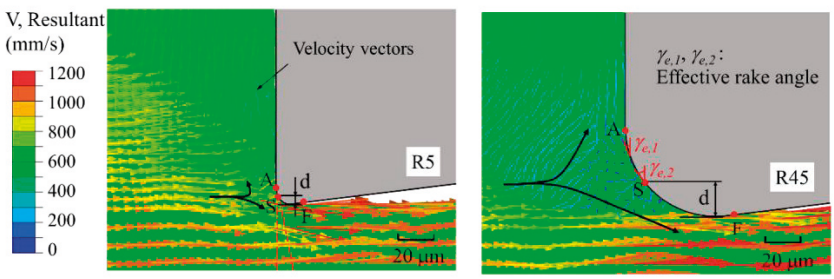

Figure 5.12
The material flow around the tool tip with edge radius.

Fig. 5.10c shows that a larger magnitude and area of the high temperature is generated in the machined surface when the tool changes from a new to a worn one. This can be explained that the frictional work between tool flank wear and machined surface significantly increases with a worn tool, thus, a higher and larger area temperature field in the surface/near-surface layer is generated.

5.3.2 Cutting forces and local normal/tangential stress

It is shown in Fig.5.9a that both the cutting force and feed force increase with the rake angle changing from positive to negative, which is due to the more seriously squeezed chip with a smaller shear angle. Thus, an increased local normal/tangential stress acting on the material behind the tool tip is obtained, as shown in Fig. 5.14a.

As a result, more tensile deformation behind the cutting edge is generated by increased stretching stress. Fig. 5.13b shows that an increasing edge radius leads to a larger cutting force and feed force. As it is known, increasing the bluntness of the cutting edge tends to release the stress concentration between the tool tip and the workpiece. Therefore, larger forces are required to produce stress that achieves the workpiece material shearing stress with a rounded edge to accomplish the cutting process. However, the local normal/tangential stress shows a different trend with the cutting force and feed force. As illustrated in Fig. 5.14b, the local normal/tangential stress increases when the edge radius increased from the sharp one to the medium one, while decreases when the edge radius continue increasing to the larger one. This phenomenon is likely attributed to the contact area. The increase of cutting force is not significant enough to compensate the influence of contact area increasing when edge radius varies from 25 μm to 45 μm, thus, a decline of the local normal/tangential stress is obtained. As to the variation of flank wear, it is reported [105] that tool flank wear does not affect the shear angle and shear stress, but results in an additional rubbing or ploughing force on the wear land and thus an increase in the overall cutting forces. The increasing force components with flank wear is also found in Fig. 5.13c. It is noticed in Fig. 5.14c that the local normal stress significantly decreases from a new tool to a worn tool, which is caused by the large degree of the increased flank/workpiece contact area. In addition, as the increased friction coefficient with a worn tool (Table 5.2), the tangential stress increases by 209 MPa as a result.

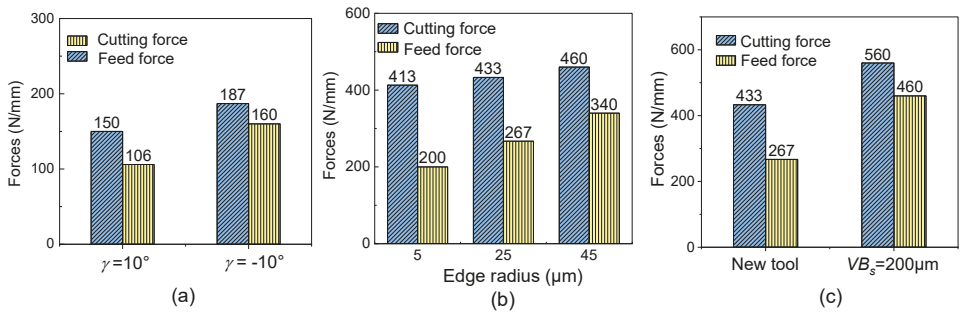

Figure 5.13
Influence of tool geometry on cutting and feed force. Effect of (a) tool rake angle; (b) edge radius; and (c) flank wear.

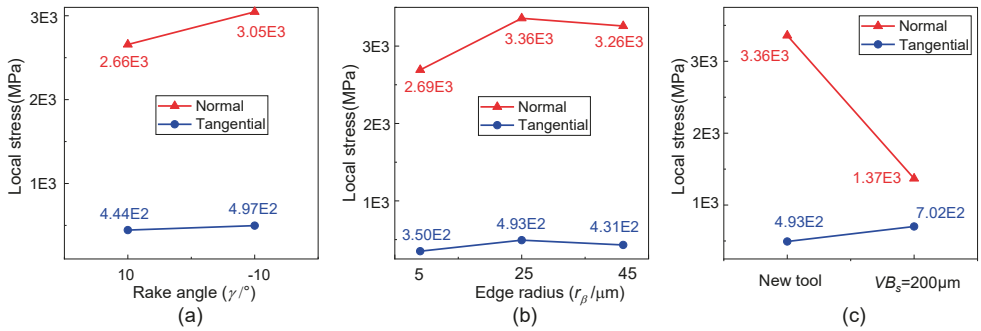

Figure 5.14
Influence of tool geometry on local normal and tangential stress. Effect of (a) tool rake angle; (b) edge radius; and (c) flank wear.

5.3.3 Residual stresses and plastic deformation depth

Fig. 5.15a shows the influence of rake angle on the residual stress distribution. When the rake angle decreases from 10° to -10°, the tensile stress at the surface decreases even though the temperature at the machined surface increases. As explained in section 2.4, the magnitude of surface tensile residual stress is not only determined by the thermal effect but also the mechanical loads contribute a lot as well. When the rake angle changes from 10° to -10°, the local normal/tangential stress applied on the material behind the tool tip increases significantly (Fig. 5.14a). The increase of mechanical induced tensile plastic deformation overwhelms the increase of thermal induced compressive strain in surface/near-surface layer. Therefore, a slightly decrease in surface tensile residual stress is obtained. In addition, the increased tool stretching effect with a negative rake angle extends to the subsurface layer, leading to a larger degree and thickness of the tensile plastic deformation in this region. Therefore, the negative rake angle induces higher compressive residual stress in the subsurface layer, and penetrates deeper into the workpiece. This can be validated from the equivalent plastic strain variation caused by rake angle changing. The equivalent plastic strain in Abaqus/Explicit 6.14-2 stands for the sum of the absolute value of the plastic strains induced by the thermal-mechanical load, and it will continue to increase if the material is plastically deformed regardless of compressed or stretched. As shown in Fig. 5.16a, a larger and deeper plastic strain is induced by a negative rake angle tool compared to that by a positive one.

When comparing residual stress generated from the tool edge radius of 5 μm and 25 μm, it is found that the surface stress has significantly increased with a larger edge radius. It is shown in Fig. 5.10b that the temperature in these two scenarios only increased slightly and in Fig. 5.14b that the stretching effect is more pronounced with a 25 μm tool edge, which are supposed to generate more compressive residual stress in surface/near-surface and sub-surface layer. This is

opposite to the result shown in Fig. 5.15b. Actually, the reason for the increased surface residual stress when the edge radius increases from 5 μm to 25 μm is related to the ploughed effect of the tool edge. When using the edge radius of 5 μm, there is a small amount of compressed material ahead of the tool edge being ploughed into the newly machined surface, while when the edge radius increases to 25 μm, a larger amount of compressed material is ploughed under the tool edge. These increased amounts of compressively deformed material have brought significant additional tensile residual stress in surface and near-surface layers that contributes to the final residual stress profile. When the edge radius increases from 25 μm and 45 μm, the increased surface tensile residual stresses is due to the combined effect of ploughed effect and increased temperature as shown in Fig. 5.10b.

Regarding the maximum compressive stress comparison, Fig. 5.15b shows that it increases when the edge radius changes from 5 μm to 25 μm, but decreased as the edge radius continues to increase to 45 μm. This is attributed to the corresponding normal/tangential stress variation with edge radius changing, which are found to increase at first and then decrease (Fig. 5.14b). Thus, the material in subsurface experiences more tensile deformation when edge radius increases from 5 μm to 25 μm, leading to an increase in the magnitude of compressive residual stress. While when edge radius changes from 25 μm to 45 μm, the subsurface material is loaded less tensile deformation because the normal/tangential stress has decreased due to a larger contact area; therefore, the compressive residual stress generated with the edge radius of 45 μm becomes smaller. In addition, with increasing edge radius, the mechanical tensile plastic deformation depth becomes larger (Fig. 5.16b) due to a larger amount of material being ploughed into the same volume; therefore, a deeper distribution of compressive residual stress in subsurface layer is observed.

It can be seen from Fig. 5.15c that the magnitude and depth of the machined surface tensile residual stress are significantly increased with an increasing flank wear. The reason for that is the higher and larger temperature field in the surface/near-surface layer with flank wear as shown in Fig. 5.10c. In addition, it is clear in Fig. 5.15c that the maximum compressive residual stress in subsurface varies from -411 MPa for the new tool to -321 MPa for the worn tool which is caused by the largely decreased normal stress as already shown in Fig. 5.14c. Even if local tangential stress increases, the normal stress also has a significant influence on residual stress in the cutting direction. The decreased normal stress results in a less degree of tensile plastic deformation in surface/near-surface and subsurface layer caused by mechanical load, thus less compressive residual stress. On the other hand, it is obvious that compressive residual stress penetrates much deeper when using the tool with the flank wear. This is because a considerably higher temperature is produced by the flank wear in the sublayer material, and this elevated temperature field tends to reduce the yield strength of the material in this area [106]. Therefore, it leads to a deeper plastic deformation even if less stretching stress is applied, thus, much deeper compressive residual stress is generated as a result.

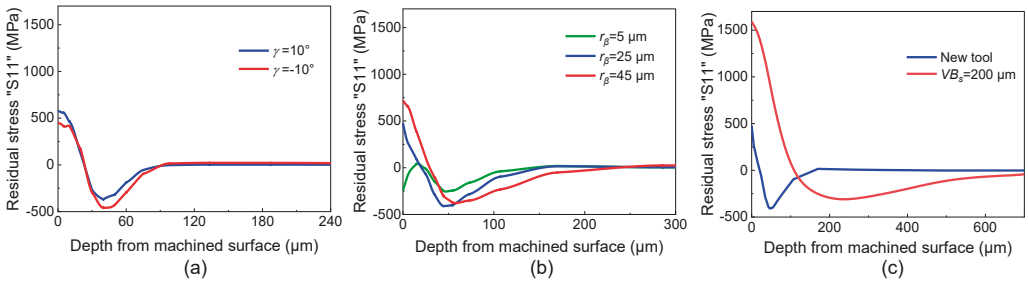

Figure 5.15
Influence of tool geometry on residual stresses distributions. Effect of (a) rake angle; (b) edge radius; and (c) flank wear.

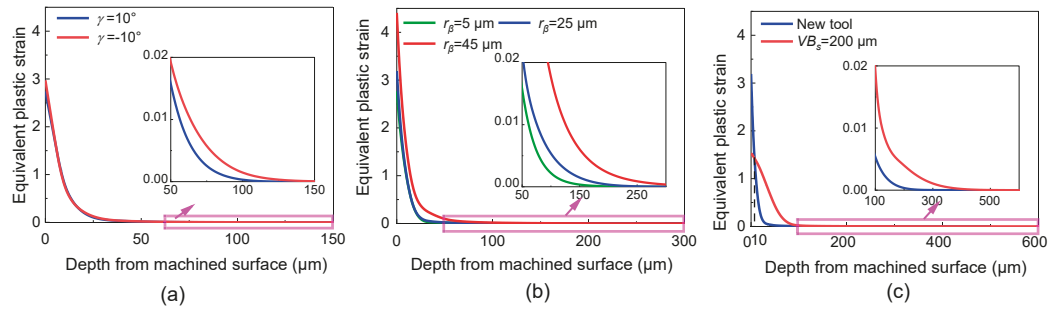

Figure 5.16
Influence of tool geometry on the equivalent plastic strain. Effect of (a) rake angle; (b) edge radius; and (c) flank wear.

It can be concluded that the residual stress profile induced by a negative rake angle becomes more compressive on the whole compared to that with a positive rake angle, which is mainly due to the increased tool stretching effect caused by the enhanced cutting force components. When using a tool with a larger edge radius or flank wear, the magnitude of surface/near-surface tensile stress will increase due to the enhanced temperature field. It is noted that the compressive stress is generated in surface/near-surface layer by a 5 μm edge radius, which is due to the absence of compressed material being ploughed into newly machined surface. Furthermore, it is found that the maximum value of compressive residual stress in sublayer is mainly determined by local normal/tangential stress exerted by the tool. The tool stretching effect will increase when tool rake angle changes from 10° to -10° or edge radius increases from 5 μm to 25 μm due to the increased cutting and feed forces, while decreases with edge radius increasing from 25 μm to 45 μm or a worn tool due to a larger contact area. As for the penetration depth of compressive residual stress, it is basically consistent with the plastic deformation depth that is influenced by many different aspects: local normal/tangential stress, ploughed effect, thermal-induced

reduced yield stress. The depth of compressive residual stress increases when using a negative rake angle due to the increased local normal/tangential stress of the tool. The depth is also increased when using a larger edge radius since more material is ploughed into the same volume and this tends to increase the thickness of the plastically deformed region. In addition, the reduction of the yield strength of the sublayer material under the elevated temperature effect allows a deeper plastic deformation and compressive residual stress distribution when using a worn tool.

5.4 Residual stress evolution in multiple cuts

As discussed in section 2.8.3, there are few studies investigating the effect of cutting conditions and tool geometries utilized in the previous cut on the residual stress evolution during multiple cuts. Therefore, 4 simulation cases (Table 5.3) are conducted in this section dedicating to explore the influence of previous cuts on the final residual stress distributions in multiple cutting of Inconel 718 alloy.

Table 5.3.
Simulation conditions.

Cutting sequences	Cutting conditions	Case 1	Case 2	Case 3	Case 4
1st cut	h_1/mm	0.05	0.25	0.25	0.25
	γ/°	10	10	0	10
	r_β/μm	25	25	25	45
2nd cut	h_1/mm	0.05	0.05	0.05	0.05
	γ/°	10	10	10	10
	r_β/μm	25	25	25	25

According to the experimental results, the values of the friction coefficient for different cuts are shown in Table 5.4. All the second cuts are performed using a constant coefficient equal to 1.32, which method was also used in previous literature [74,107].

Table 5.4.
The calculated friction coefficient for different multiple cuts.

Cases	Case 1	Case 2	Case 3	Case 4
1st cut	1.32	0.66	0.45	0.75
2nd cut	1.32	1.32	1.32	1.32

5.4.1 Effect of previous cuts

Effect of previous cuts on the residual stress evolution during multiple cuts are shown in Fig. 5.17. It is shown in Fig. 5.17a that residual stress become more compressive when uncut chip thickness increases from 0.05 mm to 0.25 mm, which is in line with the literature [62]. Even if an increased temperature at the machined

surface (Fig. 5.18a and b) is generated with uncut chip thickness of 0.25 mm, the machined workpiece in this case experience a significant increased stretching effect of the tool caused by the larger cutting and feed forces (Fig. 5.18c). Thus, a larger magnitude and a deeper depth of compressive stress is generated. Regarding the influence of the tool rake angle and edge radius on the residual stress distribution after the first cut, it has been previously analysed in detail in section 5.3, in which the trend of residual stress with different rake angle and edge radius is consistent with what presented here.

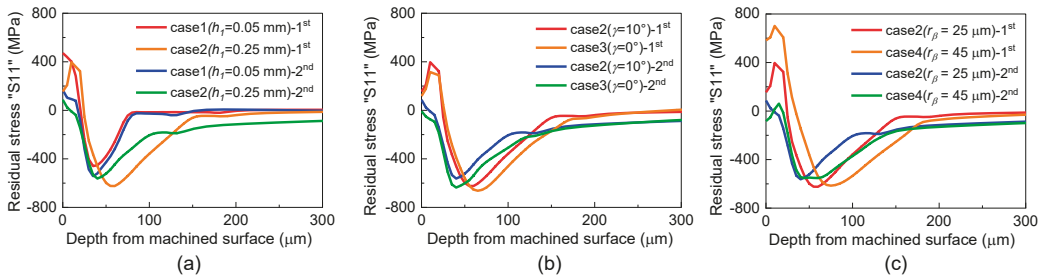

Figure 5.17
Effect of previous cuts on the residual stress evolution during multiple cuts; (a) effect of uncut chip thickness; (b) effect of rake angle; (c) effect of edge radius.

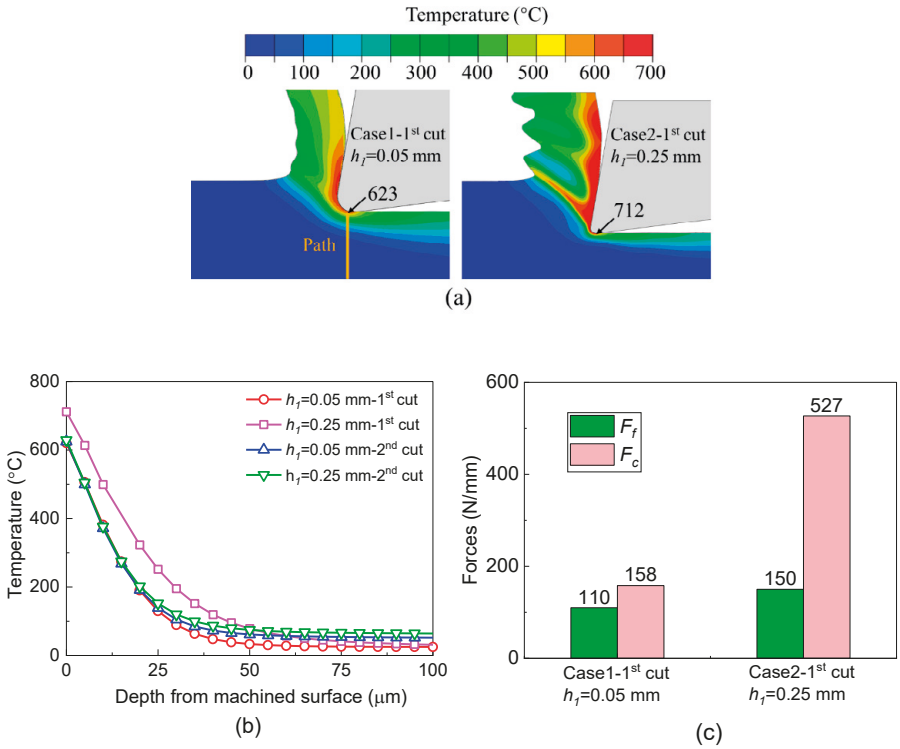

Figure 5.18
Effect of uncut chip thickness on temperature and forces: (a) temperature distribution during the first cut; (b) temperature evolution during multiple cuts; (c) forces during the first cut.

Under the mentioned various stress field produced by different first cuts, the second cut is carried out with the same cutting conditions for all the cases. Generally, Fig. 5.17 shows that the final residual stress becomes more compressive with the existence of the previous cut than the ones without it. In addition, the final residual stress will be more compressive when the previous cut is implemented at a larger uncut chip thickness or using a more negative rake angle, a larger edge radius tool.

It should be noted that for all the cases the secondly machined surface is located within the compressive residual stress area produced by the first cut. Another phenomenon worthy of attention is that the larger magnitude and depth of compressive residual stress in the subsurface left by the first cuts, the final stress state becomes more compressive. Therefore, it can be concluded that under the cutting conditions in the present study, the influence of various first-cut conditions (uncut chip thickness, rake angle, edge radius) on the final residual stress distribution is closely related to the firstly produced compressive stress distribution. Accordingly, investigating the origin of the first-cut induced compressive stress

states and their influence on finished residual stresses alteration are of utmost importance to understand the underlying mechanism of the residual stress evolution during multiple cuts

5.4.2 Loading cycle behaviours

Researchers have introduced the loading cycle behaviours of the machined material to provide an easier understanding of residual stress formation [20]. As explained in section 2.4, when a material element passes through the stress field along the cutting direction, it is subjected to a loading cycle by mechanical load. For mechanical loading conditions that are predominantly compressive, the resulting residual stress will be tensile, as presented on the left of Fig. 5.19b. In this figure, the material node is firstly compressed to a value beyond the yield strain, and the compressive stress is then unloaded and turn to be tensile to accomplish yield a second time. As the tool moves away, the tensile load is relaxed again until the elastic strain disappears, visualised by point A. These permanent compressive deformations are restrained by the underlying elastic region, continuing to be elastically stretched until the material returns to a state of zero strain (Point A′). Accordingly, the underlying elastically deformed region is compressed along the dashed line to reach a balanced state. Therefore, the resulting residual stress of the plastically compressed material point is represented by the distance between the beginning (point O) and end points (point A′) of the loading cycle. For the same reason, under the predominantly tensile loads, the material presents compressive residual stress owing to the action of the bulk material, as shown on the right of Fig. 5.19b. It can be applied to the thermal-induced tensile residual stress formation as well. It was already found that the thermal stress along the cutting direction is predominantly compressive [20]. As shown in Fig. 5.19c, thermal-induced compressive stress is generated in the superficial layer during the cutting process, causing compressive strain in this area. After cooling down, the inner part tends to prevent these materials from being compressed, and the resulting residual stress in the superficial layer is therefore tensile.

In the following sections, the loading cycle is used to explain the underlying mechanisms of residual stress alteration from the first cut to the second cut. It is noted that that the Johnson-Cook model used in the present study is the isotropic constitutive model [87], and it cannot take the Bauschinger effect into account in cyclic deformation of Inconel 718. Thus, all the loading cycles characterised in present study follows the isotropic stress-strain relation.

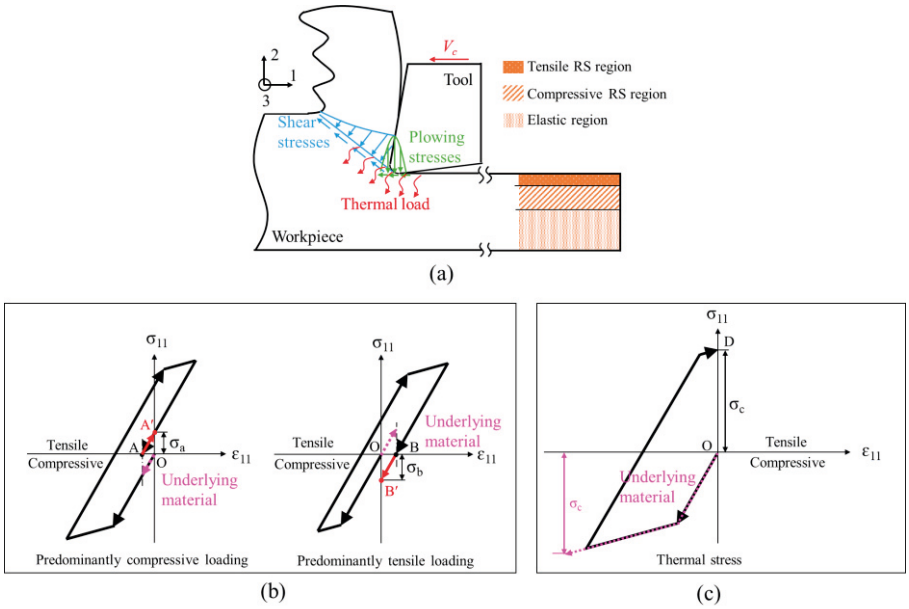

Figure 5.19
Residual stress formation in the orthogonal cutting process: (a) thermal-mechanical load acting on the machined surface; (b) mechanical-induced residual stress formation; (c) thermal-induced residual stress generation ([20,108]).

5.4.3 Plastic strain and stress analysis of the material nodes

It is already known that the existence of intermediately produced compressive residual stress tends to strengthen the compressive stress distribution within the final machined workpiece. In this dissertation, the loading cycles of the material nodes "A_1", "B_1", "A_2", "B_2" are characterized to investigate the reason behind this (Fig. 5.20a and b). Take material node A_1 as an example, the suffered compressive strain is indicated by the average value of maximum plastic strain (PE11) ahead of the tooltip, and the final strain of this node can be directly obtained from the final plastic strain distribution (Fig. 5.21a). Also, the compressive effect of the tool is expressed by the average value of maximum compressive stress (S11) ahead of the tooltip, and the stretching effect of the tool can be reflected by the local normal/tangential stress (Fig. 5.21b).

As for the thermal-induced residual stress, it is shown in Fig. 5.18b that during the first cut the workpiece temperature in the region deeper than 50 μm are slightly changed by the h_1 employed in the first cut. In addition, the workpiece temperature underneath the tool edge in the second cut is not influenced by different h_1 in the first cut. Therefore, it is reasonable to ignore the influence of thermally induced residual stress when comparing the loading cycle of the selected material nodes at the same depth.

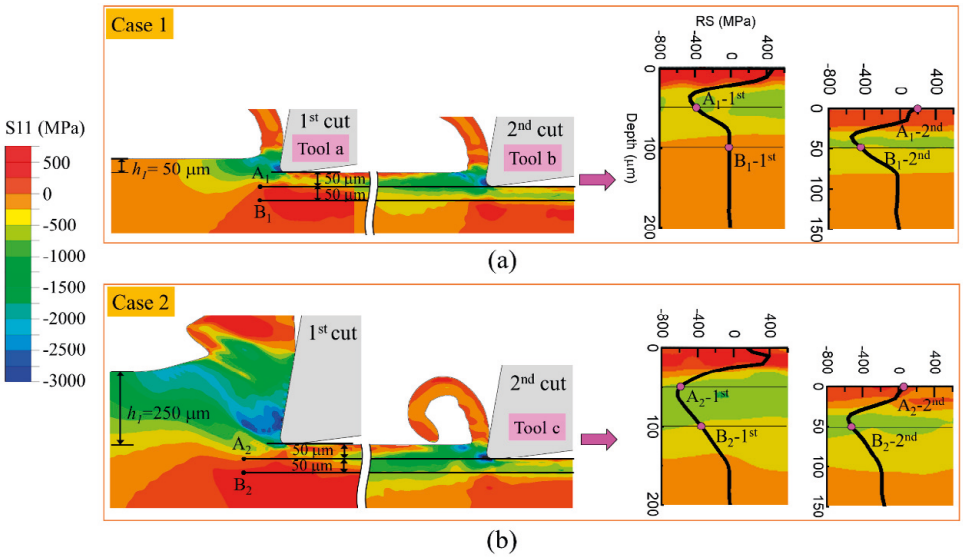

Figure 5.20
The position of the selected material nodes and the corresponding residual stress evolution during cutting sequences in (a) case 1; (b) case 2.

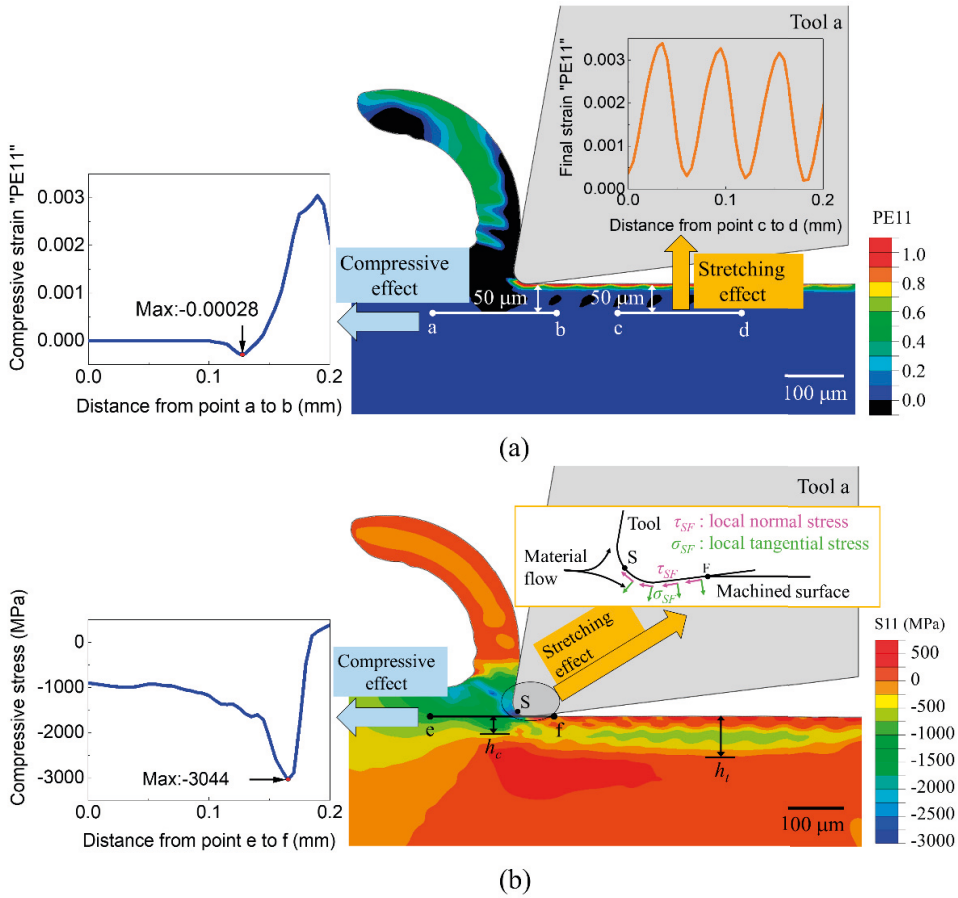

Figure 5.21
(a) The method for quantifying the compressive and final strain suffered by point "A_1" induced by mechanical load; (b) the method for indicating tool compressive and stretching effect.

5.4.4 Loading cycles of the selected material nodes

It is observed from Fig. 5.22a that during the first cut the compressive strain suffered by the material nodes A_2 and B_2 is much larger than that of the nodes A_1 and B_1, respectively. This is related to the increased length of the shear plane with an increasing uncut chip thickness. Thus, the material in front of the tooltip is to be compressed more severely with a larger uncut chip thickness. Fig. 5.22b shows the final tensile plastic strain of these material nodes after the first cut. It is noticed that this parameter becomes larger at material points A_2 and B_2 than that at points A_1 and B_1 respectively as the result of the increasing tool stretching effect with an increased uncut chip thickness. The loading cycle of these four material nodes after the first

cut are shown in Fig. 5.23a and c, in which the evolution of the residual stress produced by first cut is in line with the results shown in Fig. 5.17a.

Prior to continue to characterize the loading cycles induced by the second cut, the compressive/stretching effect of the tool used in the second cut is analysed. Fig. 5.24 shows that both the mechanical compressive and stretching effect of tool b is more significant than that of tool a. This is likely due to the material work-hardening induced by the first cut. Thus, a larger compressive and tensile stress is needed to accomplish the cutting process with a work-hardened material. Accordingly, with more hardened material generated by a larger h_1 in the previous cut, the compressive and stretching stress of tool c is higher than that of tool b.

Although suffering higher compressive stress during the second cut, the compressive strain of the material point A_2 and B_2 are less than that at point A_1 and B_1, respectively, especially at point "B_2" (Fig. 5.22c). It can be noted in Fig. 5.22b and c that the average value of PE11 at the material point B_2 is generated positive (around 0.002) after the 1st cut, and keeps almost constant in front of tool tip during the second cut. This means that this material node is too hardened to be further compressed by the second cut tool even though with an improved compressive stress induced by the tool c. Regarding the load cycle of material node B_1, it is shown in Fig. 5.22a and b that this material node is undeformed during the first cut. Thus, having no experience in work-hardened, this node is more easily compressed to yield stress compared to material node B_2. This explains the decreased compressive plastic strain (ahead of the tool) during the second cutting process in the study [73] and the smaller equivalent plastic strain (PEEQ) in the near machined surface layer after the second cut in the simulation work [70,74]. Furthermore, it is shown in Fig. 5.22d that the average value of final tensile strain is larger at material nodes A_2 and B_2 than that at A_1 and B_1 respectively. This is likely attributed to the fact that the stretching effect of tool c is larger than that of tool b. As a result, more compressive residual stress is generated at nodes A_2, B_2 than the ones at nodes A_1, B_1 respectively, as shown in Fig. 5.23b and d.

It is noticed that the mechanical compressive stress, which is capable of achieving the yield point of the machined material, spreads much shallower than that of the mechanical tensile stress ($h_c<h_t$ in Fig. 5.21b). This is the reason that the increased compressive effect of the tool cannot reach the newly yield condition of point B_2 during the second cut, while the increased tensile effect of the tool can realise it.

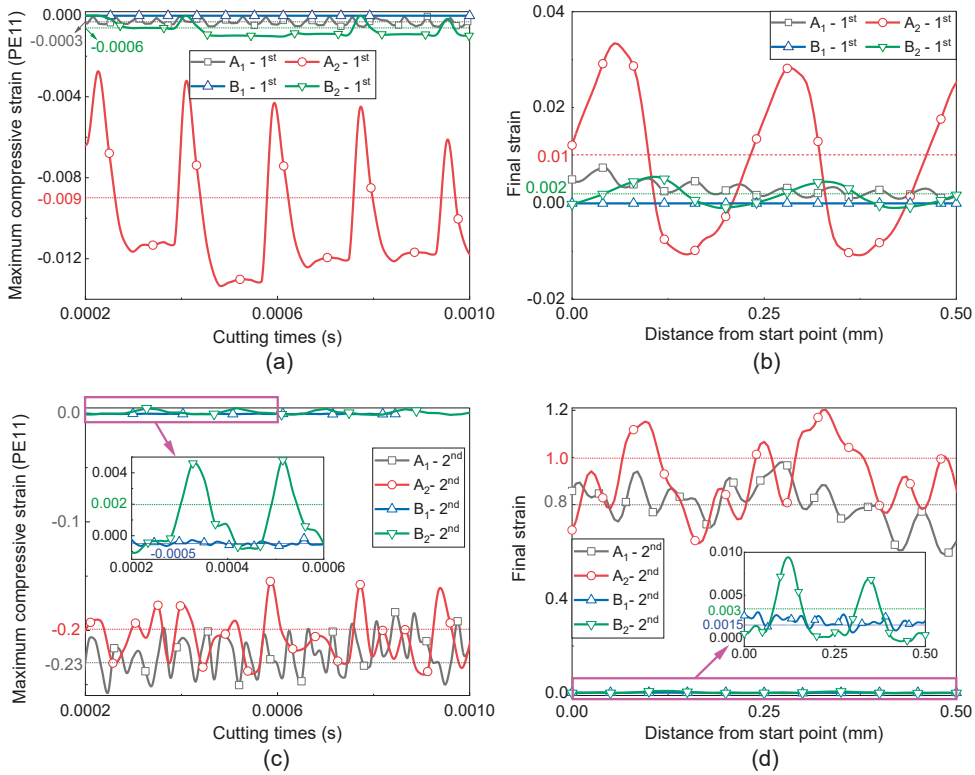

Figure 5.22
The compressive and final strain suffered by the selected points during multiple cuts. (a) Compressive strain during the first cut; (b) final strain after the first cut; (c) compressive strain during the second cut; (d) final strain after the second cut.

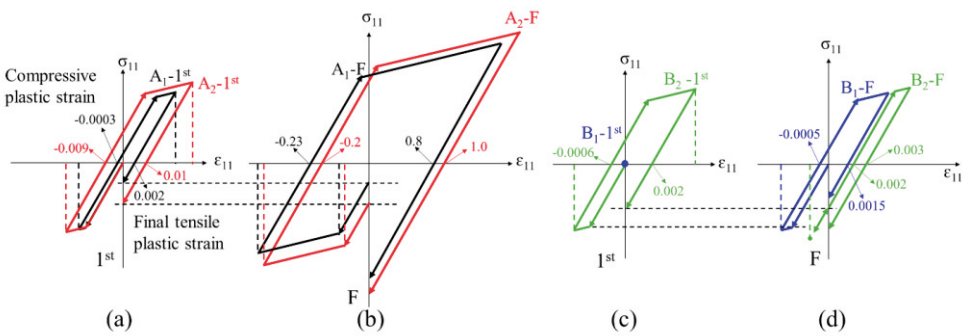

Figure 5.23
Loading cycles of the material nodes: (a) A_1 and A_2 during the first cut; (b) A_1 and A_2 during the final cut; (c) B_1 and B_2 during the first cut; (d) B_1 and B_2 during the final cut.

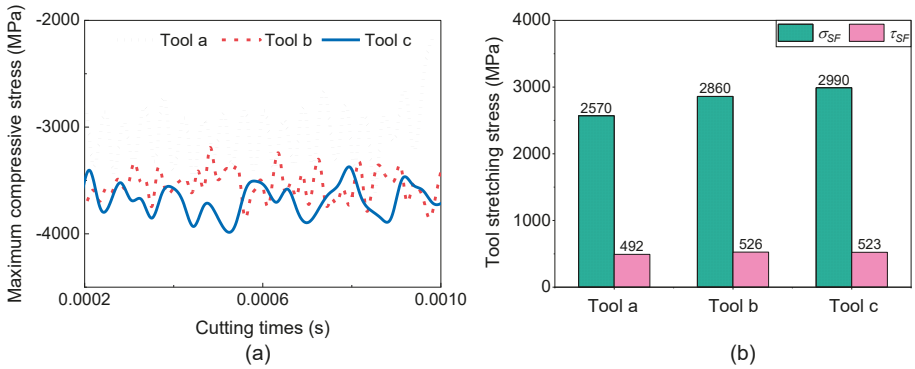

Figure 5.24
Compressive and tensile effect of the tool a, b, c and d: (a) compressive effect; (a) tensile effect.

It is concluded that the previously generated compressive residual stress tends to strengthen the final compressive residual stress. Through analysing the stress-strain response of the selected points, it is found that the reason could be related to the variation of the yield strength of workpiece material and the tool compressive/stretching effect. Since the first cut leads to an increased yield strength of the workpiece material, less compressive plastic strain ahead of the tooltip is generated during the second cut. Simultaneously, the material behind the tooltip is stretched more severely by the increased tool stretching effect during the second cut. Both effects cause the final residual stress to be more compressive. Such results were more significant when a larger intermediately generated compressive stress/tensile strain are generated by the first cut (by a larger h_1 or the tool with a more negative or a larger edge radius).

5.5 Residual stress evolution in fillet surface turning

During the fillet surface turning, the variation of uncut chip area will cause the change of cutting forces and temperature distribution, leading to the variation of residual stresses during this process. To explore the reason for the residual stress evolution during the fillet surface turning, the thermal and mechanical loads acting on the machined surface during this process are investigated.

5.5.1 Cutting forces variation

It can be seen from Fig. 5.3 that the force components in tangential and cutting speed direction increase firstly and then decrease during the fillet surface turning, while the force component in radial direction increase in this process. To explain the

evolution of force components, the change of uncut chip geometry during the fillet turning are investigated. As shown in Fig. 5.25, the shape of uncut chip shows a arc-shaped region at the outer face and a long thin band region at the end face. Therefore, the increase of radial depth of cut in the early stage of the process is likely the reason for the increased cutting force components F_t and F_c increase. After that, the shape of uncut chip area becomes longer and thinner and the area gets smaller, causing a decrease of these two force components in the later stage. Regarding the increasing trend of F_r, it is likely due to the increased length of the uncut chip cross section from turning outer face to end face.

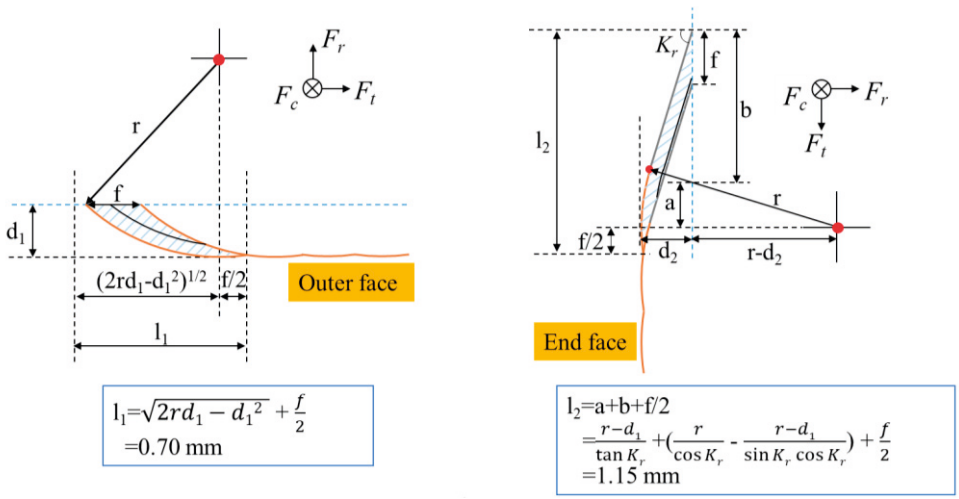

Figure 5.25
Uncut chip cross-section geometry at outer face and end face.

5.5.2 Temperature variation

Fig. 5.26 shows the temperature distribution of the workpiece at the four specific cutting faces. It is shown that the maximum temperature at the machined surface shows an increasing trend from outer face turning to end face turning, which is likely due to the change of the engagement of the edge rounding. As shown in Fig. 5.25, the chip formation taking place on the edge rounding significantly increases with the tool moving from the outer face to the end face. That is, a larger amount of workpiece material is deformed by the edge rounding where the cutting conditions are effectively negative rake. Thus, more heat is generated due to more severely plastic deformation of the workpiece during this process. In addition, Fig. 5.27 shows the evolution of the local normal rake angle (γ_l) of the direct-contact edge from outer face turning to end face turning. It is illustrated that this angle is firstly reduced from -4° to -8° when the tool position moves from the outer face to Deg60

face and then slightly increases to -7° at the end face turning. More heat generated from the plastic deformation caused by the decreased local normal rake angle is another reason for the increased temperature from the outer face turning to end face turning.

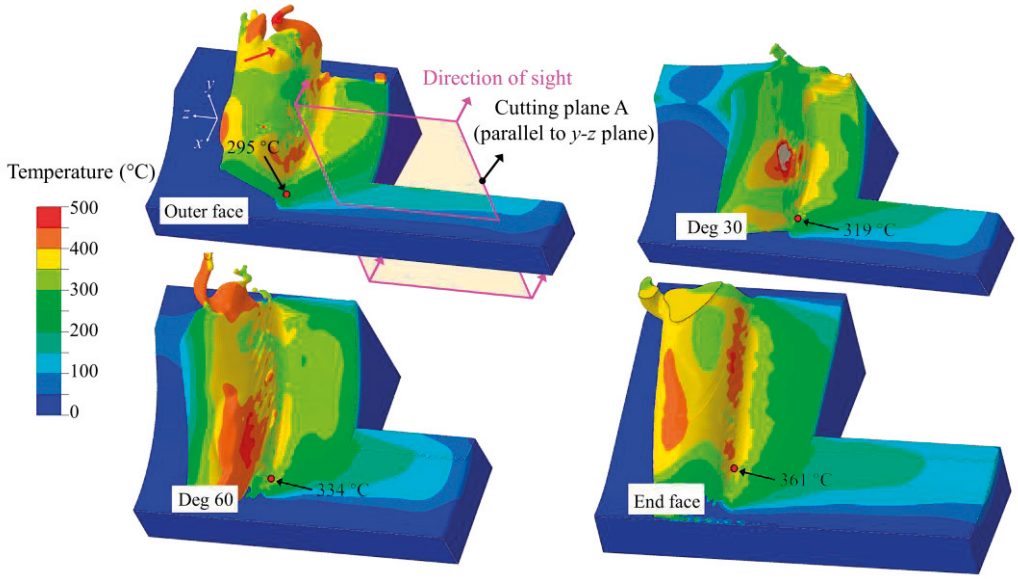

Figure 5.26
Tempearture distributions in the chip and the workpiece after 0.5 ms of cutting time.

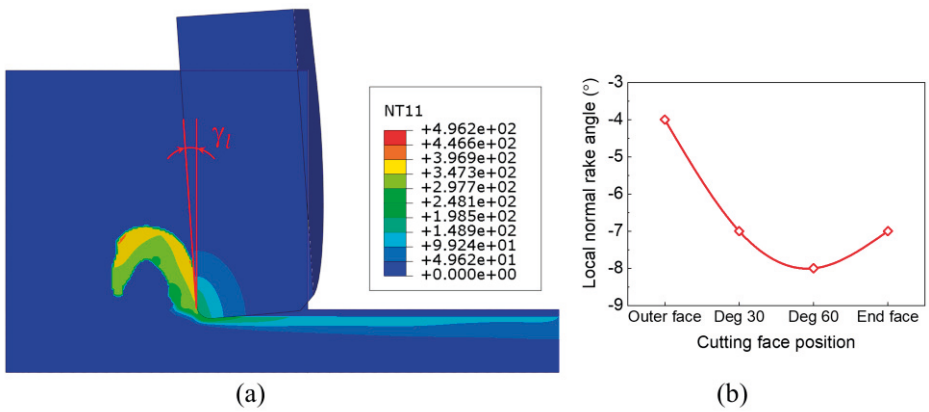

Figure 5.27
The variation of the local normal rake angle on the Cutting plane A; (a) the extraction of local normal rake angle; (b) the variation of the local normal rake angle from outer face to end face.

5.5.3 Residual stress variation

It is shown from both experimental and simulated results that a more compressive residual stress distribution is obtained at end face turning than that at outer face turning, although the difference is not significant (Fig. 5.28). Although the thermal-induced tensile residual stress could be larger in the end face turning than that in the outer face turning due to the mentioned temperature evolution, the mechanical loads play a dominant role in determining the residual stress evolution in these two cutting faces. As illustrated in Fig. 5.3, both the force components F_c and F_r are larger in end face turning compared to that in outer face turning, causing a larger degree of tensile plastic deformation in the surface and subsurface layer of the end machined workpiece, thus, a larger magnitude of compressive residual stress is generated in these regions as a result.

For this section, it can be concluded that both F_t and F_c increase firstly and then decrease during the fillet turning process due to the same variation trend of depth of cut, while F_r is increased which is likely attributed to the increased length of the uncut chip cross-section. The maximum temperature on the machined surface increases from outer face turning to end face turning because the combined effect of the increased engaged edge rounding area and more negative local normal rake angle during this process. Residual stress becomes more compressive when the tool position changes from outer face to end face, although the difference is not significant. This is caused by the increased mechanical load applied on the machined surface.

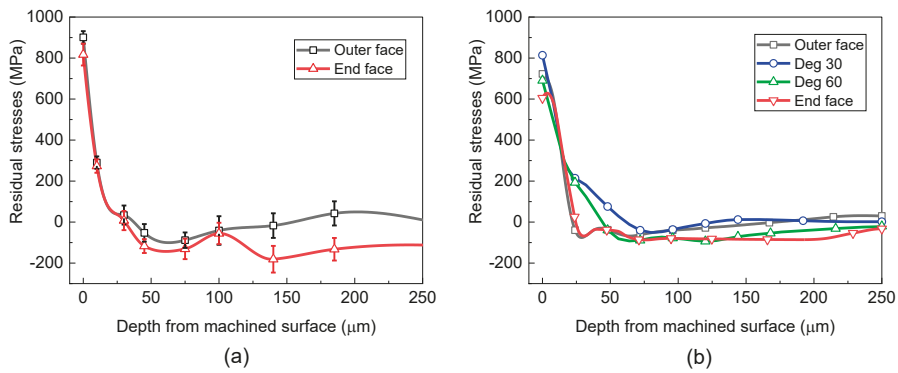

Figure 5.28
Residual stresses distributions: (a) measured residual stress profiles; (b) simulated residual stress profiles.

6 Conclusions and future work

This dissertation aims to explore the formation mechanism of the residual stress and investigate the evolution of the residual stress field under various operations through numerical analysis and simulation. With numerical investigation, the mechanically or thermally induced plastic deformation during the cutting process is distinguished by extracting different physical quantities. For example, the local normal/tangential stress acting on the material behind the tooltip can be considered as an indicator for evaluating the extent of mechanical induced compressive residual stress in surface/near-surface and subsurface layers. The magnitude of the maximum compressive stress/strain ahead of the tooltip can reflect the degree of mechanical induced tensile residual stress. The temperature as a function of depth beneath the machined surface can indicate the level of thermal-induced compressive strain in the surface/near-surface layer. Thus, through the analysis of these parameters, the effect of cutting parameters, tool geometries and cutting procedures, etc. on residual stress evolution can be easily understood. The conclusions of the results are given in this chapter, followed by suggestions for future research work.

6.1 Conclusions

- A cyclic residual stresses distribution are generated on the machined workpiece when a segmented chip is formed. This is mainly attributed to the periodical change of mechanical load on the machined surface during chip segments generation rather than the thermal load. Specifically, the feed force increase firstly and then decreases during one segment genesis. It is the increased feed force that causes an increase in the local normal/tangential stress acting on the machined surface, leading to a less tensile residual stress in the lower stress zone. This effect is more obvious when producing a larger degree of chip serration, in which compressive residual stress will be generated at the surface layer of the lower stress zone. To maintain an equilibrium state, tensile residual stress is formed in the near-surface layer in this region.
- In terms of the effect of tool geometry, the residual stress profile induced by a negative rake angle becomes more compressive on the whole compared to that with a positive rake angle. When using a tool with a larger edge radius or flank wear, the magnitude of surface/near-surface tensile stress will increase due to

the enhanced temperature field. Furthermore, it is found that the maximum value of compressive residual stress in sublayer is mainly determined by local normal/tangential stress exerted by the tool. The tool stretching effect will increase with a more negative cutting tool or a larger edge radius, while decreases with a continuous increasing edge radius or a worn tool due to a larger contact area. The depth of compressive residual stress increases when using a negative rake angle, a larger edge radius and a worn tool.

- It is found that the previously generated compressive residual stress tends to strengthen the final compressive residual stress. The reason could be related to the variation of the yield strength of workpiece material and the tool compressive/stretching effect. Since the first cut leads to an increased yield strength of the workpiece material, less compressive plastic strain ahead of the tooltip is generated during the second cut. Simultaneously, the material behind the tooltip is stretched more severely by the increased tool stretching effect during the second cut. Both effects cause the final residual stress to be more compressive. Such results are more significant when a larger intermediately generated compressive stress/tensile strain are generated by the previous cut (by a larger h_1 or the tool with a more negative or a larger edge radius).
- When turning a fillet surface, it is found that both F_t and F_c increase firstly and then decrease during this process due to the same variation trend of the depth of cut, while F_r is increased which is likely attributed to the increased length of the uncut chip cross-section. The maximum temperature on the machined surface increases from outer face turning to end face turning because of the combined effect of the increased engaged edge rounding area and more negative local normal rake angle during this process. Residual stress becomes more compressive when the tool position changes from outer face to end face, although the difference is not significant. This is caused by the increased mechanical load applied to the machined surface.

6.2 Future work

- It should be noted that the Johnson-Cook model used in the present study doesn't introduce the Bauschinger effect occurring in cyclic deformation of the workpiece. This character is important for the residual stress prediction especially in the multiple cuts because in this process the workpiece material in the surface/sub-surface is repeatedly squeezed and stretched to the yield point by cutting tools, which can be regarded as a process applying a cyclic load to the machined material. However, it is acceptable for the present study to carry out an initial investigation of the residual stress. Nevertheless, it is suggested that future research is needed to include the Bauschinger effect into the plastic

model to improve the accuracy of residual stress prediction, especially under multiple cuts.

- The selection of an appropriate material model plays a critical role in the accuracy of the residual stress prediction. It is recommended that more comprehensive models including the coupling between the strain-softening and temperature [51], the coupling between the strain softening and strain [55], and the coupling between the temperature and the strain rate [53] should be involved in the future modelling research to investigate the influence of different material models on residual stress prediction.
- The proposed CEL FE model has a good correlation for the primary cutting force, but it underestimates the feed force. These deviations are probably caused by the changing of tool edge geometries during the practical experiment. Thus, it is suggested that a finite element model considering the variation of tool geometry or tool wear with the cutting time should be established to evaluate the influence of this factor on the feed force or residual stress prediction.
- It is suggested to include user defined subroutine in present model to capture more aspects of surface integrity, such as white layer, hardness, etc.

7 References

[1] Withers PJ. Residual stress and its role in failure. Reports Prog Phys 2007;70:2211–64. doi:10.1088/0034-4885/70/12/R04.

[2] Capello E. Residual stresses in turning: Part I: Influence of process parameters. J Mater Process Technol 2005;160:221–8. doi:10.1016/j.jmatprotec.2004.06.012.

[3] Malakizadi A, Larsson R, Semih A. A thermomechanically motivated approach for identification of flow stress properties in metal cutting 2020:1055–68.

[4] Rossini NS, Dassisti M, Benyounis KY, Olabi AG. Methods of measuring residual stresses in components. Mater Des 2012;35:572–88. doi:10.1016/j.matdes.2011.08.022.

[5] Arrazola PJ, Özel T, Umbrello D, Davies M, Jawahir IS. Recent advances in modelling of metal machining processes. CIRP Ann - Manuf Technol 2013;62:695–718. doi:10.1016/j.cirp.2013.05.006.

[6] Duan C, Kong W, Hao Q, Zhou F. Modeling of white layer thickness in high speed machining of hardened steel based on phase transformation mechanism. Int J Adv Manuf Technol 2013;69:59–70. doi:10.1007/s00170-013-5005-y.

[7] Shah SM, Nélias D, Zain-Ul-Abdein M, Coret M. Numerical simulation of grinding induced phase transformation and residual stresses in AISI-52100 steel. Finite Elem Anal Des 2012;61:1–11. doi:10.1016/j.finel.2012.05.010.

[8] Jafarian F, Imaz Ciaran M, Umbrello D, Arrazola PJ, Filice L, Amirabadi H. Finite element simulation of machining Inconel 718 alloy including microstructure changes. Int J Mech Sci 2014;88:110–21. doi:10.1016/j.ijmecsci.2014.08.007.

[9] Iurea P. Finite Element Modeling of Residual Stresses Obtained By Cutting Pieces: a Review. Int J Mod Manuf Technol I 2014;2:44–62.

[10] Mabrouki T, Girardin F, Asad M. Numerical and experimental study of dry cutting for an aeronautic aluminium alloy (A2024-T351). Int J Mach Tools Manuf J Home n.d. doi:10.1016/j.ijmachtools.2008.03.013.

[11] Ulutan D, Ozel T. Machining induced surface integrity in titanium and nickel alloys: A review. Int J Mach Tools Manuf 2011;51:250–80. doi:10.1016/j.ijmachtools.2010.11.003.

[12] Dahlman P, Gunnberg F, Jacobson M. The influence of rake angle, cutting feed and cutting depth on residual stresses in hard turning. J Mater Process Technol 2004;147:181–4. doi:10.1016/j.jmatprotec.2003.12.014.

[13] Outeiro JC, Umbrello D, M'Saoubi R. Experimental and numerical modelling of the residual stresses induced in orthogonal cutting of AISI 316L steel. Int J Mach Tools Manuf 2006;46:1786–94. doi:10.1016/j.ijmachtools.2005.11.013.

[14] M'Saoubi R, Outeiro JC, Changeux B, Lebrun JL, Morão Dias A. Residual stress analysis in orthogonal machining of standard and resulfurized AISI 316L steels. J Mater Process Technol 1999;96:225–33. doi:10.1016/S0924-0136(99)00359-3.

[15] Ståhl J-E and Seco Tools AB. Metal cutting theories and models. Div Prod Mater Eng 2012.

[16] Yin Q, Liu Z. Recent progress of machinability and surface integrity for mechanical machining Inconel 718 : a review. Int J Adv Manuf Technol 2020:215–45. doi:10.1007/s00170-020-05665-4.

[17] Withers PJ, Bhadeshia HKDH. Residual stress Part 2 – Nature and origins 2001.

[18] Ui A, Mohsan H, Liu Z, Padhy GK. A review on the progress towards improvement in surface integrity of Inconel 718 under high pressure and flood cooling conditions 2017:107–25. doi:10.1007/s00170-016-9737-3.

[19] Nasr MNA, Ng EG, Elbestawi MA. Modelling the effects of tool-edge radius on residual stresses when orthogonal cutting AISI 316L. Int J Mach Tools Manuf 2007;47:401–11. doi:10.1016/j.ijmachtools.2006.03.004.

[20] Wu DW, Matsumoto Y. The Effect of Hardness on Residual Stresses in Orthogonal Machining of AiSI 4340 Steel 2014;112:245–52.

[21] Brinksmeier E, Cammett JT, König W, Leskovar P, Peters J, Tönshoff HK. Residual Stresses - Measurement and Causes in Machining Processes. CIRP Ann - Manuf Technol 1982;31:491–510. doi:10.1016/S0007-8506(07)60172-3.

[22] Schwach DW, Guo YB. A fundamental study on the impact of surface integrity by hard turning on rolling contact fatigue. Int J Fatigue 2006;28:1838–44. doi:10.1016/j.ijfatigue.2005.12.002.

[23] Zhang W, Fang K, Hu Y, Wang S, Wang X. Effect of machining-induced surface residual stress on initiation of stress corrosion cracking in 316 austenitic stainless steel. Corros Sci 2016;108:173–84. doi:10.1016/j.corsci.2016.03.008.

[24] Torres MAS. An evaluation of shot peening , residual stress and stress relaxation on the fatigue life of AISI 4340 steel 2002;24:877–86.

[25] Thumser R, Bergmann JW, Vormwald M. Residual stress fields and fatigue analysis of autofrettaged parts. Int J Press Vessel Pip 2002;79:113–7. doi:10.1016/S0308-0161(01)00137-5.

[26] Rodríguez A, Lacalle LNL De, Celaya A, Lamikiz A, Albizuri J. Surface improvement of shafts by the deep ball-burnishing technique. Surf Coat Technol 2012;206:2817–24. doi:10.1016/j.surfcoat.2011.11.045.

[27] Guo YB, Warren AW, Hashimoto F. The basic relationships between residual stress, white layer, and fatigue life of hard turned and ground surfaces in rolling contact. CIRP J Manuf Sci Technol 2010;2:129–34. doi:10.1016/j.cirpj.2009.12.002.

[28] Withers PJ, Turski M, Edwards L, Bouchard PJ, Buttle DJ. Recent advances in residual stress measurement. Int J Press Vessel Pip 2008;85:118–27. doi:10.1016/j.ijpvp.2007.10.007.

[29] Ruud CO. A review of selected non-destructive methods for residual stress measurement. NDT Int 1982;15:15–23. doi:10.1016/0308-9126(82)90083-9.

[30] Fitzpatrick ME, Fry AT. Determination of Residual Stresses by X-ray Diffraction

Determination of Residual Stresses by X-ray Diffraction - Issue 2 2002.

[31] Lord JD, Fry AT. A review of residual stress measurement methods--a guide to technical selection. NPL Mater Cent 2001.

[32] Hutchings, M. T., & Krawitz AD (Eds.). Measurement of residual and applied stress using neutron diffraction. Springer Science & Business Media; 2012.

[33] Schajer GS. Hole-Drilling Residual Stress Measurements at 75 : Origins , Advances , Opportunities 2010:245–53. doi:10.1007/s11340-009-9285-y.

[34] Ruud CO. A Review of Nondestructive Methods for Residual Stress Measurement n.d.:35–40.

[35] Šarga P, Menda F. Comparison of Ring-Core Method and Hole-drilling Method Used for Determining Residual Stresses 2013;1:335–8. doi:10.12691/ajme-1-7-36.

[36] Karabutov A, Devichensky A, Ivochkin A, Lyamshev M, Pelivanov I, Rohadgi U, et al. Laser ultrasonic diagnostics of residual stress. Ultrasonics 2008;48:631–5. doi:10.1016/j.ultras.2008.07.006.

[37] Sadeghifar M, Sedaghati R, Jomaa W, Songmene V. A comprehensive review of finite element modeling of orthogonal machining process: chip formation and surface integrity predictions. Int J Adv Manuf Technol 2018;96:3747–91. doi:10.1007/s00170-018-1759-6.

[38] Huang JM, Black JT. An Evaluation of Chip Separation Criteria for the FEM Simulation of Machining. J Manuf Sci Eng 1996;118:545. doi:10.1115/1.2831066.

[39] Grissa R, Zemzemi F, Fathallah R. Three approaches for modeling residual stresses induced by orthogonal cutting of AISI316L 2018;135:253–60. doi:10.1016/j.ijmecsci.2017.11.029.

[40] Sun SI. A study of different FEM techniques for modelling 3D metal cutting process with an emphasize on ALE and CEL formulations 2014.

[41] Agmell M, Ahadi A, Zhou JM, Peng RL, Bushlya V, Ståhl JE. Modeling subsurface deformation induced by machining of Inconel 718. Mach Sci Technol 2017;21:103–20. doi:10.1080/10910344.2016.1260432.

[42] Zhang C, Choi H. Study of segmented chip formation in cutting of high-strength lightweight alloys. Int J Adv Manuf Technol 2021. doi:10.1007/s00170-020-06057-4.

[43] Moussa N Ben, Sidhom H, Braham C. Numerical and experimental analysis of residual stress and plastic strain distributions in machined stainless steel. Int J Mech Sci 2012;64:82–93. doi:10.1016/j.ijmecsci.2012.07.011.

[44] Ducobu F, Rivière-Lorphèvre E, Filippi E. Numerical contribution to the comprehension of saw-toothed Ti6Al4V chip formation in orthogonal cutting. Int J Mech Sci 2014;81:77–87. doi:10.1016/j.ijmecsci.2014.02.017.

[45] Arrazola PJ, Özel T. Investigations on the effects of friction modeling in finite element simulation of machining. Int J Mech Sci 2010;52:31–42. doi:10.1016/j.ijmecsci.2009.10.001.

[46] Filippi E, Ducobu F, Rivi E. Application of the Coupled Eulerian-Lagrangian (CEL) method to the modeling of orthogonal cutting 2016;59:58–66. doi:10.1016/j.euromechsol.2016.03.008.

[47] Klocke F, Döbbeler B, Peng B, Lakner T. FE-simulation of the cutting process under consideration of cutting fluid. Procedia CIRP 2017;58:341–6. doi:10.1016/j.procir.2017.03.235.

[48] Agmell M, Bushlya V, Saoubi RM, Gutnichenko O, Zaporozhets O, Va S, et al. Investigation of mechanical and thermal loads in pcBN tooling during machining of Inconel 718. Int J Adv Manuf Technol 2020:1451–62. doi:10.1007/s00170-020-05081-8.

[49] Shuang F, Chen X, Ma W. Numerical analysis of chip formation mechanisms in orthogonal cutting of Ti6Al4V alloy based on a CEL model 2018:185–98. doi:10.1007/s12289-017-1341-z.

[50] Chen L, El-Wardany TI, Harris WC. Modelling the effects of flank wear land and chip formation on residual stresses. CIRP Ann - Manuf Technol 2004;53:95–8. doi:10.1016/S0007-8506(07)60653-2.

[51] Calamaz M, Coupard D, Girot F. Numerical simulation of Titanium alloy dry machining with a strain softening constitutive law 2010;0344. doi:10.1080/10910344.2010.500957.

[52] Calamaz M, Coupard D, Girot F. A new material model for 2D numerical simulation of serrated chip formation when machining titanium alloy Ti–6Al–4V. Int J Mach Tools Manuf 2008;48:275–88. doi:10.1016/j.ijmachtools.2007.10.014.

[53] Iturbe A, Giraud E, Hormaetxe E, Garay A, Germain G, Ostolaza K, et al. Mechanical characterization and modelling of Inconel 718 material behavior for machining process assessment. Mater Sci Eng A 2017;682:441–53. doi:10.1016/j.msea.2016.11.054.

[54] Kim S, Yoo Y. Dynamic recrystallization behavior of AISI 304 stainless steel. Mater Sci Eng 2001;311:108–13. doi:10.1016/S0921-5093(01)00917-0.

[55] Sima M, Özel T. Modified material constitutive models for serrated chip formation simulations and experimental validation in machining of titanium alloy Ti-6Al-4V. Int J Mach Tools Manuf 2010;50:943–60. doi:10.1016/j.ijmachtools.2010.08.004.

[56] Atlati S, Haddag B, Nouari M, Zenasni M. Analysis of a new Segmentation Intensity Ratio SIR to characterize the chip segmentation process in machining ductile metals. Int J Mach Tools Manuf 2011;51:687–700. doi:10.1016/j.ijmachtools.2011.05.007.

[57] Zhang Y, Mabrouki T, Nelias D, Gong Y. FE-model for Titanium alloy (Ti-6Al-4V) cutting based on the identification of limiting shear stress at tool-chip interface. Int J Mater Form 2011;4:11–23. doi:10.1007/s12289-010-0986-7.

[58] Agmell M, Bushlya V, Laakso SVA, Ahadi A. Development of a simulation model to study tool loads in pcBN when machining AISI 316L 2018:2853–65. doi:https://doi.org/10.1007/s00170-018-1673-y.

[59] Schlauer C, Odén M. Residual stress evolution and near-surface microstructure after turning of the nickel-based superalloy Inconel 718. Zeitschrift Fuer Met Res Adv Tech 2005;96:385–92. doi:10.3139/146.018124.

[60] Pawade RS, Joshi SS, Brahmankar PK. Effect of machining parameters and cutting edge geometry on surface integrity of high-speed turned Inconel 718. Int J Mach Tools Manuf 2008;48:15–28. doi:10.1016/j.ijmachtools.2007.08.004.

[61] Sharman ARC, Hughes JI, Ridgway K. An analysis of the residual stresses generated

in Inconel 718™ when turning. J Mater Process Technol 2006;173:359–67. doi:10.1016/j.jmatprotec.2005.12.007.

[62] Hua J, Umbrello D, Shivpuri R. Investigation of cutting conditions and cutting edge preparations for enhanced compressive subsurface residual stress in the hard turning of bearing steel. J Mater Process Technol 2006;171:180–7. doi:10.1016/j.jmatprotec.2005.06.087.

[63] Hua J, Shivpuri R, Cheng X, Bedekar V, Matsumoto Y, Hashimoto F, et al. Effect of feed rate, workpiece hardness and cutting edge on subsurface residual stress in the hard turning of bearing steel using chamfer + hone cutting edge geometry. Mater Sci Eng A 2005;394:238–48. doi:10.1016/j.msea.2004.11.011.

[64] Shen Q, Liu Z, Hua Y, Zhao J, Lv W, Mohsan AUH. Effects of cutting edge microgeometry on residual stress in orthogonal cutting of inconel 718 by FEM. Materials (Basel) 2018;11. doi:10.3390/ma11061015.

[65] Liu M, Takagi JI, Tsukuda A. Effect of tool nose radius and tool wear on residual stress distribution in hard turning of bearing steel. J Mater Process Technol 2004;150:234–41. doi:10.1016/j.jmatprotec.2004.02.038.

[66] Sharman ARC, Hughes JI, Ridgway K. The effect of tool nose radius on surface integrity and residual stresses when turning Inconel 718™. J Mater Process Technol 2015;216:123–32. doi:10.1016/j.jmatprotec.2014.09.002.

[67] Tang ZT, Liu ZQ, Pan YZ, Wan Y, Ai X. The influence of tool flank wear on residual stresses induced by milling aluminum alloy. J Mater Process Technol 2009;209:4502–8. doi:10.1016/j.jmatprotec.2008.10.034.

[68] Ee KC, Dillon OW, Jawahir IS. Finite element modeling of residual stresses in machining induced by cutting using a tool with finite edge radius. Int J Mech Sci 2005;47:1611–28. doi:10.1016/j.ijmecsci.2005.06.001.

[69] Liu CR, Guo YB. Finite element analysis of the effect of sequential cuts and tool-chip friction on residual stresses in a machined layer. Int J Mech Sci 2000;42:1069–86. doi:10.1016/S0020-7403(99)00042-9.

[70] Zhao H, Liu C, Cui T, Tian Y, Shi C, Li J, et al. Influences of sequential cuts on micro-cutting process studied by smooth particle hydrodynamic (SPH). Appl Surf Sci 2013;284:366–71. doi:10.1016/j.apsusc.2013.07.106.

[71] Pu Z, Umbrello D, Jr OWD, Jawahir IS. Finite element simulation of residual stresses in cryogenic machining of AZ31B Mg Alloy. Procedia CIRP 2014;13:282–7. doi:10.1016/j.procir.2014.04.048.

[72] Zhang XM, Huang X Da, Chen L, Leopold J, Ding H. Effects of sequential cuts on white layer formation and retained austenite content in hard turning of AISI52100 Steel. J Manuf Sci Eng Trans ASME 2017;139:1–12. doi:10.1115/1.4035125.

[73] Nasr MNA. Effects of sequential cuts on residual stresses when orthogonal cutting. Procedia CIRP 2015;31:118–23. doi:10.1016/j.procir.2015.03.032.

[74] Guo YB, Liu CR. FEM analysis of mechanical state on sequentially machined surfaces 2007;0344:20–41. doi:10.1081/MST-120003183.

[75] Sasahara H, Obikawa T, Shirakashi T. FEM analysis of cutting sequence effect on mechanical characteristics in machined layer. J Mater Process Technol 1996;62:448–53. doi:10.1016/S0924-0136(96)02451-X.

[76] Ma Y, Yu D, Feng P, Wu Z, Zhang J. Finite element method study on the influence of initial stress on machining process. Adv Mech Eng 2015. doi:10.1177/1687814015572457.

[77] Ruitao P, Linfeng Z, Jiawei T, Xiuli F, Meiliang C. Application of pre-stressed cutting to aviation alloy : The effect on residual stress and surface roughness. J Manuf Process 2021;62:501–12. doi:10.1016/j.jmapro.2020.12.021.

[78] Aiswaresh R, Gupta TVK. The influence of tool-path strategies and cutting parameters on cutting forces , tool wear and surface quality in finish milling of Aluminium 7075 curved surface 2020:589–601.

[79] Ma J, Hu G, Jia Z, Zhang N, Wang F. Effect of geometric feature and cutting direction on variation of force and vibration in high-speed milling of TC4 curved surface 2018:2207–18.

[80] Ma J, Wang F, Jia Z, Xu Q. Study of machining parameter optimization in high speed milling of Inconel 718 curved surface based on cutting force 2014:269–77. doi:10.1007/s00170-014-6115-x.

[81] Mahajan KA. Effect of machining parameters and vibration on polymethylmethacrylate curved surface in single-point diamond turning 2020:1–10. doi:10.1177/2516598420941728.

[82] Jiang X, Kong X, Zhang Z, Wu Z, Ding Z, Guo M. Modeling the effects of Undeformed Chip Volume (UCV) on residual stresses during the milling of curved thin-walled parts. Int J Mech Sci 2020;167:105162. doi:10.1016/j.ijmecsci.2019.105162.

[83] Zhang X, Zhang J, Zhao W. A new method for cutting force prediction in peripheral milling of complex curved surface. Int J Adv Manuf Technol 2016:117–28. doi:10.1007/s00170-015-8123-x.

[84] Ma J, Jia Z, Wang F, Gao Y, Liu Z. A new cutting force modeling method in high-speed milling of curved surface with difficult-to-machine material. Int J Adv Manuf Technol 2016:2195–205. doi:10.1007/s00170-015-7856-x.

[85] Valiorgue F, Rech J, France F, Stief P, Dantan J, Etienne A, et al. Evolution of the surface integrity while turning a fillet radius in a martensitic stainless steel 15-5PH. Procedia CIRP 2020;87:101–6. doi:10.1016/j.procir.2020.02.038.

[86] Ducobu F, Rivière-Lorphèvre E, Filippi E. Mesh influence in orthogonal cutting modelling with the Coupled Eulerian-Lagrangian (CEL) method. Eur J Mech - A/Solids 2017;65:324–35. doi:10.1016/j.euromechsol.2017.05.007.

[87] Abaqus Analysis User's Guide, Version 6.14 n.d.

[88] Nie D, Lu Z, Zhang K. Hot bending behavior of SUS 304 stainless steel sheet assisted by resistance heating : multi-field coupling numerical simulation and experimental investigation. Int J Adv Manuf Technol 2016:2763–74. doi:10.1007/s00170-016-8653-x.

[89] MatWeb (2016) http://www. matweb. com 2016. Material property data n.d.

[90] Zhang W, Wang X, Hu Y, Wang S. Predictive modelling of microstructure changes, micro-hardness and residual stress in machining of 304 austenitic stainless steel. Int J Mach Tools Manuf 2018;130–131:36–48. doi:10.1016/j.ijmachtools.2018.03.008.

[91] Johnson G, Cook W. Fracture characteristics of three metals subjected to various strains, strain rates and temperatures and pressures. Eng Fract Mech 1985;21(1):31–48.

[92] Hillerborg A, Modéer M, Petersson P-E. Analysis of crack formation and crack growth in concrete by means of fracture mechanics and finite elements. Cem Concr Res 1976;6:773–81. doi:10.1016/0008-8846(76)90007-7.

[93] Farahmand B. Virtual testing and predictive modeling: For fatigue and fracture mechanics allowables. 2009. doi:10.1007/978-0-387-95924-5.

[94] Zorev NN. Inter-relationship between shear processes occurring along tool face and shear plane in metal cutting. Int Res Prod Eng 1963;49:143–52.

[95] Artozoul J, Lescalier C, Bomont O, Dudzinski D. Extended infrared thermography applied to orthogonal cutting: mechanical and thermal aspects. Appl Therm Eng 2014;64:441–52. doi:10.1016/j.applthermaleng.2013.12.057.

[96] Atlati BHS, Zenasni MNM. Analysis of the heat transfer at the tool – workpiece interface in machining : determination of heat generation and heat transfer coefficients. Heat Mass Transf 2015:1355–70. doi:10.1007/s00231-015-1499-1.

[97] Muñoz-Sánchez A, Canteli JA, Cantero JL, Miguélez MH. Numerical analysis of the tool wear effect in the machining induced residual stresses. Simul Model Pract Theory 2011;19:872–86. doi:10.1016/j.simpat.2010.11.011.

[98] Sartori E. Convection coefficient equations for forced air flow over flat surfaces. Sol Energy 2006;80:1063–71. doi:10.1016/j.solener.2005.11.001.

[99] M'Saoubi R, Outeiro JC, Chandrasekaran H, Dillon OW, Jawahir IS. A review of surface integrity in machining and its impact on functional performance and life of machined products. Int J Sustain Manuf 2008;1:203–36. doi:10.1504/IJSM.2008.019234.

[100] Korkut I, Kasap M, Ciftci I, Seker U. Determination of optimum cutting parameters during machining of AISI 304 austenitic stainless steel. Mater Des 2004;25:303–5. doi:10.1016/j.matdes.2003.10.011.

[101] Sharman ARC, Hughes JI, Ridgway K. Workpiece surface integrity and tool life issues when turning inconel 718^{TM} nickel based superalloy. Mach Sci Technol 2004;8:399–414. doi:10.1081/MST-200039865.

[102] Laakso SVA, Zhao T, Agmell M, Hrechuk A, Ståhl JE. Too Sharp for its Own Good – Tool Edge Deformation Mechanisms in the Initial Stages of Metal Cutting. Procedia Manuf 2017;11:449–56. doi:10.1016/j.promfg.2017.07.135.

[103] Dumas M, Valiorgue F, Robaeys A Van, Rech J. Interaction between a roughing and a finishing operation on the final surface integrity in turning. Procedia CIRP, vol. 71, Elsevier B.V.; 2018, p. 396–400. doi:10.1016/j.procir.2018.05.050.

[104] Cakir FH, Gurgen S, Sofuoglu MA, Celik ON, Kushan MC. Finite element modeling of ultrasonic assisted turning of Ti6Al4V Alloy. Procedia - Soc Behav Sci 2015;195:2839–48. doi:10.1016/j.sbspro.2015.06.404.

[105] Wang J, Huang CZ, Song WG. The effect of tool flank wear on the orthogonal cutting process and its practical implications. J Mater Process Technol 2003;142:338–46. doi:10.1016/S0924-0136(03)00604-6.

[106] Liu CR, Barash MM. The mechanical state of the sublayer of a surface generated by chip-removal process—Part 2: cutting with a tool with flank wear. J Eng Ind 1976;98:1202–8. doi:10.1115/1.3439085.

[107] Dehmani H, Salvatore F, Hamdi H. Numerical study of residual stress induced by multi-steps orthogonal cutting. Procedia CIRP 2013;8:299–304. doi:10.1016/j.procir.2013.06.106.

[108] Liu CR, Barash MM. The mechanical state of the sublayer of a surface generated by chip - Remove process part 2 : cutting with a tool with flank wear. J Eng Ind 1976;98:1202–8. doi:10.1115/1.3439085.